EXPERIMENTAL AND THEORETICAL ANALYSIS OF FLOW AND SEDIMENT TRANSPORT IN 90-DEGREE FLUVIAL DIVERSIONS

by

Albert Herrero Casas

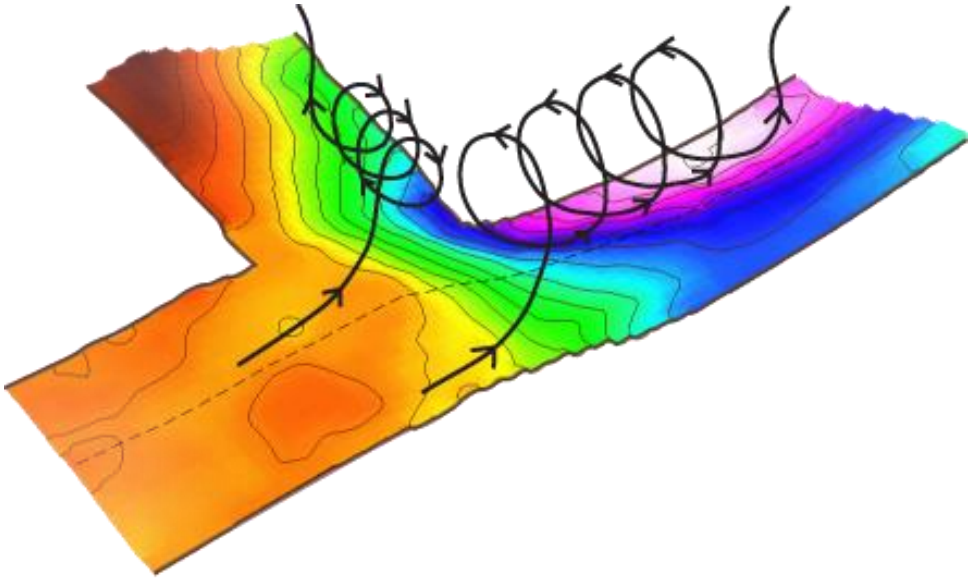

Supervised by:

Prof. Dr. Allen Bateman Pinzón

GRUP D'INVESTIGACIÓ EN MODELITZACIÓ DE CONQUES I TRANSPORT DE SEDIMENTS

UNIVERSITAT POLITÈCNICA DE CATALUNYA

Barcelona

May 2013

Funded by:

Abtract

Fluvial bifurcations are systems that have a great influence on human society. Their formation and evolution can affect to activities as agriculture or industry and a good knowledge of the mechanisms that affect the processes involved can be determinant for a proper land management. From a geometrical point of view, diversions or lateral intakes are a particular case of fluvial bifurcations in which one of the downstream branches exits laterally while the other follows the same direction as the incoming channel. Diversions are characterized by a significant trend of sediment to deviate towards the lateral branch.

The first part of this study describes the experimental work performed in the Fluvial Morphodynamic Laboratory in BarcelonaTech University. Water and solid discharge distributions, as well as bed and water surface levels are measured along the model, during tests with different total water discharges. Results confirm the sediment distributions reported in the literature but also highlight the influence of bed bathymetry evolution and three-dimensional flow patterns in the local sediment transport of the diversion area. A threshold value is found for the momentum flux ratio between the lateral branch flow and the main channel flow, above which a vortex is formed in front of the diversion entrance and a scour hole is formed in the first stretch of the main channel downstream of the diversion.

An energy balance equation is proposed between upstream and downstream of the diversion taking into account the energy losses associated with the vortex, and a good comparison is found when tested against the experimental results. A nodal equation that relates water discharge to sediment discharge distribution is developed considering separately bed load and suspended sediment transport. Calculated values of sediment discharge ratio compare reasonably well with experimental values. Joining these equations, uniform flow, transport capacity and mass continuity equations for water and sediment, a theoretical model is proposed to evaluate the equilibrium situation of a fluvial diversion in terms of water discharge, sediment discharge, water depth and bed slope in both downstream branches.

Preface

The research reported in this document was carried out in the Sediment Transport Research Group (GITS) of the Department of Hydraulic, Marine and Environmental Engineering in BarcelonaTech University, between September 2008 and February 2013. The dissertation is the result of my own work and the scientific discussions held with my tutor Dr. Allen Bateman and Dr. Vicente Medina, who are both members of the GITS research group. Chapters 3, 4 and 5 correspond to adapted versions of articles that are planned to be submitted to the Journal of Hydraulic Engineering. The authors of the articles are Albert Herrero, Allen Bateman and Vicente Medina.

The experimental work was carried out by myself with the help of Pr. Allen Bateman and Vicente Medina, as well as Pablo Bejarano and Guillaume Houot, two master thesis students whose works were related to the studies presented herein.

The development of the conceptual model presented in chapters 4 and 5 was performed by myself, with the assessment and help of Pr. Allen Bateman and Vicente Medina.

Table of Contents

List of Tables

List of Figures

List of Symbols

The following symbols refer to the studies developed in the frame of this thesis work and appear in chapters 3, 4 and 5. Symbols appearing in chapter 2 have been maintained as they appear in the original works that are referred there and are appropriately described along the text.

Symbol

A	Vortex energy loss coefficient
a_l	Lateral acceleration of the suspended sediment in the diversion area ($m \cdot s^{-2}$)
B_l	Lateral branch width (m)
B_m	Main channel width (m)
C	Sediment concentration (sediment volume/water volume)
C_b	Near-bed sediment concentration used in the Rouse profile
C_l	Sediment concentration in the lateral branch
C_m	Sediment concentration in the main channel
D	Sediment diameter (m)
g	gravity acceleration ($m \cdot s^{-2}$)
H	Energy height at the corresponding section (m)
I_1	Integral resulting from the nodal equation development
I_2	Integral resulting from the nodal equation development
k_s	Effective roughness length (m)
L_i	Length of the axis in vortex *i* (cylinder height) used in the energy balance (m)
l_i	Characteristic length of the vortex *i* used in the energy balance (m)
L_l	Length of the lateral branch (m)
L_m	Length of the main channel (m)
m_i	Mass involved in vortex *i* used in the energy balance (kg)
M_r	Flow momentum ratio between the lateral branch and the main channel
P	Power associated with the flow at the corresponding section ($kg \cdot m^2 \cdot s^{-3}$)

Q_l	Water discharge in the lateral branch ($m^3 \cdot s^{-1}$)
Q_m	Water discharge in the main channel ($m^3 \cdot s^{-1}$)
Q_{sbl}	Bed load discharge in the lateral branch ($m^3 \cdot s^{-1}$)
Q_{sbm}	Bed load discharge in the main channel ($m^3 \cdot s^{-1}$)
Q_{sbt}	Bed load discharge in the upstream channel ($m^3 \cdot s^{-1}$)
Q_{sl}	Solid discharge in the lateral branch ($m^3 \cdot s^{-1}$)
Q_{sm}	Solid discharge in the main channel ($m^3 \cdot s^{-1}$)
Q_{ssl}	Suspended sediment discharge in the lateral branch ($m^3 \cdot s^{-1}$)
Q_{ssm}	Suspended sediment discharge in the main channel ($m^3 \cdot s^{-1}$)
Q_{sst}	Suspended sediment discharge in the upstream channel ($m^3 \cdot s^{-1}$)
q_s	Solid discharge per unit width ($m^2 \cdot s^{-1}$)
q^*	Dimensionless solid discharge
R	Sediment density relative to water
r_Q	Water discharge ratio (Q_m/Q_l)
r_S	Sediment discharge ratio (Q_{sm}/Q_{sl})
r_{sb}	Bed load sediment discharge ratio (Q_{sbm}/Q_{sbl})
r_{ss}	Suspended sediment discharge ratio (Q_{ssm}/Q_{ssl})
S	Channel bed slope
u	Longitudinal flow velocity ($m \cdot s^{-1}$)
u_i	Characteristic velocity of the vortex i used in the energy balance ($m \cdot s^{-1}$)
u_*	Shear velocity associated with the longitudinal velocity profile ($m \cdot s^{-1}$)
v	Water flow velocity ($m \cdot s^{-1}$)
v_*	Transversal shear velocity associated with the lateral branch flow ($m \cdot s^{-1}$)
v_l	Water flow velocity in the lateral branch ($m \cdot s^{-1}$)
v_m	Water flow velocity in the main channel ($m \cdot s^{-1}$)
v_s	Sediment fall velocity ($m \cdot s^{-1}$)
w	Depth dependent width of the flow captured by the lateral branch (m)
y	Water depth at the corresponding section (m)

z_b	Bed level (m)
Z_R	Exponent introduced in the Rouse profile
z_0	Bed roughness length (m)
z_{0l}	Bed level at the downstream end of the lateral branch (m)
z_{0m}	Bed level at the downstream end of the main channel (m)
Δp	Transversal pressure difference in the diversion entrance ($kg \cdot m^{-1} \cdot s^{-2}$)
δ	Close-to-bed height introduced in the Rouse concentration profile (m)
κ	Von Karman constant
ρ_s	Bed sediment density ($kg \cdot m^{-3}$)
ρ_w	Water density ($kg \cdot m^{-3}$)
τ^*	Dimensionless shear stress
τ_c^*	Critical dimensionless shear stress
τ_s^*	Dimensionless skin shear stress

Acknowledgements

Many people have influenced on me and my work during my PhD studies, each in their own special way. I would like to express my most sincere gratitude to all of them.

First of all, I would like to express my gratitude to my supervisor, Professor Allen Bateman, for trusting me and giving me the opportunity to carry out my research work, providing a great amount of useful ideas for the development of the thesis and participating in the experimental work with enthusiasm, no matter the narrowness or unconfortability of the situation. Thanks also for inviting me to participate in numerous congresses and conferences. It has been a pleasure to learn from him.

I greatly appreciate Vicente Medina for all the help he has given me in the most diverse aspects, from rescuing me from my typical informatics problems to providing useful ideas to improve the conceptual models or solving practical problems in the laboratory. But I would really like to thank him for the altruism he has shown with me since the first day I arrived to work in GITS research group during my master thesis.

I would like to thank both, Allen and Vicente, for their help and coauthorship of the different publications that are product of the research work exposed in this thesis, as well as the publication related to the master thesis on sediment resuspension by density currents.

I would also like to express my thanks to Pablo Bejarano and Guillaume Houot, for their invaluable help with the experimental model construction and the performance of the laboratory measurements, many times in hard and cold conditions. Without their cooperation, the work of this thesis would have hardly been possible.

I am also grateful to all my fellows in the Hydraulics Section in Civil Engineering School in Barcelona, with whom I have shared a longer or shorter part of my PhD studies. Our friendship has taken us to celebrate uncountable “asados”, long and surrealistic nights in places from Barcelona to Cartagena de Indias and even some storm-threatening excursion in the Catalan Pyrenees. Francesco, Andrés, Anaïs, Sergi, Anna, Francisco, Guillaume, Gonzalo, Ana María, Cristina, Khaled with, again, Allen and Vicente, have shared all these wonderful moments that surely have contributed to provide excitement and positive energy to my research activities.

I would like to extend my special thanks to the friends I made at the Civil Engineering School of Barcelona: Carles, Guindu, Roberto, Lluis, Roma, Víctor, Ignasi, with whom I have shared uncountable laughs, football discussions, orienteering races and mountain “sometimes-long” trips, and specially to Javi with whom the discussions were not only about football but some stranger and

surrealistic topics, with whom I shared a wonderful experience that helped me to undertake my PhD studies with energy and optimism and who has advised me at different moments of my thesis from a mixed scientific, linguistic and friendly point of view.

I would like to express my special thanks to my brother and my parents, who have always given me support and whose knowledge of the scientific world, even if in a different area, has smoothed the way in many situations.

Last but not least, my dearest thanks to Gail for the good moments we have lived and for the support and understanding of the day-to-day problems and worries. Thanks also for the accuracy when revising my surely-improvable English, for being patient with my recurrent mistakes and make it possible to guaranty a good quality in the text of this document and the publications related to it.

Chapter 1: Introduction

Fluvial bifurcations are the points where a river divides into two different channels that carry part of the flow and sediment further in the downstream direction. Both downstream channels can join again at a confluence or flow separately to their mouths at the sea.

Bifurcations in rivers can occur naturally or be built artificially. The low course of the Rhin River presents several examples of both, as the Pannerdense Kop, at the border between Germany and the Netherlands, the branches of which are connected further downstream by artificial channels that join them to improve the connectivity and transportation of the area. Deltaic zones represent another example of how the evolutionary processes of consecutive bifurcations, most of which originate naturally, influence the terrain's morphology feeding sediment to different zones of the coast. Deltas in large rivers such as the Lena (Russia) or the Orinoco (Venezuela) present a complex ramified structure with many interconnected channels (Figure 1.1 and Figure 1.2). Lastly, braided rivers constitute another case in which bifurcations and confluences, usually at a spatial scale smaller than in the previous examples, interact in a determinant manner for further evolution of the river course.

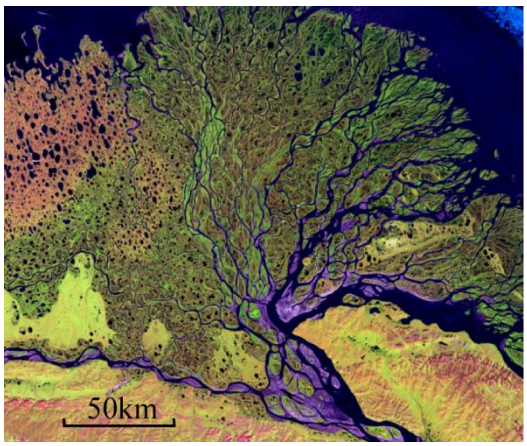

Figure 1.1. Aerial view of the delta of Lena River (Russia)

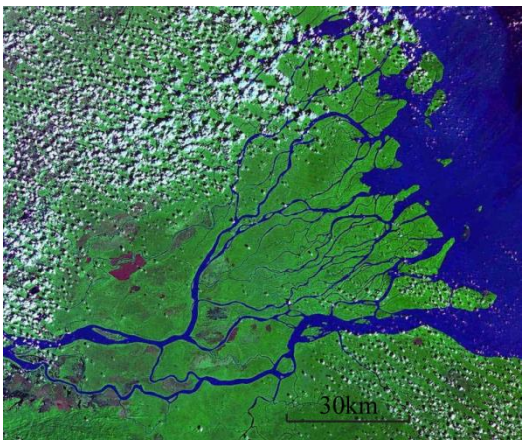

Figure 1.2. Aerial view of the delta of Orinoco River (Venezuela)

Water and sediment distribution at the bifurcation condition the evolution of both branches in terms of slope and planimetric geometry. This is a concern for society in those areas where the river plays a role in human activities. For instance, water discharge evolution can affect the navigability of a certain reach and the increase of discharge in one of the branches can inundate crops or trigger floods in urban areas. On the other hand, the eroding processes related to the flow can destroy human infrastructures such as roads or the centers of population. Solid discharge distribution can also have problematic consequences, such as sediment deposition when the feeding material exceeds the transport capacity associated with the flow. This can

affect navigability at the entrance of the corresponding branch. In other cases, an excess of sediment can damage turbines or other devices that may be placed in the river for different purposes.

From an environmental point of view, a modification of the water and sediment discharge can dramatically alter the habitat of plants and animals in the area, as many of these species require specific conditions concerning water content in their environment. On the other hand, an excess of sediment can affect the ecosystem where fluvial fish lay their eggs or where river plants grow. An example of this kind of problem can be found in the Magdalena River (Colombia), where a side channel was constructed in the 17th century in order to improve the communication between Cartagena de Indias and the inner part of the country. Some modifications performed during the last decades in the planimetry of the channel, have caused an excess of sediment transported by the branch and the generation of deposition fans inside the Cartagena Bay, affecting the choral ecosystems in the nearby Islas del Rosario (Figure 1.3).

Figure 1.3. Aerial view of the Canal del Dique from Magdalena River to Cartagena Bay

1.1 Motivation

The motivation behind the research on fluvial bifurcations in the Sediment Transport Research Group, arose from the group's participation in a project for the restoration of a bifurcation in the Patía River delta, in Colombia. The Patía River is one of the most important rivers in Colombia and the second largest flowing into the Pacific Ocean along the Colombian coast. The mean discharge is around 1500m^3/s, its length is around 400km and the watershed area is 26000km^2. The discharge variability is relatively low, being around 6700m^3/s and the discharge corresponding to a peak event with 500 years of return period. The source of the Patía River is in the south Colombian Andes range, at a height of 4500m in the Cauca province, and flows south towards the border with Ecuador and turns west descending towards de Pacific coast. At this point, the river has created a large delta covering an area of around 5000km^2 that constitutes a semi-circular peninsula, significantly noticeable in the shape of the Pacific coast in south Colombia (Figure 1.4).

The Patía River watershed can be divided into two parts concerned with climatic characteristics. The first part of its course goes along the Andes range, where there is a humid climate with two

seasons (spring and autumn) of higher rainfall. The last stretch traverses the delta plain, where very high and relatively uniform rainfall is found year round. This difference can be observed between the mean annual rainfall of Pasto, around 600mm, which is located at a height of 2500m in the first part of the river, and the corresponding data of Barbacoas, approximately 60km upstream from the river mouth, that rises to an extremely high value of 6500mm. These climatic patterns give way to a very densely vegetated area in the delta plain of the Patía River, the mangrove being the most typical specie along the river course.

Focusing on a social point of view, most of the people living in the delta of the Patía River are afro-Colombians, that is, come from the slave groups that were introduced to the American continent by the Spanish settlers during the late 16th century. The provinces in the Colombian Pacific coast (Nariño, Cauca, Valle del Cauca and Chocó), together with some areas in the Amazon basin, are the most disadvantaged regions in Colombia from an economic point of view. There is a very significant lack of infrastructures and road links are almost non-existent. Specifically in the area of the delta of the Patía River, the only existing road is one going from Pasto, the department capital, to Tumaco, which is located in the southern part of the delta and near the border with Ecuador. Three small runways in the principal inhabited nuclei of the delta offer flights in light aircrafts to Cali, the third largest city in Colombia. Therefore, as the only means of communication, fluvial transport has a determinant importance for the people living in the area.

The main economic activities are fishing, wood exploitation and fruit cultivation of mainly bananas and coconuts. However, the existence of clandestine but numerous coca fields cannot be ignored, as they represent an important source of income of a significant and not easily determined amount of people. Parallel to this, coca traffic is often the onset of an armed conflict between the national army, the FARC guerrillas and paramilitary groups that has affected Colombia for the last 60 years with dramatic consequences. The inaccessibility of areas like the Patía River offers an appropriate shelter for these

Figure 1.4. Location of the delta of the Patía River in Colombia

groups, which in turn spread coaction and fear over the population of the region, conditioning their life and activities.

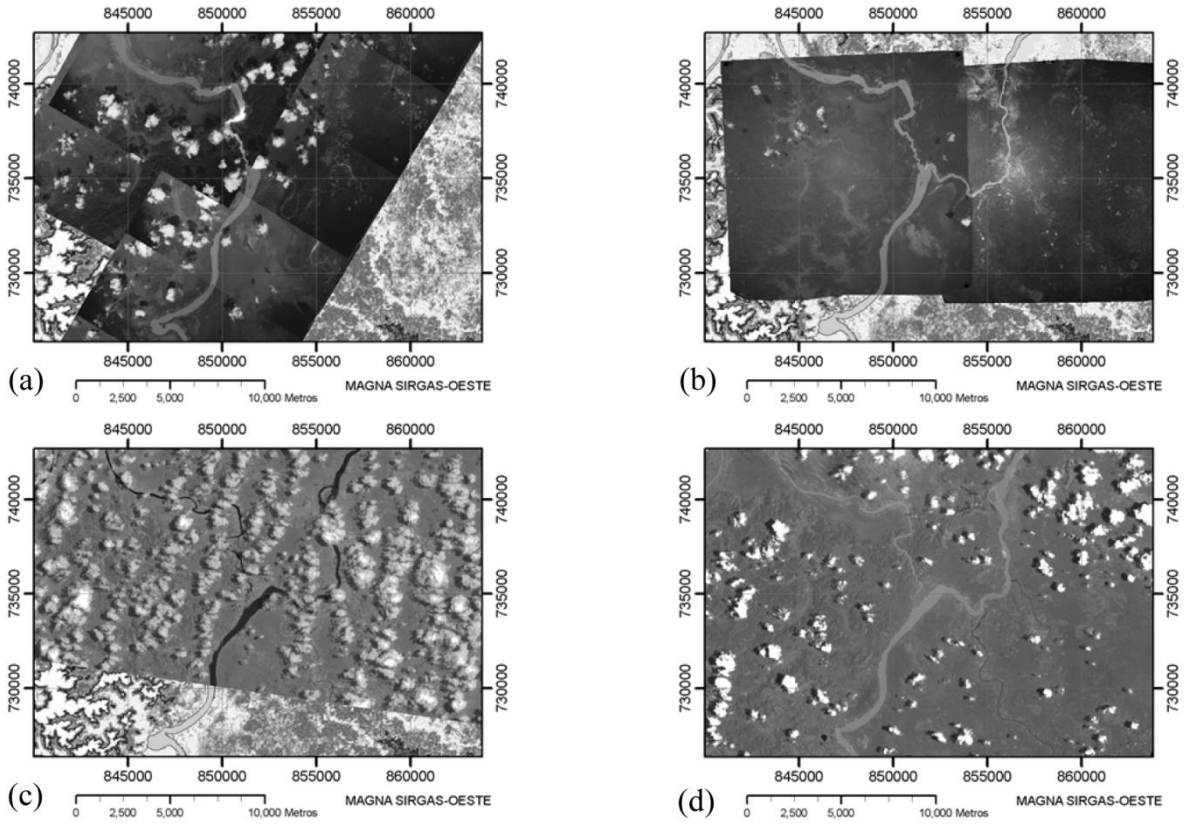

Figure 1.5. Aerial views of the Patía River before the formation of the bifurcation in 1962 (a) and after it, in 1986 (b), 2001 (c) and 2008 (d). It is clearly seen how the old branch is progressively abandoned whereas the new one currently captures nearly all the discharge (Bateman, 2009).

In this frame, in 1970 the proprietor of a wood sawmill constructed a small channel connecting what was then the main course of the Patía River with another secondary river that flowed towards his sawmill. In this way, he was able to transport wood from upstream to his factory, reducing the travel distance and avoiding the sea traverse, which was both more dangerous and more costly in terms of fuel. At the beginning, the small channel was separated from the Patía River and a wincher was used to lift the trunks from the river and place them into the channel. From there, another boat carried them to their final destination. However, during the first flood event after its construction, the flow overtopped the banks and entered the channel, increasing its depth and width. A sluicegate was built to maintain the separation between the river and the channel but some days later it was destroyed by some local people who thought that the new situation was positive for them. Indeed, the presence of this new bifurcation represented a benefit for many people in the area, as it implied an improvement in the communication links of the region, and they pressed against the restoration of the previous situation. Therefore due to the construction of the channel, a bifurcation was created in the Patía River.

The bifurcation evolved in such a way that the new branch widened and the bed level descended, with the subsequent rise of the discharge flowing through it. During a certain period of time, the consequent communication improvement was beneficial to the inhabitants of the area, but over the years, the system evolved into a configuration in which the new branch became predominant and the discharge in the old branch descended progressively (Figure 1.5). This fact was a problem for the people living along the old branch course because it implied navigability problems during low flow conditions. Figure 1.6 shows a close aerial view of the present situation of the Patía River bifurcation. The sedimentation area between the branches has caused a decrease in the diversion angle throughout the years and driftwood retention contributes to the old branch blockage.

Figure 1.6. Close aerial view of the present situation of the Patia River bifurcation.

On the other hand, the increase of the discharge in the new branch impelled changes in the planimetric geometry of the downstream reach, with consequential erosion problems. One example of this is found in the town of Bocas de Satinga, the largest nucleus of the lower delta. During the last 20 years, the river has been meandering through the town which is on the outer shore. Therefore, bank erosion has directly affected some neighborhoods and their inhabitants have been obliged to move to the inner part of the town (Figure 1.7). This area was formerly occupied by a waste dump, so a layer of land and sawdust was displayed in order to separate residuals from the new houses. However, the heavy rains make this separation difficult and there is a lack of basic services in this part of the town. Moreover, the river erosion also affected the water supply treatment plant, destroying it between 2008 and 2009. Another problem, originated by the increase of discharge in the new branch of the Patía River, consists of the increase of sediment deposited at the mouth of the river. Gorgona Island is located 30km north of the new Patía River mouth and is considered a UNESCO World Heritage site. The increase of sediment deposited in the area is affecting the choral ecosystems and their biodiversity.

Figure 1.7. Erosion problems in the town of Bocas de Satinga, located on the external bank of a forming meander of Patía River

Therefore, different aspects of diverse origins make the new bifurcation a problem for both the society and the natural environment of the Patía River delta and a solution to these inconveniences was demanded. However, it should be noted that avulsion and shifting processes of rivers in deltas occur naturally, and this or another change could have happened in the future.

1.2 Establishment of the objectives

From a geometrical point of view, those bifurcations in which one of the downstream branches exits laterally while the other follows the same direction as the incoming channel, are known as diversions or lateral intakes. In this regard, the geometry of the new bifurcation at the Patía River fits well into this group. The old branch direction has evolved from a nearly perpendicular configuration to the present angle of 35º with the common direction of the incoming channel and the new branch.

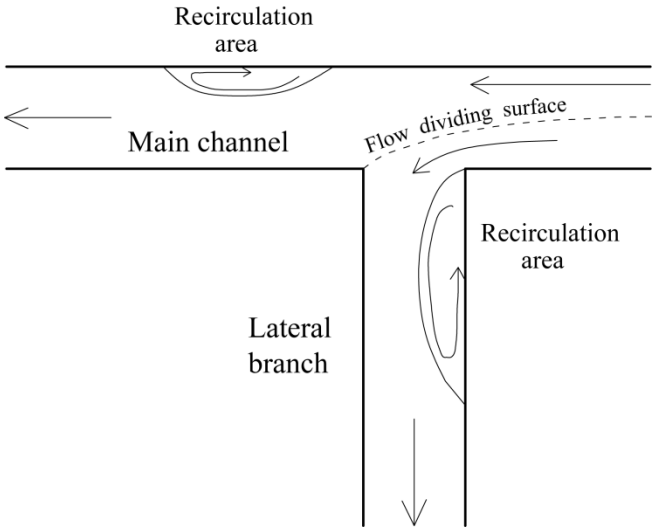

Figure 1.8. Scheme of the main flow patterns in a 90-degree diversion

Inspired by the Patía River case, we decided to focus the analysis on fluvial diversions. However, the objective of this thesis is not to reproduce the Patía River case but to analyze the different general patterns that govern the flow and sediment transport in 90-degree diversions.

Apart from natural examples like the one exposed above, this geometry is also found in artificial lateral intakes built for communication, irrigation or energy production. A complete state-of-the-art compilation is provided in chapter 2, mainly regarding 90-degree diversions in which the lateral branch is perpendicular to the main channel. The flow patterns in these systems have been observed to be highly tridimensional and turbulent, but some general characteristics are identified (Figure 1.8). Flow dividing surface separates the discharge following the main channel from that which deviates toward the lateral branch. This surface extends further into the main channel next to the bed, where velocities are low and flow is captured more easily by the lateral branch. Flow separation occurs in the upstream corner of the diversion and a recirculation area is observed next to the adjacent wall. This implies a flow contraction in the opposite wall that generates relatively high velocities. When the discharge through the lateral branch is sufficiently high in relation to the discharge following the main channel, a second recirculation area is observed to form in the first stretch of the main channel and next to the wall opposite the diversion.

With regard to sediment transport the repercussions are less clear, as most analyses in this area have been performed without considering the presence of sediment and only indirect conclusions can be drawn about sediment movement. However, a remarkable trend of sediment to deviate towards the lateral branch has been observed in experimental and field studies and is commonly known as the Bulle effect in honor of Henri Bulle, who first studied experimentally and described this pattern in 1926.

However, the connection between flow patterns and sediment transport, and the causes of the sediment deviation are not well understood. Given this background, we opted for an experimental approach in order to avoid the uncertainty of sediment transport calculations using numerical models in such complex flow conditions. The experiments were conducted under mobile bed conditions so that the bathymetry evolution in the diversion area could be analyzed, together with its influence in flow and sediment transport patterns. Moreover, the tests were maintained until the system reached equilibrium, in order to study the evolution from a horizontal bed initial condition and to identify the system trends in different flow conditions. Initially, the variables studied were the total water discharge, the diversion angle and the bed discordance, defined as the bed level difference between the lateral branch and the main channel. However, due to the obtained results and a time constriction, only the influence of total discharge was studied, leaving the other variables as the aim of future studies.

In view of the present state of knowledge and considering the previous comments, the objectives of this thesis could be summarized as follows:

- Performance of a set of experiments in a 90-degree diversion laboratory model, in mobile-bed conditions and registering the system evolution to the state of equilibrium.
- Provide experimental data for validation of future numerical and theoretical models
- Characterization of the flow and sediment transport patterns that take place in the diversion area
- Development of a conceptual model to describe water discharge and sediment discharge distribution in a 90-degree diversion

1.3 Experimental setup

The experimental model was constructed at the Fluvial Morphodynamic Laboratory of the Hydraulics, Coastal and Environmental Engineering Department at BarcelonaTech University. It consisted of a 9m long and 20cm wide flume with a 2.5m long and 20cm wide lateral branch located 6m downstream from the inlet of the main channel (Figure 1.9). Lateral walls along the whole model were 35cm high. The flume was made of methacrylate and it was elevated to a height of 1.6m by means of steel supports in order to facilitate observations. The choice of these dimensions was conditioned by the space available in the laboratory and taking into account the coexistence of this model with other previous facilities. A new pipe was installed to supply the model with water from a previously available reservoir with a volume of 8 cubic meters and an Arquimedes screw hopper was installed at the inlet of the model in order to provide sediment feeding to the facility. Figure 1.10 shows two images of the experimental model downstream of the diversion.

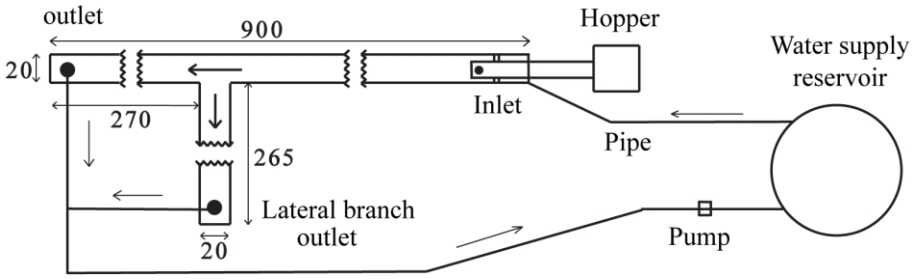

Figure 1.9. Schematic plant view of the experimental model used in this analysis

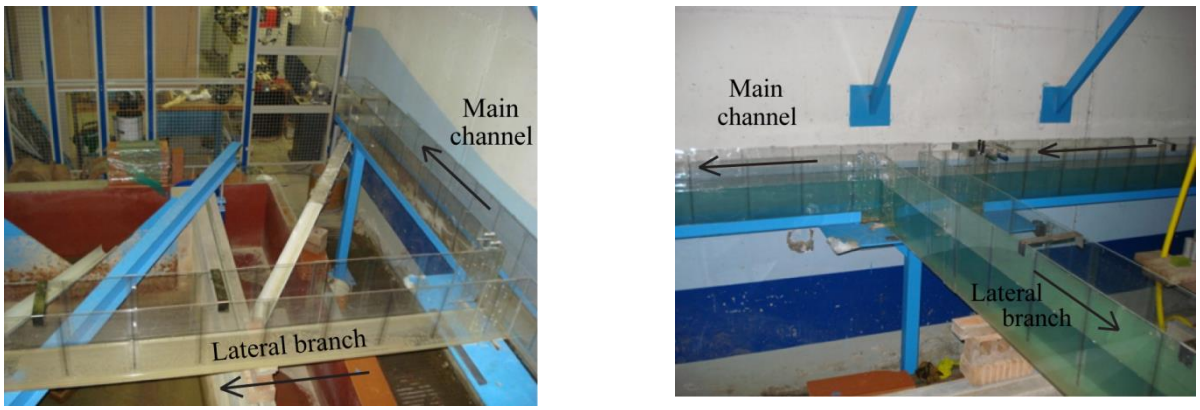

Figure 1.10. Preliminary view of the downstream part of the experimental model before the introduction of sediment.

In order to study the influence of the diversion angle and the bed discordance between the lateral branch and the main channel, a special piece was used to connect both parts of the model. The scheme of the piece is shown in Figure 1.11. It consists of a rectangle 70cm wide and 55cm high with a rectangular hole 20cm wide and 35cm high that corresponds to the entrance of the lateral branch. A fixed stretch of the lateral branch is glued to this space forming a certain angle with the rectangular sheet. There is a specific bifurcation piece for each of the angles to be studied, which in our case were planned as 30º, 60º and 90º. A 70cm-long piece of the lateral wall of the main channel was removed and the bifurcation piece was fitted into the remaining space. The lateral branch was then connected to the bifurcation piece, therefore forming the desired angle with the main channel. On the other hand, two grooves were performed on the rectangular sheet and parallel to the vertical sides of the entrance of the lateral branch, in order to be able to displace the lateral branch vertically and fix it at different heights. Thus, a certain bed discordance can be established between the lateral branch and the main channel.

Figure 1.11. Scheme and photograph of the bifurcation piece. The piece extends deeper than the main channel to allow its raising to establish a bed discordance between both branches.

The range of discharges applied during the tests ran from 3.5l/s to 6l/s and was partly chosen based on the model dimensions. Before introducing sediment, some calibration tests were performed in order to obtain water discharge ratios in fixed bed conditions and to test the volumetric measurement method of the water discharge at the end of each branch. However, no further analysis was carried out in relation to these results and attention was mainly paid to the tests with the mobile bed.

The sediment used during all the test sets consisted of fine-medium sand with a mean diameter of 0.25mm. This kind of sediment was chosen due to its high availability in the laboratory and its relatively high mobility, which facilitated the observation of the bathymetry patterns and allowed for a relatively low time of evolution until equilibrium could be reached.

Each experiment began from a horizontal bed condition and constant water and solid discharges were introduced into the model inlet. The experiment was maintained until equilibrium occurred, which is identified when water and solid discharges at the outlet of both branches, as well as the main bathymetry patterns in the diversion area, are approximately constant. A complete set of measurements is carried out every 60 minutes, which include water and sediment discharges at the outlet of each branch and bed and water surface levels along the entire model and every 25cm. Additionally, water and sediment discharges introduced into the model are measured in order to check that they correspond to the predetermined values.

In chapter 3, further details on the experimental setup and procedure are given.

1.4 Document structure

The content of chapters 3, 4 and 5 of this thesis correspond to two articles written about the research on flow and sediment transport in 90-degree diversions. These articles are planned to be submitted to the Journal of Hydraulic Engineering of the American Society of Civil Engineers (ASCE). Each chapter includes its own introduction, as well as the final conclusions drawn from its analysis.

Chapter 2 consists of an extensive review of the existent bibliography on fluvial bifurcations. In the first part of the chapter, general characteristics of fluvial bifurcation behavior are explained, concerning to the formation process, the evolution and the equilibrium states. Moreover, the influence of factors as migrating bars, bank erodibility, discharge variability and the bifurcation angle are discussed, as well as the behavior of fluvial bifurcations as part of a larger braided network. On the other hand, the second part

of the chapter is referred to those bifurcations which are geometrically classified as diversions. The Bulle effect is first explained in the context of the experimental work of Henri Bulle (1926) and general flow characteristics typical from this kind of bifurcations are commented based on the literature. Particular aspects of conceptual models, numerical methods and experimental studies when applied to the analysis of lateral intakes are commented next and a specific subsection is destined to movable-bed experimental studies. Lastly, several measures related with sediment control at lateral intakes are commented, together with some results of their application in the field.

Chapter 3 consists of the article "Experimental analysis of sediment transport in a 90-degree diversion". This paper presents the approach and main results of the experimental study carried out in the Fluvial Morphodynamics Laboratory. Previous analyses on flow and sediment transport are summarized in the introduction, with an explanation of the main characteristics observed and a special emphasis on the idea of the Bulle effect. A detailed explanation of the experimental setup, measured variables and measurement methods is provided. Then, a qualitative description of the observed behavior is presented, followed by the main quantitative results in terms of water discharge distribution, solid discharge distribution and bed bathymetry evolution in the area of the diversion. A linkage between all these characteristics is observed and further discussed, focusing on the formation of an eroded area and an associated vortex in the main channel and downstream from the diversion for certain total discharge conditions and its consequences over sediment and flow distribution. Finally, the main conclusions of this analysis are summed up.

Chapter 4 consists of the article "Flow energy balance in a 90-degree diversion". In order to develop a theoretical model that describes the behavior of lateral intakes, an equation that quantifies and relates the energy losses along both branches is needed. In previous models of fluvial bifurcations, this equation was substituted by the compatibility of water surface heights. The vortex associated with the erosion area in the main channel generates energy losses that should be taken into account when setting out the energy balance equation of the system. In this paper, after a summary of the experimental analysis results in which the performed balance is framed, a theoretical approach is carried out to quantify the vortex associated energy losses based on Batchelor (1953). The resulting equation is then tested against the experimental results and a discussion about this contrast is provided. Final conclusions are drawn in the last chapter of the article.

Chapter 5 is constituted by the article "Theoretical model for flow and sediment transport in fluvial diversions". The main objective of this paper is to develop a nodal equation to

describe solid discharge distribution between both branches as a function of water discharge distribution, which together with the energy balance equation on which chapter 3 is focused, constitutes an essential tool for describing fluvial diversions behavior. A summary of the background on previous nodal equations is presented, based on two examples developed for Y-shaped bifurcations, in which flow patterns are significantly different. Then, a recapitulation on the experimental analysis is carried out, developing a proposal about the conditions that give rise to the erosion area in the main channel and the associated vortex, which have a determinant effect on sediment movement in the diversion area. Afterwards, an equation that relates the solid discharge distribution to water discharge distribution is developed based on the logarithmic velocity profile and dealing separately with bed load and suspended sediment. Then the proposed equation is tested against the experimental results and the virtues and limitations of the model are discussed. Finally, the nodal equation is joined with the energy balance equation presented in chapter 3, uniform flow and sediment transport equation for both branches, establishing a system of equations that may be used to solve the different variables that intervene in the diversion evolution, that is, water and solid discharge, water depth and slope in both the lateral branch and the main channel.

Lastly, chapter 6 summarizes the most important conclusions drawn from the experimental and conceptual analysis developed throughout the thesis.

Chapter 2: Previous studies

According to the diverse applications and influence that fluvial bifurcations have on different aspects of human society, their dynamics has been studied since early stages of fluvial engineering. Some of the areas of application have already been mentioned in the introduction chapter and refer to transport and communication (Bateman et al. 2009, Ordóñez, 1972), agriculture crops (Ryad, 1961) or power energy plants (Odgaard, 2009). The symbols that appear throughout this chapter are the ones adopted by the authors in their original works and are described conveniently where they are used. Therefore, they do not correspond to the notation that appears in the list of symbols, which refers only to the work developed in the frame of this thesis and is shown in chapters 3, 4 and 5.

2.1 General behavior of fluvial bifurcations

2.1.1 Formation of a bifurcation

Different aspects influence in the process of formation of a bifurcation. Bertoldi and Tubino (2005) performed a laboratory analysis in which they studied the evolution of an unconstrained channel until the onset of a bifurcation in different conditions of discharge and slope for uniform and non-uniform sediment. From an initial straight channel, migrating alternate bars were formed and a slight meandering pattern developed, resulting from the interaction between altimetric and planimetric interaction. The Shields parameter and the channel geometry determine the migrating velocity of the bars and the possibility, for the slower ones, to establish a static pattern of successive bumps and bars typical from meandering channels. In these cases the bifurcation occurs through the mechanism of chute cutoff. On the other hand, in those conditions where bars migrate faster bifurcation occurs due to the different mobility of two single bars, which may lead a bar front to merge into a scour hole left by the preceding bar. The Shields parameter determines the shift between both behaviors, which can be explained in terms of linear stability analysis of free bars (Colombini et al. 1987, Seminara and Tubino, 1989). In a common natural situation, the previous evolution becomes more complicated due to the interaction between bifurcation and confluence processes that usually take place in a braided river network (Ashmore, 1991).

Federici and Paola (2003) classify the bifurcation formation processes in five types. Central bar deposition is the process whereby an elongated, more or less symmetric,

medial bar without avalanche face develops in the middle of a channel, separating the two resulting branches. Transverse bar conversion is observed when flow expands out of a pool because at these sites of flow convergence appreciable scour occurs, generating enough sediment for substantial downstream deposition where the flow subsequently diverges. The chute cutoff mechanism consists of a headward incision by flow taking a shortcut across an alternate or point bar. The multiple-bar dissection process occurs in multiple-bar braiding, in which local decline of competence in a flow expansion or over a bar top initiates dissection of the submerged bars. Finally, avulsion consists of the overtopping of part of the stream over a channel bank, resulting typically from bank erosion or from a rise in the local water level due to local deposition or increasing discharge.

2.1.2 Evolution and equilibrium states of a bifurcation

The problem of the evolution of a general bifurcation is approached theoretically by Wang et al. (1995). They consider a river with given water and solid discharges that bifurcates in two branches of a certain geometry that flow into the same lake or sea, and use a one-dimensional model to study the conditions in which the system tends to an equilibrium with both branches open and those in which one of the branches tends to close. The equilibrium situation is described through the imposition of uniform flow and sediment transport equal to the capacity in both branches. Moreover, mass continuity is applied to water and sediment in the bifurcation to relate water and solid discharges in the branches to the known incoming values from the channel upstream and a geometrical relation is introduced to consider the equality of height difference along both branches. The eighth equation that allows solving the problem unknowns (for each branch: water depth, slope, water discharge and sediment discharge) is a nodal equation that relates solid discharge distribution to water discharge distribution and other variables of the problem. The equation proposed by Wang et al. is:

$$\frac{Q_{s1}}{Q_{s2}} = \left(\frac{Q_1}{Q_2}\right)^k \left(\frac{B_1}{B_2}\right)^{1-k} \tag{2.1}$$

Where Q_{sj}, Q_j and B_j are respectively the solid discharge, water discharge and channel width in each branch (j =1,2), and k is an certain exponent. The meaning of this equation is to relate the specific solid discharge (discharge per unit width) to the specific water discharge through a potential relation, in which the exponent k determines which of the branches is favored in terms of sediment transport and how much an increment of water discharge ratio represents over sediment discharge ratio. However, this equation deals with

the difficulties of simplifying a process that is three-dimensional to a formulation that uses one-dimensional variables. Other aspects as bifurcation angle, roundness of its end, transversal slope, etc. and the flow patterns induced by them, have to be represented by a single parameter that is exponent *k*. Wang et al. themselves carried out a least squares fitting of equation (2.1) with both field and scaled-model data from Pannerdense bifurcation in river Rhine, finding significantly different values for *k*. In our opinion, the ignorance of the relation between this parameter and the different aspects that describe the three-dimensionality of the bifurcation limits so far the utility of this model.

Islam et al. (2006) performed an experimental study in order to test equation (2.1) for different values of the nose angle (defined as the angle between the tip of the nose and the symmetrical line of the bifurcation) and the upstream discharge. Regression analyses were carried out to fit the data to the proposed potential law and parameter *k* was found to have a higher dependence on the nose angle.

On the other hand, Wang et al (1995) used their model to describe the temporal evolution of the bifurcation and performed a mathematical stability analysis to determine the dependence of this evolution on the problem parameters. They found that the final state of the bifurcation depends on the values of *k* and *n*, being *n* the exponent of the power-law which they use for calculating sediment transport in the branches. In this way, when $k > n/3$ the system would evolve to an equilibrium situation in which both branches remain open, whereas in those situations in which $k < n/3$ one of the downstream channels would silt up. The interpretation of this result is that in the first case, an increment (increase or decrease) of the water depth in a certain branch implies a more important increment in the amount of sediment that feeds that branch than in its transport capacity. Therefore, if we consider an initial situation in which branch 1 is fed in excess, the subsequent decrease in its water depth implies a relatively high decrease in the sediment feeding amount and a relatively low decrease in sediment transport capacity, in such a way that both quantities tend to converge. The opposite evolution occurs in the other branch and the system attains an equilibrium situation with both branches open. On the other hand, for $k < n/3$, the branch that starts silting suffers a relatively high decrease in its sediment transport capacity and although the sediment feeding decreases too, the branch tends to close. However, the fact that this stability condition depends on an exponent *k* that is not well determined and a parameter *n* that depends on the sediment transport formula chosen, makes it of less practical use.

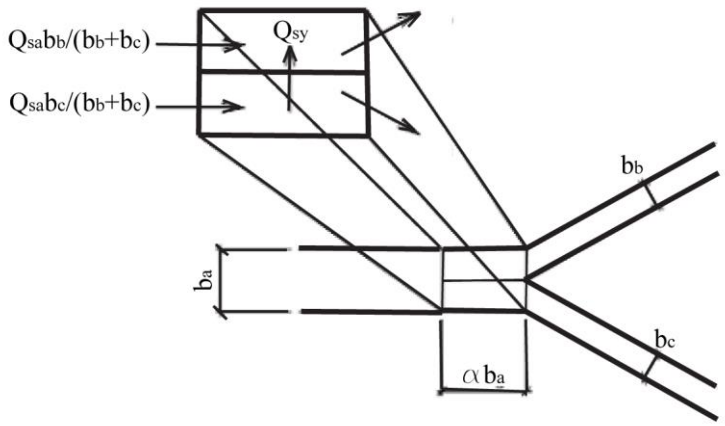

Figure 2.1. Scheme of the quasi-2D model developed by Bolla Pittaluga et al. (2003)

An alternative theoretical approach was carried out by Bolla Pittaluga et al. (2003), who developed a quasi-2D model to represent the flow and sediment processes that take place in the bifurcation (Figure 2.1). This contribution is very important and has been used as a basis for posterior analyses. They consider the last part of the upstream channel as divided into two cells of a certain length characterized by a parameter α, that is related to the distance for which the effects of the bifurcation on the bed bathymetry were no longer visible, and was determined experimentally. Similar to Wang et al., uniform flow and sediment transport capacity equations are applied in the downstream branches, and a common water surface level is imposed at the bifurcation. Moreover, mass continuity equation is applied for water and sediment in each cell, thus substituting the nodal equation of Wang et al. The sediment mass continuity equation involves transversal sediment exchange between both cells, which is determined following Ikeda et al. (1981) as a function of depth-averaged flow direction and transversal bed slope.

$$q_y = q_x \left[V\left(U^2 + V^2\right)^{-1/2} - \frac{r}{\sqrt{\theta}} \frac{\partial \eta}{\partial y} \right] \tag{2.2}$$

Where x and y are respectively the longitudinal and transversal directions, U and V the x and y depth-averaged velocity components, θ is Shields parameter and η is the bed level height. In this model the upstream channel, as well as the downstream branches, were considered to have a fixed width. Kleinhans et al. (2008) developed a modification of the previous equation in order to take into account the effect of spiral flow associated with a bend located upstream from the bifurcation, based on the direction of the bed shear stress vector including the mentioned effect (Struiksma et al. 1985).

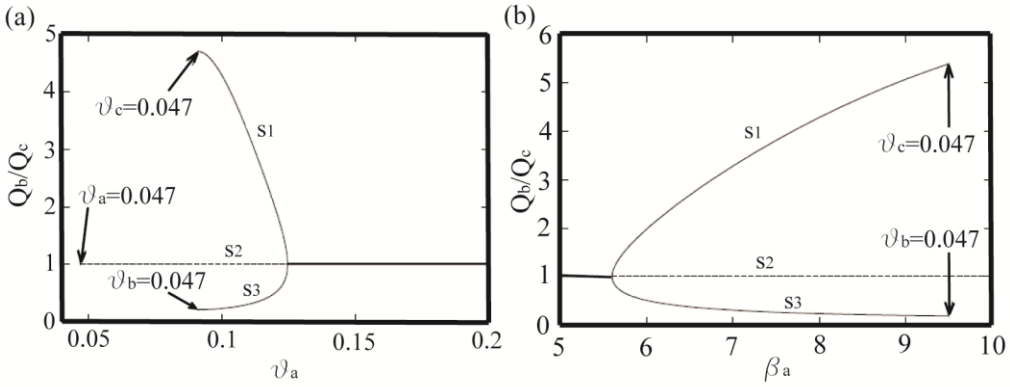

Figure 2.2. Results of water discharge ratio as a function of Shields parameter (a) and aspect ratio (b) (half-width to depth ratio) obtained by Bolla Pittaluga et al. (2003)

The equilibrium configurations of the system were found to be highly dependent on the upstream channel Shields parameter (Figure 2.2). For values over a certain threshold only one equilibrium solution exists, in which water discharge ratio is dependent on branches length ratio and is characterized by a symmetrical discharge distribution for a geometrically symmetrical bifurcation (branches with equal length). On the other hand, for Shields parameter values below the mentioned threshold three possible equilibrium configurations occur, one of them symmetrical for symmetrical geometry conditions and the other two, which are reciprocal, present an asymmetrical discharge distribution even for branches with equal length. The threshold value for Shields parameter that separates the situations with one or three possible solutions was found to depend on the upstream channel aspect ratio (half-width divided by water depth). A stability analysis was performed to verify the stable or unstable character of the different equilibrium solutions. The single solution found for high Shields values was found to be stable whereas below the threshold value this symmetrical solution became unstable, being the asymmetrical solutions the stable ones. This result represents a very important contribution, as highlights the possibility of a stable asymmetrical discharge distribution, even when both branches have the same length. On the opposite, Wang et al. (1995) model determined an equitable discharge distribution for equal-length cases, and stable when the mentioned stability criterion involving exponents *k* and *n* was verified.

Experiments performed by Bertoldi and Tubino (2007) confirmed the trend of a bifurcation system towards an asymmetrical discharge distribution in certain conditions of the upstream flow, corroborating Bolla Pittaluga's results (Figure 2.3). Moreover, Federici and Paola (2003) performed experiments in a widening channel, that enhances the formation of a central bar associated to the divergence of the streamlines. The subsequent symmetrical bifurcation is observed to be stable or unstable depending on the shields stress and the

aspect ratio of the upstream channel. The results agree quite well with the results obtained with Bolla Pittaluga's model. In addition to this, the final equilibrium configuration is found to depend on the widening ratio of the channel.

Burge (2006) reports field data in five bifurcations in the gravel-cobble bedded Renous River (New Brunswick, Canada). The results are opposite to the mentioned experimental observations, showing that stable bifurcations displayed lower Shields stresses than unstable bifurcations.

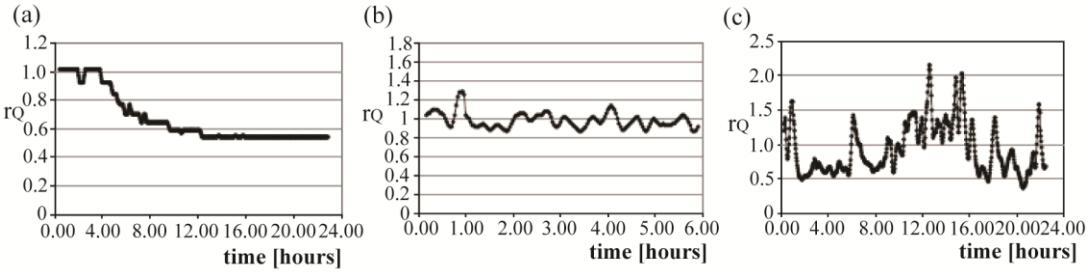

Figure 2.3. Time evolution of water discharge ratio r_Q of downstream branches measured in three different runs by Bertoldi and Tubino (2007): without bar formation (a), with bar formation and high Shields value (b), with bar formation and low Shields value.

The existence of asymmetrical solutions can be interpreted as follows. The presence of a certain transversal step generates a water depth difference between both branches that in uniform flow conditions implies a difference in water discharges. For low Shields values in the upstream channel, the transversal flow that compensates that water discharge difference, together with the bed level difference associated to the transversal step, generate a transversal sediment transport that makes possible that each branch is fed with a solid discharge equal to the transport capacity associated to its flow conditions (water discharge and water depth).

One limitation of the model resides on the fact that the results depend on the parameter α, which is only defined as having the same order of magnitude as the upstream distance from the diversion required for the effects of the bifurcation on bed topography to decay. In spite of its imprecise definition, no sensitivity analysis related to this parameter is provided. Bertoldi and Tubino (2007) approach the study of the upstream impact of the bifurcation in terms of the theory of morphodynamic influence (Zolezzi and Seminara, 2001). This theory establishes the existence of a resonant aspect ratio that separates those situations in which the influence of a planimetric discontinuity of the river is propagated upstream (super-resonant conditions) from those in which this propagation is rapidly dumped (sub-resonant conditions), playing a similar role to Froude number's separation of subcritical and supercritical flows. When applied to a fluvial bifurcation situation, the consequence is

that in super-resonant conditions, when a bed level difference appears between the entrances of both branches, this transversal step propagates upstream and generates a transversal flow that entails different water discharges in both branches. On the other hand, in sub-resonant conditions the upstream bed profile is almost unaffected by the bifurcation and water discharges in the branches tend to be similar. Therefore, according to this study it could be said that super-resonant conditions favor unbalanced water discharge distributions whereas sub-resonant conditions tend to equitable ones. Moreover, Bertoldi and Tubino (2007) performed a calibration of parameter α relating it to the separation of the aspect ratio with respect to resonant conditions, finding values that ranged from 1 to 7.

The time evolution that takes the system to arrive to the equilibrium is also influenced by the upstream geometry and the morphodynamic influence of the bifurcation (Bertoldi et al., 2005). In super-resonant conditions, the further the aspect ratio is from the resonant value, the faster the system evolves from a balanced discharge distribution to the unbalanced stable equilibrium state. On the other hand, for resonant or sub-resonant conditions the response of the system to a perturbation is much slower.

A relatively simple theoretical approach was carried out by Kobayashi et al. (2006). They consider a straight flow dividing surface and control volumes of length equal to the upstream channel width formed by the flow entering into each branch (Figure 2.4). They apply momentum equations into each volume considering pressure, gravity and friction forces and mass continuity equation relating incoming and outgoing flow. Moreover, they consider uniform flow equations in the branches and suppose the water surface height at the wall separating the branches as the average value of the heights considered in the branches. They also assumed the hypothesis that friction and gravitational terms cancelled each other and they solved the resulting equations to find values of water discharge ratio and water depth in the upstream channel, for different slope ratios between the downstream branches. Two solutions were found in each case, one corresponding to sub-critical and the other to super-critical conditions. Experiments were performed over flat-bed and the results agreed quite well with the sub-critical ones obtained from the theoretical model. By increasing the discharge and subsequently the Shields stress, they carried out movable-bed experiments. A significant difference in the water discharge ratio is not observed in the results when comparing with the flat-bed experiments.

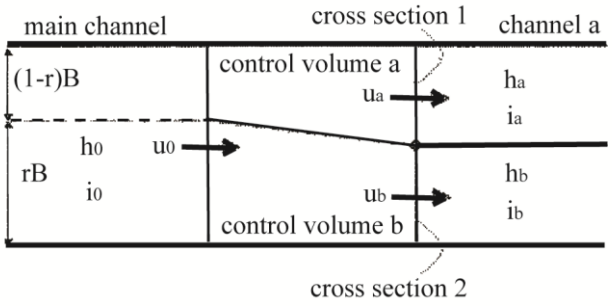

Figure 2.4. Scheme of the conceptual model used by Kobayashi et al (2005)

As noticed above, there is an interconnection between solid discharge distribution, water depth difference, and water discharge ratio between branches. Therefore, not considering solid discharge limits considerably the application of this model for most real cases of bifurcation evolution. On the other hand, the model geometry reproduces a bifurcation generated by a dividing wall parallel to the upstream channel direction, which would hardly correspond to natural bifurcations but to artificial flow divisions. Moreover, the hypothesis related to the water surface height at the division wall requires further verification, as the wall should produce a water surface level increase that could alter the results significantly. Lastly, the idea of establishing a length equal to the channel width for the control volumes used in this theoretical model, is cast into doubt by the values of parameter α introduced by Bolla Pittaluga et al. (2003) representing the area of influence of the bifurcation in the upstream channel.

2.1.3 Influence of migrating bars

Another limitation of the previous model that was already highlighted by the authors resides on the fact that the influence of migrating bars is not considered. Bolla Pittaluga et al. (2003) performed some experiments in which large-scale migrating bed forms were formed in the upstream channel (Figure 2.5). Its alternating pattern caused a periodical shifting in the transversal slope in the area upstream from the bifurcation, causing that the water discharge ratio between both branches presented an oscillating behavior. Bertoldi and Tubino (2007) deepened some more into the relationship between bar formation and the balanced and unbalanced solutions found in the theoretical study, by means of several experimental runs in a bifurcation with non-erodible banks and branches with equal length. For high Shields parameter values, the migrating bed forms generated an oscillating pattern around the symmetrical stable equilibrium. However, for low Shields values in which the stable equilibrium solutions present an unbalanced distribution of discharge between both

branches, the influence of the bars generate a more complex situation in which the system shifts alternatively from one solution to the other (Figure 2.3).

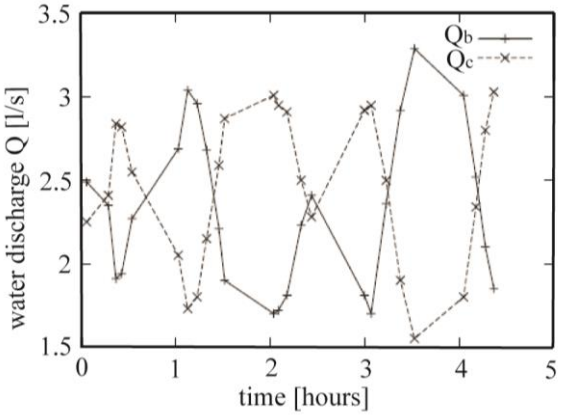

Figure 2.5. The water discharges measured in the two branches (b and c) of the experimental flume are plotted versus time in a test in which alternate bars were migrating along the upstream channel (Bolla Pittaluga et al. 2003)

Bertoldi et al. (2005) carried out some experiments with erodible banks, both in the upstream channel and the downstream branches, in which the interaction between planimetric and altimetric processes generated a more complex situation. In these cases, the lateral evolution give place to situations in which two consecutive bed forms enter into the same channel, shifting definitively the discharge towards the other branch (Figure 2.6). Moreover, the bifurcation has an influence on the bar migrating patterns, causing a decrease in the bars speed. In turn, this slowing down process favors the formation of a slightly meandering structure in the channel upstream that decreases even more the bars speed, with the possibility of reaching a static pattern.

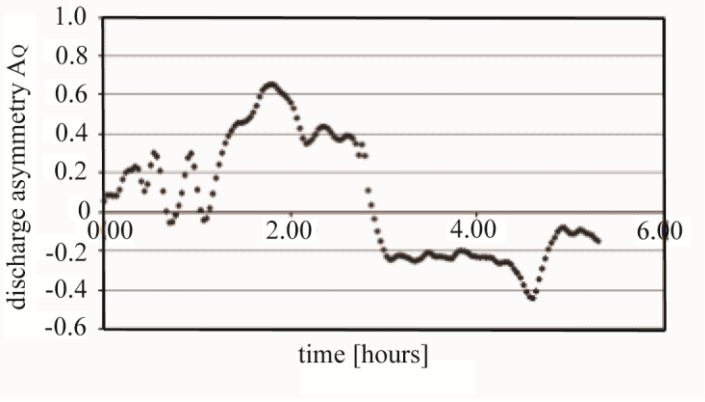

Figure 2.6. Evolution of discharge assymetry in time, defined as Q_b-Q_c/Q_b+Q_c, being Q_b and Q_c the water discharges through each branch (Bertoldi et al. 2005)

From a theoretical point of view, Hirose et al. (2003) developed an analytical model to explain the oscillating behavior of water discharge ratio in a bifurcation in the presence of alternating bars. Based on the approach of Bolla Pittaluga et al. (2003), they considered the

last stretch of the upstream channel divided in two cells and considered the Exner equation in each of them, accounting for the sediment mass balance. However, instead of relating the solid discharge exiting through each branch to the associated transport capacity, they described it as a function of the local bed gradient of each cell:

$$Q_{sb} = \left(1 - k\frac{Z_1}{\lambda}\right)Q_{s1} + m\frac{Z_2}{\lambda}Q_{s1} \tag{2.3}$$

$$Q_{sc} = \left(1 - k\frac{Z_2}{\lambda}\right)Q_{s2} + m\frac{Z_1}{\lambda}Q_{s2} \tag{2.4}$$

In these equations, Q_{sb} and Q_{sc} are the solid discharges entering to cells 1 and 2, and Q_{s1} and Q_{s2} are the solid discharges exiting them, Z_1 and Z_2 are the cells bed levels, λ their length and *k* and *m*, two parameters to be calibrated. Introducing these expressions in the Exner equations and rearranging terms, they arrived to dumped oscillating equation describing bed level evolution in each cell. They performed several experiments in supercritical flow conditions, non-uniform bed sediment and a bifurcation with an angle of 20º, and measured the oscillating period of the bed forms that were formed, therefore using the results to calibrate the parameters of the conceptual model.

Miori et al. (2006) used the model of Bolla Pittaluga to propose an alternative approach to consider the influence of bar migration. They assume alternate sinusoidal in time sediment discharge distributions feeding each of the cells of the last stretch of the upstream channel:

$$Q_{sb} = \frac{1}{2}b_a\left[q_a + A\sin\left(\omega_b t\right)\right] \tag{2.5}$$

$$Q_{sc} = \frac{1}{2}b_a\left[q_a - A\sin\left(\omega_b t\right)\right] \tag{2.6}$$

In these equations b_a is the upstream channel width, q_a is the sediment discharge per unit width, *A* is the amplitude of the oscillations and ω_b its frequency.

The results show that the frequency of oscillation is a determinant parameter for the behavior of the system (Figure 2.7). For rapid migrating bars in which the time-scale associated with the bar migration is of the same order of magnitude as the intrinsic time scale of evolution of the bifurcation, the water discharge ratio oscillates around the stable equilibrium solution of the system which, considering equal-length downstream branches, is symmetrical for high upstream Shields values and unbalanced for low upstream Shields values. The oscillations are due to the alternative lateral step that is established between both cells, directing the flow towards one cell or the other. Being the bars rapid and small, the system does not change its stability conditions. However, when the time scale of the

bars is larger than the morphodynamic one, the system has time to adapt to the changing flow conditions. For low Shields values situations, this means that the system shifts between the two reciprocal unbalanced equilibrium situations, giving place to a some more complex behavior.

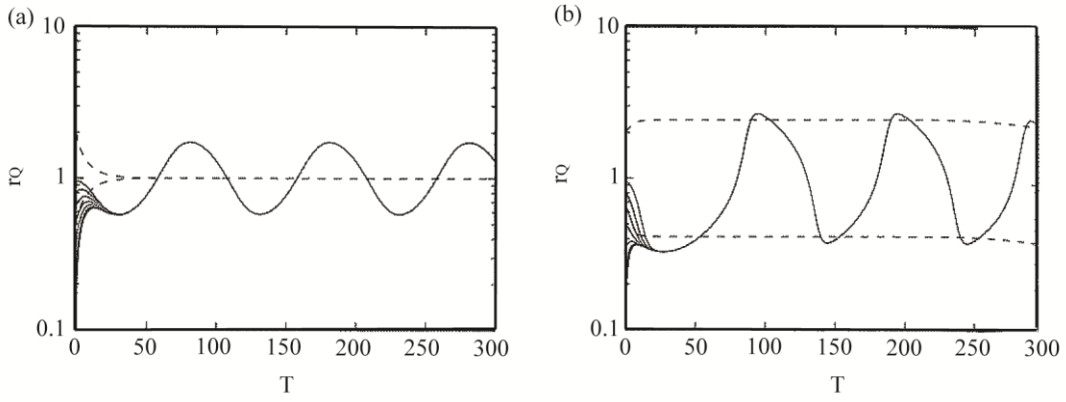

Figure 2.7. Time evolution of water discharge ratio starting from different initial conditions in the presence of alternate bars along the upstream cannel: high Shields value (a), low Shields value. Dashed lines correspond to steady forcing conditions (Miori et al. 2006)

2.1.4 Influence of bank erodibility

Bolla Pittaluga's model considers channels with fixed banks. This situation is representative of rivers in which bank evolution processes occur over a much larger time scale than bed evolution processes, such as rivers with cohesive or vegetated banks. However, in gravel-bed braided rivers both phenomena have similar time scales and the non-erodible banks hypothesis may not be appropriate. Miori et al. (2005) and Miori et al. (2006) develop the Bolla Pittaluga model to take into account the effects of bank erosion. For this purpose, the authors consider different regime relationships to link the river width with the flow conditions and finally adopt the one proposed by Ashmore (2001) on the basis of a statistical regression on field data mainly from gravel bed rivers. The relatively low Shields values that derive from this equation suggest that this kind of rivers present the conditions to enhance the establishment of unbalanced stable bifurcations. The upstream channel is considered to have a given width and discharge according to the regime relationship, whereas the mentioned equation is imposed in the downstream branches when solving the problem. The equilibrium configurations are studied and compared to the fixed width discharge distributions obtained by Bolla Pittaluga et al. (2003) and more asymmetrical solutions are found for a certain aspect ratio. A more pronounced lateral step is also predicted between the two cells of the last stretch of the upstream channel in the

cases with erodible banks. These results agree with field observations carried out by Zolezzi et al. (2006) in two streams of Canada and Italy.

The time evolution of a bifurcation with erodible banks is studied by means of this analytical model, including the following equation to account for width time evolution:

$$\frac{db}{dt} = \frac{1}{T_w}\left(b_r - b\right) \tag{2.7}$$

Where b denotes the actual channel width, T_w is the time scale of the width adaptation process and b_r is computed through the corresponding regime formula. However, the different response of channel width to discharge rise or fall is incorporated in the model, as time scale associated to widening process due to erosion is much shorter than narrowing process due to deposition. Therefore, whereas equation (2.7) is applied when the channel width increases, the opposite process is not permitted by the model. Due to these considerations, the final state attained by the bifurcation is influenced by the initial condition of the bifurcation. In other words, the mechanism of formation of the bifurcation is determinant on the final equilibrium configuration, and significantly different situations are found if the bifurcation is generated from the incision of a new channel, through a chute cutoff or an avulsion process or it is formed as a consequence of a central bar. Figure 2.8 shows the time dependence of water discharge ratio and width ratio for different initial conditions.

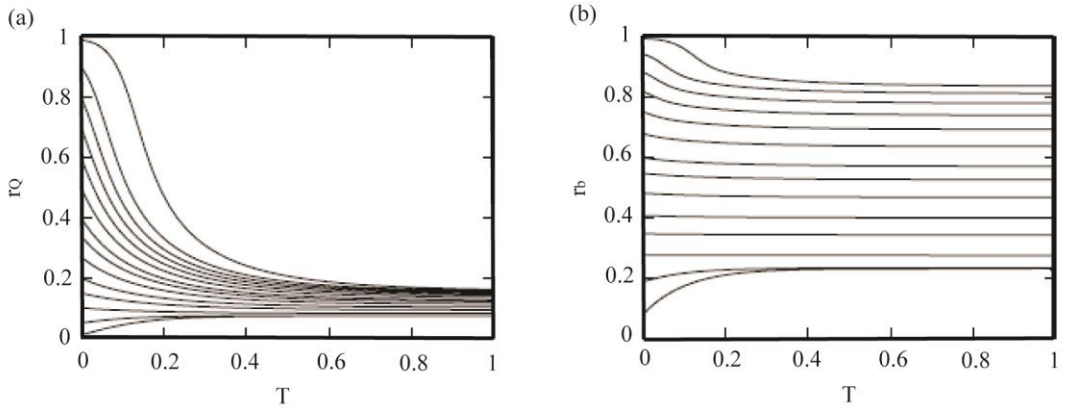

Figure 2.8. Time evolution of water discharge ratio (a) and width ratio (b) of a bifurcation for different initial conditions, calculated by the 1D model of bifurcations with erodible banks (Miori et al. 2006)

2.1.5 Influence of discharge variability

Miori et al. (2006) studied the influence of water discharge fluctuations on the evolution of water discharge distributions between both branches of a bifurcation. Starting from the

conceptual model of Bolla Pittaluga (2003), they considered a simple hydrograph described by the following equation:

$$Q(t) = Q_0 \left[1 + A_Q \sin\left(\omega_Q t \right) \right] \tag{2.8}$$

The considered incoming discharge consists in a certain average value, Q_0, and oscillations of amplitude A_Q and frequency ω_Q. This situation simulates the possible forcing conditions in a river bifurcation affected by an ice-melt type annual hydrograph. Similarly to the case of alternate migrating bars that has been discussed above, the ratio between the time scale associated to the hydrograph oscillations and the intrinsic morphodynamic time scale is determinant for the evolution of the system. Moreover, the range of Shields values associated with the range of discharges causes the balanced or unbalanced pattern of the flow distribution. Thus, for low-frequency oscillations that cover only high shields values, the system rapidly evolves to an equilibrium characterized by a constant equitable distribution of the discharge, even if the total discharge fluctuates in time. However, depending on Q_0, A_Q and the upstream geometry, the system can fluctuate between flow conditions that, in case they were steady, would lead the system to balanced discharge distributions and flow conditions that would enhance unbalanced situations. In these cases the system behavior is more complex and the discharge ratio oscillates. Depending on the value of ω_Q, the discharge ratio is able to attain the equilibrium values corresponding to the steady conditions or simply oscillates between unity and the low value corresponding to the low Shields situation (Figure 2.9).

An experimental analysis carried out by Miori et al. (2008) corroborates the results obtained with the previous conceptual model. A hysteresis loop was obtained by the water discharge ratio when comparing the raising and the falling branch of a hydrograph cycle, which is interpreted in terms of the relatively slow time scale of morphological adaptation of the inlet step. In some of the runs alternate bars developed making more complex the evolution of the system, but the general patterns predicted by the theoretical model were confirmed.

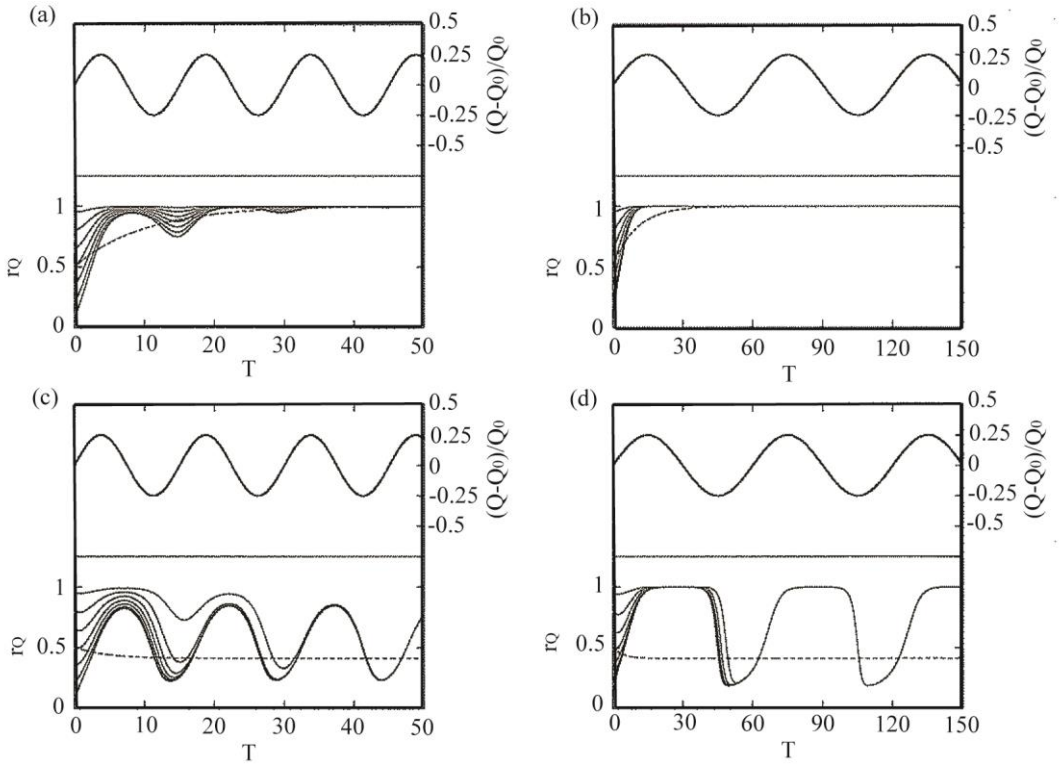

Figure 2.9. Time evolution of water discharge ratio between the branches starting from different initial conditions, in the case of water discharge fluctuations (continuous lines) and in the case of steady forcing conditions (dotted lines). In each plot the value of the water discharge is also plotted (right axis scale): (a) fast fluctuations and high Shields number; (b) slow fluctuations and high Shields number; (c) fast fluctuations and low Shields number; (d) slow fluctuations and low Shields number

2.1.6 Influence of the bifurcation angle

Another aspect of interest that has been experimentally analyzed is the angle to which a developing bifurcation tends. In their experiments on bifurcations evolving to an equilibrium state, Bertoldi et al. (2005) measured the angle between the downstream branches during the system evolution. From the onset of the bifurcation, when the angle value ranges between 60 and 70 degrees, deposition occurs at the bar front and the angle decreases to values around 50 degrees at the equilibrium state. On the other hand, Federici and Paola (2003) measured the angle at the front of the central bar formed in the widening channel that they use to study the onset of a bifurcation, obtaining values ranging from 60 to 75 degrees. They compared these values to the angle between the center lines of the branches, finding these to be lower and ranging between 40 and 60 degrees. Furthermore, Bertoldi et al. (2005) and Bertoldi and Tubino (2005) report bifurcation angles ranging from 20 to 55 degrees, with an average value of 35 degrees, in their experiments gravel-bed baided networks. Finally, field data from Burge (2006) show an average bifurcation

angle of 47º for five bifurcations in the gravel-cobble bedded Renous River (Canada) and highlight a decrease in the angle when the branches are of similar length.

2.1.7 Studies based in field observations

Some studies have been carried out based on real bifurcations. One example of this is Pannerdense Kop (Figure 2.10), a bifurcation located in the Rhine River at the border between the Netherlands and Germany, which is considered to be the main control for water distribution in the Netherlands, its evolution being therefore of utmost important for the country. Sloff et al. (2003) report the results of a numerical modeling and experimental analysis on sediment behavior in Pannerdense bifurcation. The numerical model provides better results when compared to field data. Due to the relative geometry of the downstream branches and the upstream channel, lateral sorting is observed and coarser sediment is found in the branch located in the inner part of the bend where the
bifurcation is placed. Moreover, the main diameters that govern the bifurcation behavior are roughness and sediment diameter.

Figure 2.10. Aereal view of the Pannerdense Kop bifurcation in the Rhine River (Netherlands)

Field studies often highlight aspects that are more difficultly studied in the more idealized theoretical and experimental models. Frings and Kleinhans (2008) carried out an analysis on data of three bifurcations in the Rhine River system: the mentioned Pannerdense Kop, Ijssel Kop and Merwede Kop. The location of the bifurcation in relation to the planimetric shape of the river can play an important role in sediment distribution amongst the downstream branches. The bend sorting process that takes place in a river bend, distributing coarser sediment in the outer part of the bend and finer sediment in the inner part, causes that when a bifurcation is placed in a river bend, the outer branch receives less

sediment than the inner one due to supply-limited conditions. Another factor that can sometimes influence the bifurcation behavior when it is located near the sea is tidal influence. In these situations, a difference in the roughness of the branches channels causes a different propagation of tidal wave along them, conditioning the flow and sediment distribution between the branches. Moreover, the delayed adaptation of dunes after a change in flow conditions causes hysteresis in hydraulic roughness and bed-load transport, making more complex the solid discharge distribution at the bifurcation. Lastly, sediment waves have been observed in all three bifurcations, and characterized as intrinsic phenomena that result from bend effects or flow divergence directly upstream of the bifurcation. During periods of rising discharges, more bed-load is supplied from upstream than is evacuated through the branches, therefore causing sedimentation, whereas during the periods of falling discharge this excess of sediment is eroded, generating a sediment wave. The main parameter found to differentiate the behavior of these three bifurcations is sediment mobility.

Other analyses based on a real bifurcation were carried out by Zanichelli et al. (2004), consisting on a two-dimensional depth-averaged modeling of the bifurcation Po de Goro-Po di Venezia (Italy), in which the applied mass and momentum conservation equations together with Boussinesq's assumption to compute the bed shear stresses. These studies highlight the ability of numerical models to give acceptable results of water discharge ratios, though they happen to be sensitive to eddy viscosity. This fact is interpreted as a consequence of the predominance of turbulent stresses in the local processes that take place in the bifurcation.

2.1.8 Influence of other factors

Kleinhans et al. (2006) used 1D and 3D numerical models to study the long-term evolution of a bifurcation under the influence of an upstream meander bend and a slope difference between downstream branches (Figure 2.11). The modification of sediment transport direction due to bend-associated spiral flow causes that inner bend branch receives relatively more sediment and the bifurcate connected to the outer bend receives relatively more water. Moreover, the presence of a river bend generates a bar-pool structure associated to the change in curvature. The characteristic damping length of this morphological pattern depends on the width-depth ratio of the channel, in such a way that bars are underdamped for wider and shallower channels. Therefore, depending on the channel geometry and the distance from the bifurcation to the upstream bend, the transverse slope at the bifurcation can cause its stabilization or destabilization. The bend

radius of curvature also affect to the stabilization of the bars, so that the sharpest bends have the fastest development of a fixed bar that can partially block one of the branches.

The general trend observed is the development of highly asymmetrical bifurcations in which one of the branches tends to a very small but non-zero discharge, whereas the other becomes absolutely dominant. During the phase of increasing asymmetry, sediment discharge ratio follows the same behavior as flow division, but in the final stages sediment transport declines more rapidly than the discharge in the silting-up channel, therefore causing the establishment of a low but stable discharge. On the other hand, the results highlight the possibility of a combination of upstream bend characteristics and slope ratio between the branches, that lead to relatively stable bifurcations with an equitable discharge distribution, due to the counteracting effect of the two mentioned factors.

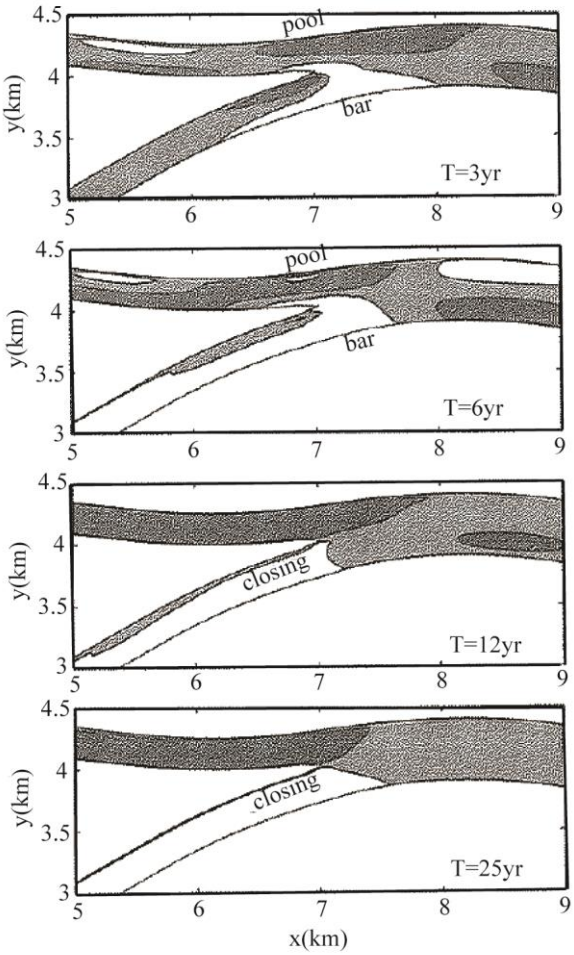

Figure 2.11. Evolution of the bed levels at 3, 6, 12 and 25 years illustrating the bar and pool evolution, according to the results by the numerical model of Kleinhans et al. (2006)

Other studies by Kleinhans et al. (2007) highlight the fact that in many situations there is not a unique relation between sediment transport and hydrodynamic parameters and investigate the consequent hysteresis process occurring at bifurcations. The analysis is based on field observations carried out in the mentioned above Pannerdense Kop. During a flood, a clockwise hysteresis of bedload against discharge is observed upstream of the bifurcation, caused by the lagging development of dunes during the hydrograph. However, counter-clockwise hysteresis is observed downstream of the bifurcation, caused by a combination of processes. On the one hand, a scour zone is formed that causes a migrating fine sediment wave. On the other hand, vertical bed sediment sorting occurs at the lee-side

of the dunes, which lead to surface-sediment fining and increase transport during and after the flood.

In his field-data based analysis, Burge (2006) highlight the stabilizing role of vegetation in fluvial bifurcations. This effect is caused by the slowing down of channel migration, helping to maintain a uniform upstream flow field. Vegetated bifurcations favor accretion at the front of the bifurcation angle, at rates observed to range between 0.9 and 2.5 meter/year.

2.1.9 Bifurcations as part of a braided network

Fluvial bifurcations have also been studied not individually but as part of a more complex braided network. Bertoldi et al. (2006) carried out a laboratory analysis in which they studied the evolution of a braided network from the initial situation consisting of a single straight channel to the equilibrium state, in different conditions of water and sediment supply. They classified the different bifurcations based on bed load activity in their constitutive branches and defined a "degree of activity" of the network, which gave an idea of the amount of branches active from the point of view of bed load transport. This parameter was found to increase with the stream power of the incoming flow, defined as $\Omega = \gamma QS$, being γ the specific weight of water, Q the water discharge and S the slope. The number of bifurcations where the three constitutive branches (the upstream channel and the two bifurcates) were active was found to decrease in time for all the experiments, where as a slight increase was reported for the number of bifurcations in which only one branch presented non-zero bed load transport. Moreover, a greater width asymmetry between the downstream branches was found for this second type of bifurcations in relation to the first type.

2.2 Flow and sediment transport on fluvial diversions

Diversions or lateral intakes constitute a particular case of fluvial bifurcations in which one of the downstream branches follows the same direction as the upstream channel, whereas the other exits laterally forming a certain angle with the former. As they are frequently found in nature and they present several patterns of behavior that are characteristic of this kind of geometry, they are usually studied separately from the general Y-shaped bifurcations that have been commented in the previous section. This system's shape can be found often in naturally formed bifurcations and corresponds also to the vast majority of the artificial intakes constructed in a river, which can be used for diverse finalities as crop

irrigation, water supply systems of inhabited nucleus or refrigeration circuits of power plants and factories.

Throughout the rest of the document, the downstream branch that forms a certain angle with the upstream channel will be referred to as 'lateral branch', whereas the branch that follows straight and parallel to the upstream channel will be referred to as 'main channel'.

2.2.1 The Bulle effect

From a sediment transport point of view, the main pattern presented by fluvial diversions consists in a significant trend of sediment to deviate towards the lateral branch. This means that solid discharge distribution tends to be more unbalanced in favor of the lateral branch than water discharge distribution. This fact often causes sedimentation problems at the entrance of the intake, when the amount of sediment that feeds the lateral branch exceeds the transport capacity associated to the diverted flow. Therefore, the performance of the intake is affected by this deposition process and correcting measures are required to assure the accomplishment of the diversion objective. This phenomenon is commonly known as Bulle Effect, in honor of Henri Bulle, the German researcher that studied it for the first time and reported this behavior.

Bulle (1926) carried out an experimental study in which he studied the relation between sediment distribution and flow distribution with different diversion angles and changing the roundness of the upstream corner of the diversion entrance. Table 2.1 shows the results of some of the runs with a total incoming discharge of 5l/s. The scope of Bulle Effect is highlighted by the fact that in situations of equitable water discharge distribution, around 97 percent of the sediment is deviated towards the lateral branch. Figure 2.12 shows a scheme of Bulle's experimental model and Figure 2.13 includes an example of Bulle's reported results for a bifurcation angle of 30º.

Table 2.1. Bulle experiment results for a diversion angle of 30 degrees and different water discharge distributions

Experiment number	Q_l		Q_m		r_Q (Q_l/Q_m)	Q_{sl} (%)	Q_{sm} (%)	r_S (Q_{sl}/Q_{sm})
	l/s	%	l/s	%				
1	2.5	50	2.5	50	1	97.3	2.7	36
2	1.9	38	3.1	62	0.613	93	7.0	13.3
3	1.45	29	3.55	71	0.408	71.5	28.5	2.5
4	1.25	19.3	3.75	80.7	0.240	29.8	70.2	0.425

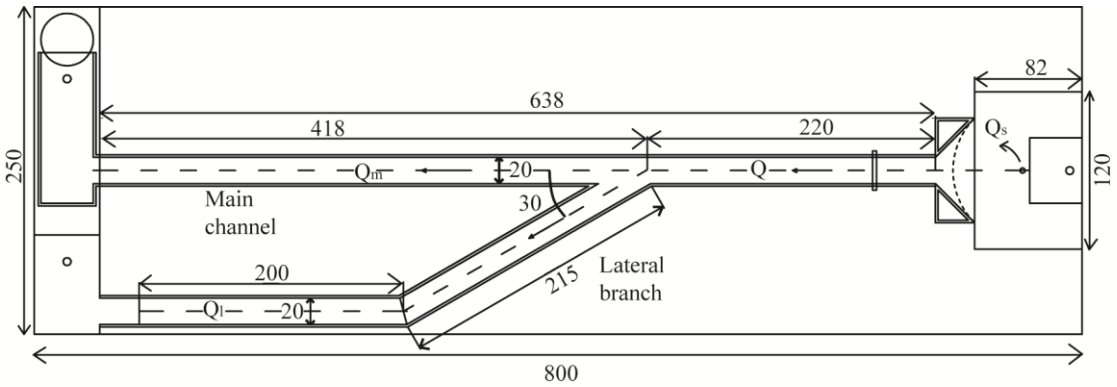

Figure 2.12. Scheme of Bulle experimental model (lengths in centimeters)

Experiments were carried out with diversion angles of 30º, 60º, 90º, 120º and 150º. An increase in the diversion angle is observed to slightly decrease the percentage of sediment that is deviated towards the lateral branch, although this trend is inverted from 120º to 150º. On the other hand, for the same general geometry but re-shaping the upstream corner of the diversion entrance to give it a round profile, the solid discharge in the lateral branch decreases, although the effect is not very significant (a reduction of 0% to 5%).

The general interpretation of the Bulle effect relates it to the fact that, as flow velocities are low near the channel bed, this part of the flow is more easily deviated by the lateral pressure gradient generated by the diversion entrance. Therefore, the lateral branch discharge is formed by the flow coming from the lower layers of the upstream discharge, which constitute also the part of the flow that carries the bed load sediment and a high proportion of the suspended material (Ordóñez, 1974). The influence of the roundness in the upstream corner of the diversion entrance would be interpreted as a facilitation of the entrance of the faster flow of the near-surface layers, therefore decreasing the sediment mixed with the diverted discharge.

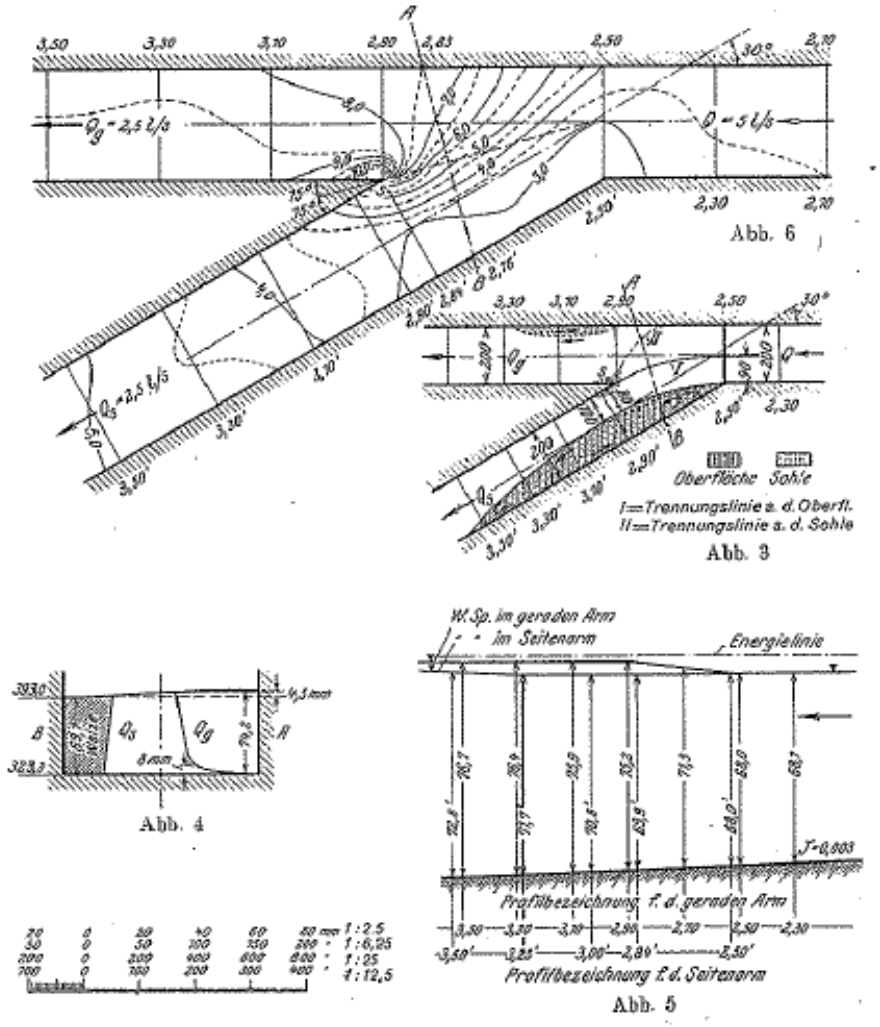

Figure 2.13. Example of Bulle's experimental results in the case of a 30-degree diversion. Scheme of the flow patterns (Abb. 3), profile of cross section β – β' (Abb. 4), energy line profile (Abb. 5) and water surface levels in the diversion area (Abb. 6)

Bulle also carried out some additional experiments in which he varied the ratio between the main channel and the lateral branch widths. The increase of the value of this ratio (a reduction of lateral branch width in relation to main channel width) causes a reduction in the percent of sediment captured by the lateral branch. For instance, setting a value of 2 for the width ratio (the main channel width is two times the lateral branch width), the percent of sediment flowing through the lateral branch decreases from 97% to 89% in relation to the equal-width case. Although the explanation of these results is not clear, a possible interpretation would relate them to the inertia of the sediment, which is higher than water's, a fact that would cause that the sediment travelling furthest from the diversion entrance would not be captured by the diverted flow in the time interval during which it crosses the diversion area.

However, the analysis performed by Bulle has several limitations. Firstly, the reported results on sediment distribution refer to experiments in which sand is fed to a fixed bed channel. Therefore, no effect of the bed bathymetry can be reproduced by this analysis. Moreover, the time length of the runs is relatively short, 45 to 75 minutes. Considering diversion morphology evolution observed in other studies (Herrero et al. 2011), this time length is too short for the system to attain the equilibrium situation. Finally, no time evolution of the variables is reported in Bulle's results, but the average values obtained considering the total amount of sediment collected at the end of each branch during the whole experiment.

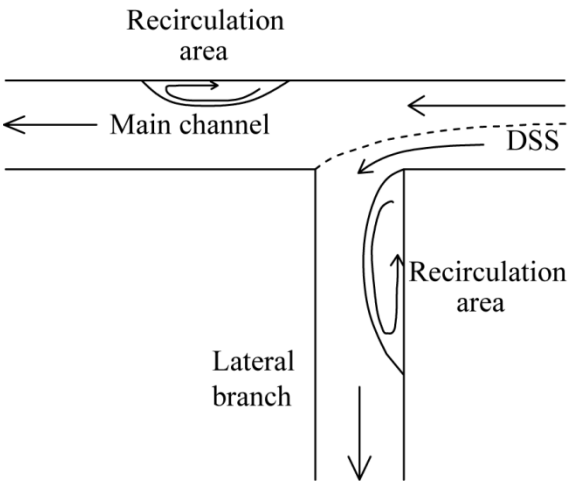

Figure 2.14. General flow patterns of a fluvial diversion

2.2.2 General flow charactreristics

Bulle's analysis as well as the whole of the numerical and laboratory studies that have been performed since then about the behavior of fluvial diversions, highlight some general patterns in the characteristics of the flow in this kind of system (Figure 2.14). However, most of them emphasize the fact that flow becomes significantly complex in the area affected by the intake, and secondary flows with a highly 3-dimensional character have a great influence on flow and sediment distribution (Neary & Sotiropoulos, 1996, 1999; De Heer & Mosselman, 2004). Moreover, non-uniform and turbulent patterns also play a certain role in the system evolution (Omidbeigi et al., 2009; Zhou & Zeng, 2009).

The surface that ideally divides the flow that is diverted to the lateral branch from the flow that follows the main channel is commonly known as the dividing stream surface (DSS) (Neary & Sotiropoulos, 1999). Its shape is related to the lateral acceleration caused by the transversal pressure gradient associated with the lateral intake. The velocity profile of the flow that is coming from the upstream channel, with relatively high velocities near the surface and relatively low ones near the bed, causes that the DSS extends further into the main channel in the near bed-layers whereas near the surface a smaller flow width is captured by the diversion. This is the reason why the flow in the lateral branch is mainly formed by the near-bed flow of the upstream channel, which carries most of the sediment

discharge of the upstream channel, therefore constituting the main reason reported in the literature to explain the Bulle Effect (Ordoñez, 1974; Van der Mark and Mosselman, 2012). The DSS finishes at the downstream corner of the diversion entrance forming a stagnation point of the flow where overpressure occurs and water surface level presents a significant rise.

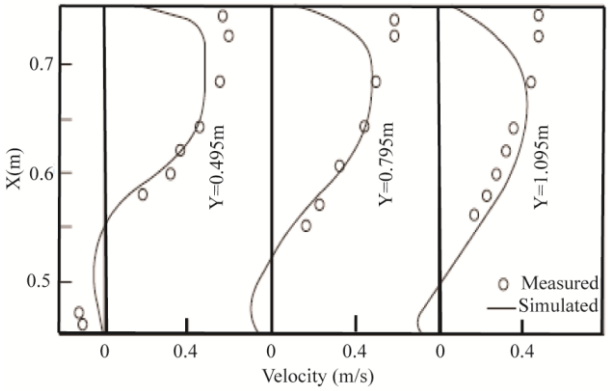

Figure 2.15. Velocity profiles in three sections of the first stretch of the lateral branch measured by Shettar and Murthy (1996) and simulated numerically by Khan et al. (2000). X and Y coordinates refer respectively to transversal direction and longitudinal direction in the lateral branch. Negative velocities are associated with the recirculation area of the lateral branch. Figure obtained from Khan et al. (2000).

The flow in the lateral branch is characterized by the formation of a recirculation area next to the upstream wall of the lateral branch, due to flow separation at the upstream corner of the diversion entrance. The recirculation of the flow generates an area of low and even negative velocities next to the wall (Figure 2.15). Bulle (1926) reports qualitatively the existence of this pattern and both laboratory measurements and numerical models reproduce it quite coherently (Neary & Sotiropoulos, 1996, 1999; Barkdoll, 1998; Khan et al. 2000; De Heer & Mosselman, 2004; Vasquez, 2005). On the other hand, Pizardeh and Shamloo (2007) carried out a 2-dimensional numerical analysis to study the dependence of the dimensions of the lateral branch recirculation area on the water discharge ratio between the lateral branch and the main channel. Mass continuity and momentum equations were solved, using Reynolds stress model as a closure scheme to consider turbulence. Channel width is used to make both length and width of the recirculation area dimensionless and their results highlight that both dimensions decrease with an increasing ratio of discharge. Measurements performed by Kasthuri and Pundarikanthan (1987) reproduce the same trend and compare well with the numerical results (Figure 2.16). Movable-bed experiments by Rezapour et al. (2009) are also coherent with the mentioned observations. This trend is caused by the blockage that the recirculation area causes in the lateral branch. Concerning the depth-dependence of these dimensions, Neary and Sotiropoulos (1999) highlight a decrease of width and length near the bed. This behavior is due to the lower velocities in this area and the subsequent lower centrifugal force, which facilitates the alignment of the

streamlines with the channel direction. On the other hand, the existence of the separation zone causes that all the lateral branch flow is constricted to a relatively narrow section with a subsequent increase in flow velocity (Barkdoll et al. 1998, Neary and Sotiropoulos, 1996, 1999). Hsu et al. (2002) report experimental values of a contraction coefficient describing the flow in this area, found in their experiments performed in a 90-degree diversion model under varied conditions of discharge ratio. In regard to sediment transport and bed morphodynamics, the recirculation area enhances sediment deposition whereas deeper bed levels should be found next to the opposite wall due to the higher transport capacity associated with the higher velocities that are present in this area.

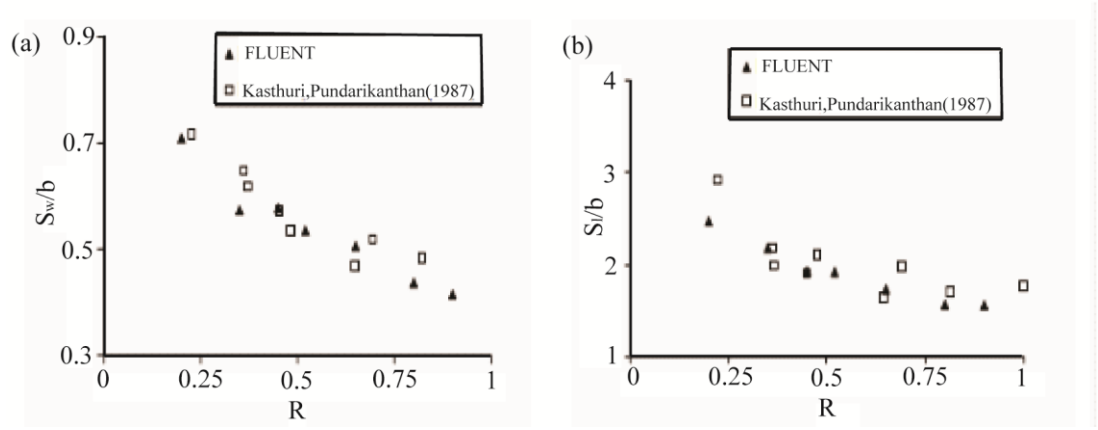

Figure 2.16. Comparison between the width (a) and length (b) of the lateral branch separation zone calculated numerically by Pizardeh and Shamloo (2007) and measured experimentally by Kasthuri and Pundarikanthan (1984). (Figure obtained from Pizardeh and Shamloo (2007))

Some studies report the occurrence of another separation zone with the subsequent flow recirculation, in the main channel, just downstream from the diversion and next to the wall opposite to the diversion entrance (Figure 2.14) (Bulle, 1926; De Heer & Mosselman, 2004; Pizardeh & Shamloo, 2007). However, this separation zone only occurs when discharge flowing into the lateral branch is high enough in relation to the total incoming discharge. This is due to the fact that this main channel recirculation area is related to the curvature of the streamlines caused by the transversal pressure gradient associated with the diversion. Therefore, in those situations where the discharge distribution is such that the lateral branch takes an important percentage of the flow, streamlines curve towards the entrance of the lateral intake and flow separation occurs just downstream from the diversion in the main channel. No clear limit about the water discharge ratio is given in the literature for the formation of this recirculation area. Bulle (1926) shows qualitatively a dependence of this phenomenon on the diversion angle, highlighting that separation is more likely to occur for angles lower than 90º, whereas for orthogonal or higher angle

diversions no recirculation area is observed in the main channel. His test with a narrow lateral branch also shows no separation zone in the main channel, a fact which is coherent if it is considered that a narrower lateral branch will provoke less curvature in the streamlines for the same lateral pressure gradient. Numerical results reproducing Bulle's 30º experiment give similar results concerning the occurrence of this phenomenon (De Heer & Mosselman, 2004). However, the simulated recirculation area is found to be larger than the one measured in the experiments. Other numerical results carried out about 90º degrees diversion show no separation area in the main channel, although a decrease in longitudinal flow velocities is observed in the area next to the wall, as a consequence of flow expansion in this region (Neary & Sotiropoulos, 1996, 1999; Barkdoll, 1998). Laboratory measurements performed by Neary & Sotiropoulos (1999) are coherent with these results and provide slightly lower velocities than those found in the numerical calculations.

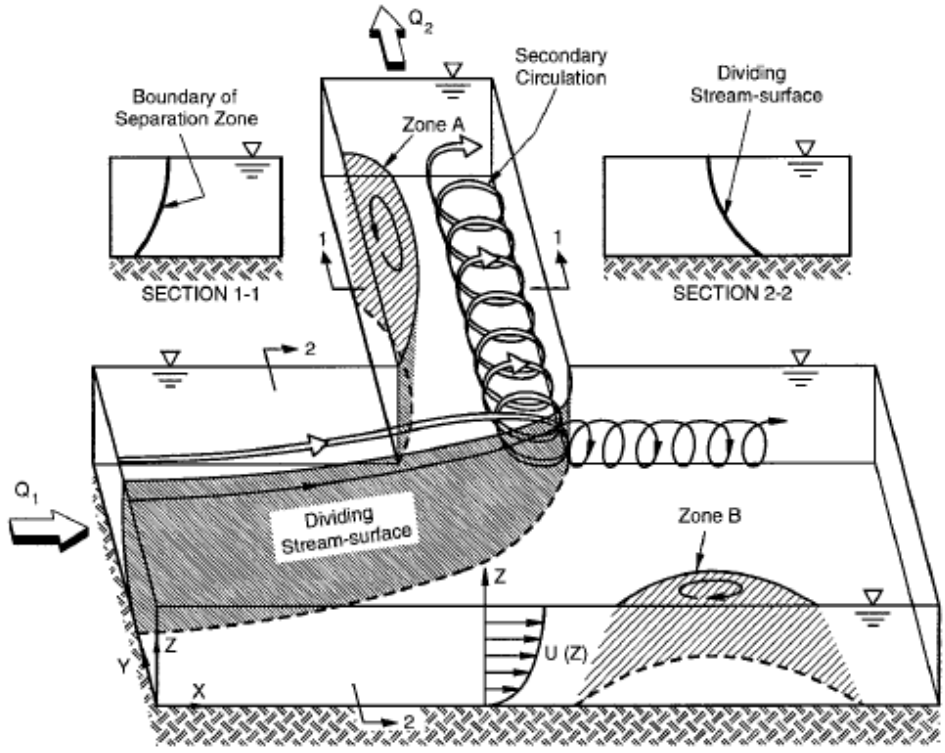

Figure 2.17. 3D flow patterns in a lateral intake as characterized by Neary and Sotiropoulos (1999)

Popp and Sallet (1983) carried out a similar experimental analysis on flow through a 90-degree tee junction in a duct and found negative velocities next to the wall opposite to the diversion, at an area located from approximately 2 to 5 channel widths downstream from the diversion. The interpretation of why separation was found in the closed duct and not in open-channel experiments is not clear and more studies under more varied conditions are

needed to clarify this point. Lastly, the occurrence of this main channel recirculation area causes flow contraction in the opposite wall (diversion side) and relatively high velocities in this area (Neary & Sotiropoulos, 1999, Khan et al. 2000).

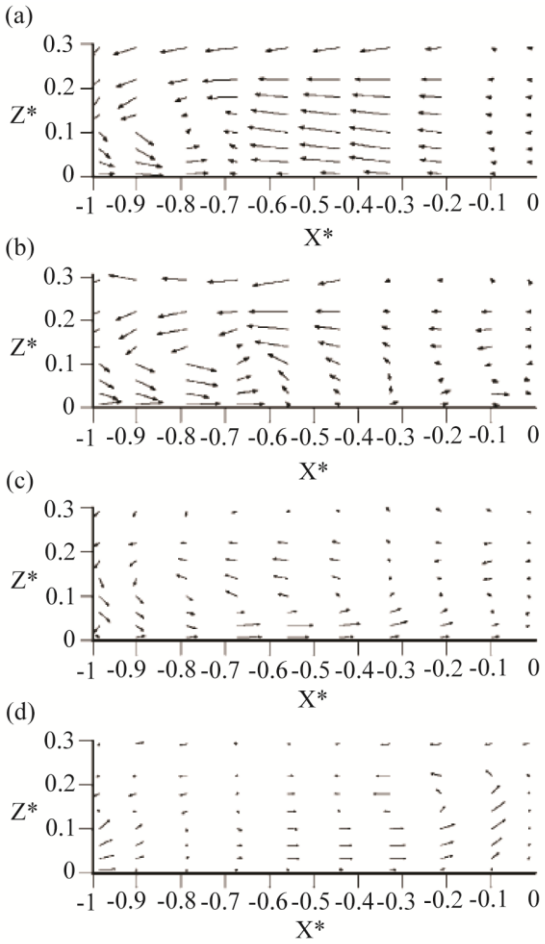

Figure 2.18. Vector velocity plots in different sections of the lateral branch (Y*=0.29 (a), Y*=0.73 (b), Y*=1.0 (c), Y*=2.5 (d)), for a discharge ratio of 0.838 (lateral branch to upstream discharge). X*, Y*, Z* are made dimensionless dividing by channel width and Y*=0 corresponds to the intake inlet (Ramamurthy et al. (2007)

Both recirculation areas commented above are related with the curvature of the streamlines provoked by the pressure field associated with the presence of the diversion. The interaction of the curved flow with the walls of the main channel and the lateral branch cause the occurrence of two helical secondary flows which are described qualitatively by Neary and Sotiropoulos (1999) (Figure 2.17). In the lateral branch, the flow hits against the right wall (looking in downstream direction) and generates a clockwise helical secondary flow in the part of the section that is not affected by the recirculated flow. On the other hand, the part of the flow that follows the main channel is deviated towards the left wall and generates an anti-clockwise helical secondary flow. Both patterns are reproduced by

numerical and experimental results carried out by Ramamurthy et al. (2007) and Yang et al. (2009) (Figure 2.18).

Another general particularity of the flow associated with lateral intakes is the transversal asymmetry in the width velocity profile in the main channel in the area upstream from the diversion. Flow acceleration occurs in the area next to the wall of the lateral intake side due to the pressure gradient generated by the diversion, which counteracts the effect of the wall friction and provokes the highest longitudinal velocities to be found next to the wall (Barkdoll et al., 1998). Khan et al. (2000) carried numerical studies that also reproduce the mentioned effect. They compared their results with laboratory measurements performed by Shettar and Murthy (1996) and found them to be in good agreement.

Yang et al. (2009) carried out a combined numerical and experimental analysis to study the influence of the diversion angle in the flow patterns around the diversion area. Experiments were performed in a 45-degree lateral intake with a width ratio of 2.3 between the main channel and the lateral branch and under diverse conditions of velocity ratio between the incoming flow and the lateral branch. Paralelly, numerical tests were carried out simulating the laboratory model geometry and changing the diversion angle to 30º and 90º. The main conclusions were that the smaller the diversion angle and the smaller the velocity ratio are, the better uniformity for the intake flow is attained. On the other hand, for low angles relative width of the flow following the main channel is smaller, whereas the diverted flow occupies a larger proportion of the upstream channel width. Therefore, to obtain a uniform flow in the lateral branch and to avoid flow separation at the entrance, small angles such as 30º or 45º are required.

Concerning water surface levels, Bulle (1926) reports quite accurate measurements in the different diversion angle and discharge ratio conditions (Figure 2.13). As a general characteristic, a significant increase is observed in the stagnation point located at the downstream corner of the diversion entrance. From there, water surface level decreases slightly towards the main channel and quite sharply towards the lateral branch. The lowest point is found next to the upstream corner of the diversion entrance. The difference between water surface levels at the main channel and the lateral branch increases with an increasing diversion angle. Numerical results from Vasquez (2005) compare well with Bulle's results, for the case of a 30º diversion. Ramamurthy et al. (2007) also report similar water surface level differences between both branches in their experiments on 90º diversions. However, their numerical analysis highlights a significantly lower level difference and a very sharp increase near the stagnation point.

2.2.3 Previous conceptual models

Apart from experimental and numerical studies, some considerations have been done in the past to carry out a conceptual approach over the problem of flow distribution in fluvial diversions. Ryad (1961) took into account the similarity between flow in river bends and flow entering into a lateral intake, to establish an equation to calculate water depth difference between both sides of this branch. He also highlighted the influence of the helical secondary flow in the sediment motion, being it another cause of the disproportionate entrance of sediment into the lateral branch.

Ramamurthy and Satish (1988) developed a theoretical model for division of flow in a short lateral branch forming a 90º angle with the main channel, considering various width ratios between both of them. The model considers momentum, energy and mass continuity equations and makes the assumption of free flow conditions in the branch lateral branch. The main idea of the model lies on the similarity of flow configuration between the division of flow into a lateral branch and in a two-dimensional lateral conduit fitted with a barrier, which is used to estimate the contraction coefficient of the converging flow entering the lateral branch. A relation between water discharge ratio and Froude number in the main channel section downstream of the junction is found and compared with previous experimental data to validate the proposed theoretical model.

A more general approach was carried out by Ramamurthy et al. (1990) to estimate the discharge ratio between the lateral branch and the main channel of right-angled diversions, in terms of the Froude numbers in the main channel upstream and downstream of the junction (Figure 2.19). The following hypothesis are considered to

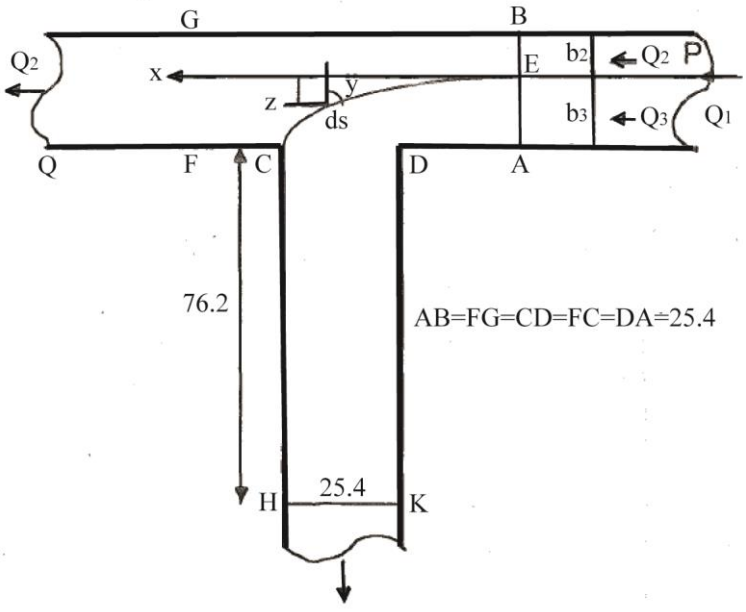

Figure 2.19. Scheme of the conceptual model developed by Ramamurthy et al. (1990). Lengths are expressed in centimeters and correspond to the experimental model used to test the results

study the characteristics of the flow: the main channel and the lateral branch have the same rectangular section and are horizontal; the incoming flow is subcritical; the flow at sections located sufficiently far upstream and downstream of the diversion is uniform; friction loss in the section ACDE and the energy loss along the streamline EC are negligible; and the depth variation from the beginning to the end of the dividing flow line (line EC) is supposed to have a parabolic shape. Applying momentum equation to section ACDE, the momentum transfer in the longitudinal direction from the main channel to the lateral branch is calculated. Then, momentum balance equation is applied in the main channel between upstream and downstream of the diversion and an equation is found that relates water discharge ratio to Froude numbers in the main channel, upstream and downstream of the diversion. Experimental studies were carried out to test the accuracy of the conceptual model and positive conclusions were drawn.

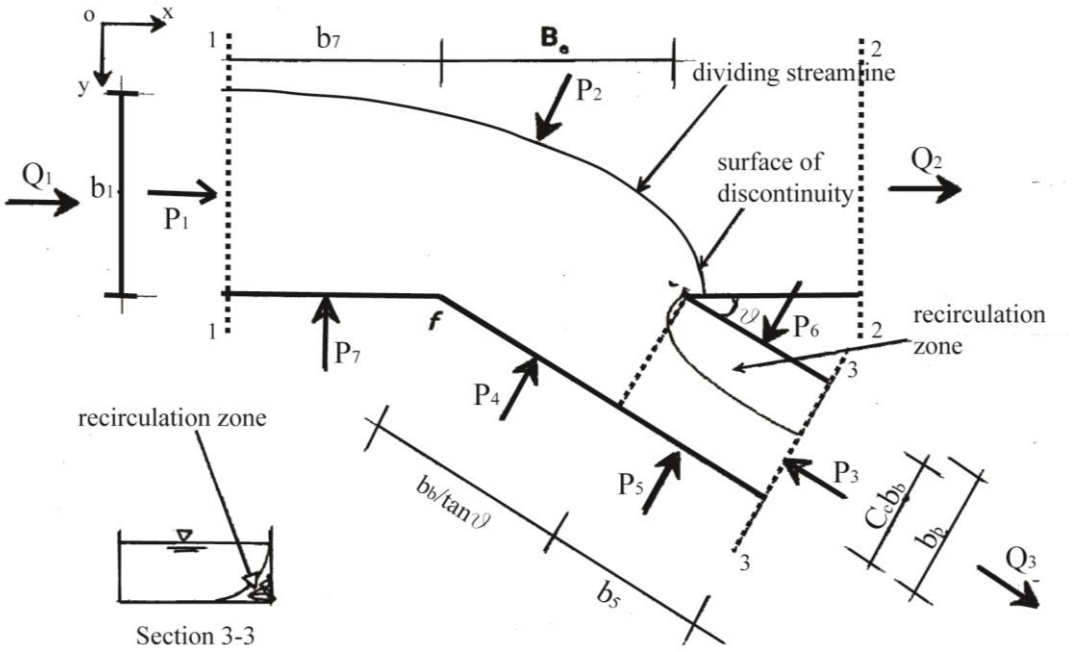

Figure 2.20. Conceptual model developed by Lama et al. (2002) for a 30-degree diversion with a narrow lateral branch in relation to the main channel width. Momentum balance is applied to the control volume located between section 1-1 and section 3-3.

A quite particular case was studied by Lama et al. (2002), consisting in a 30º degree diversion with a large width ratio that is, a significantly higher width in the main channel than in the lateral branch. They considered a control volume comprising the flow that enters the lateral branch and limited by the dividing stream surface and two sections upstream and downstream of the diversion (Figure 2.20). Momentum equations in *x* and *y* directions as well as mass continuity equation were applied in the control volume and a

theoretical relationship was developed for the discharge distribution at various flow conditions in the main channel and the lateral branch.

2.2.4 Particularities of the use of numerical models in fluvial diversions

A particular aspect concerning the use of numerical models to simulate the flow characteristics in fluvial diversions is the fact that flow is three-dimensional and highly turbulent complicates considerably the numerical computations. Therefore, the choice of an appropriate turbulence closure model to reproduce the turbulent patterns that occur in this area is a very important matter. Very diverse approaches are found in the literature, including the use of direct Navier-Stokes equations without considering turbulence (Neary and Sotiropoulos, 1996) and the use of turbulence closure models as Boussinesq (Khan et al. 2000, Vasquez, 2005), k-ε (Shamloo and Pizardeh, 2007; Omidbeigi et al. 2009), k-ω (Neary et al. 1999; Ramamurthy et al. 2007; Omidbeigi et al. 2009), RSM (Omidbeigi et al. 2009) and Spat-Almaras (Li and Zeng, 2009). Omidbeigi et al. (2009) carried out a comparison between different turbulent models including k-ε, k-ω and RSM, finding that the last was the one that provided the best comparison when contrasted to experimental results. A more complex approach was performed by Zhou and Zeng (2009), who used the LES model to simulate the diversion region and added isotropic velocity fluctuations at the inflow interface of this region to trigger the generation of resolved turbulence. This model was combined with the Reynolds-averaged Navier-Stokes model, which was applied to the rest of the domain. This approach proved to save computational effort in relation to other models and provided good results when compared to experimental data by Ramamurthy et al. (2007).

Another point to be considered when using numerical models to simulate lateral intakes is the grid's shape in relation to the system geometry. De Heer and Mosselman (2004) reproduced Bulle's experiments in a 30-degree diversion, and found that they had to establish a rounder angle in the numerical representation than in the real model, in order to minimize the truncation errors in the discretized equations due to deviations from grid smoothness and grid orthogonality. As a consequence, the recirculation areas of the main channel and the lateral branch were not well reproduced, being the former larger and the second smaller than in experimental observations. Using triangular instead of rectangular grid elements, Vasquez (2005) simulated the same Bulle's tests and found a better agreement regarding the shape and size of the recirculation areas.

2.2.5 Other aspects in the experimental analyses

Hsu et al (2002) carried out fixed bed laboratory experiments in a 90-degree diversion model and carried out an energy balance over a control volume including the diversion area, section of the upstream channel and the first stretch of each branch, based on the water depth and discharge measurements performed in the laboratory. The energy balance equation was applied as follows:

$$Q_u H_u \left(1-K_e\right) = Q_d H_d + Q_l H_l \tag{2.9}$$

Where Q refers to discharge, H to the energy head, subscripts u, d and l, refer to the main channel upstream and downstream of the diversion and the lateral branch respectively and K_e is the energy-loss coefficient across the flow division. H_u and H_d were considered to be approximately equal and an expression was obtained for K_e:

$$K_e = \left(1-\overline{Q_d}\right)\left[1-\frac{2\overline{Y_b}^3+\left(1-\overline{Q_d}\right)^2 \mathsf{F}_u^2}{\overline{Y_b}^2\left(2+\mathsf{F}_u^2\right)}\right] \tag{2.10}$$

In the equation (2.10) $\overline{Q_d}$ is the discharge ratio between downstream and upstream of the diversion in the main channel, $\overline{Y_b}$ is the depth ratio between the lateral branch and the upstream channel and F_u is the Froude number in the upstream channel.

Another experimental study in quite specific conditions was performed by Pirestani et al. (2007), in which they studied the influence of the location of a 60º diversion in different locations of a bend in a fixed bed model. A significant increase and a very sharp decrease of the longitudinal velocity are observed in the main channel, at the beginning and just after the end of the diversion entrance respectively. Based on the experimental measurements, the authors proposed equations for the decrease of the secondary flow strength associated to the flow in the bend and for the decrease of lateral flow momentum, caused both by the lateral intake. The equations were obtained empirically as a function of the discharge ratio between the lateral branch and the main channel, the intake location along the bend and the Froude number of the main channel.

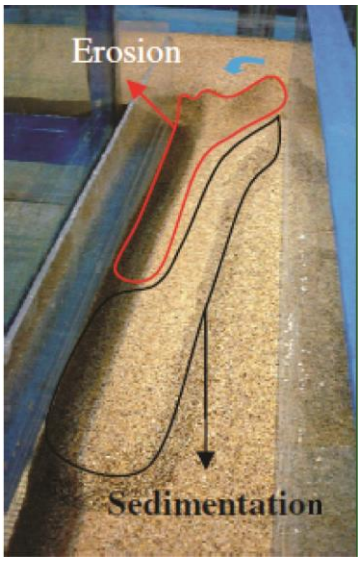

Figure 2.21. Erosion and sedimentation areas in the first stretch of the lateral branch. Figure obtained from Rezapour et al (2009)

2.2.6 Experiments with sediment transport

The main limitation of the numerical and most of the experimental studies on fluvial diversions for their application on the system morphology evolution lies in the fact that sediment transport has not been considered. Apart from the previously commented Bulle (1926) work, very few studies have been performed in diversion models over movable-bed, despite the importance of this topic and its practical application on the social and economic areas mentioned above. Ryad (1961) and Ordóñez (1974) are some of the authors that have dealt with this subject and have been commented before. However, some of the numerical analyses try to extrapolate the calculated velocity patterns to discuss how sediment behavior would be. Neary and Sotiropoulos (1996, 1999) calculates three-dimensional particle trace plots for different Reynolds numbers and discharge ratios, showing the complexity of the flow in the diversion area. From their results, sedimentation is expected in the recirculation area of the lateral branch whereas erosion is predicted in the opposite wall. Similar conclusions are drawn by different other authors without much further detail (De Heer and Mosselman, 2004; Vasquez, 2005).

Rezapour et al. (2009) carried out experiments on movable-bed conditions and under varied conditions of width ratio and discharge ratio between the lateral branch and the main channel. Froude number and Reynolds number in the main channel vary from 0.2 to 0.4 and from $2.5 \cdot 10^4$ to $5 \cdot 10^4$ respectively. Bed sediment was formed by sand with an average diameter of 0.8mm. Erosion is observed next to the downstream wall of the lateral branch even for low Froude numbers, and sedimentation is measured in the opposite branch coinciding with the recirculation area (Figure 2.21). For increasing Froude numbers both patterns extend downstream along the lateral branch. Additionally, erosion in the main channel in the area just downstream of the diversion is reported for high Froude numbers. Unfortunately, no detailed description of this erosion area is provided, neither measurements of bed level or details about its dependence on flow characteristics.

Moghadam et al. (2010) performed a laboratory analysis reproducing a common situation found in artificial lateral intakes, consisting in a trapezoidal lateral channel forming a 30º angle with the main channel. Concerning the flow characteristics in this situation, it is found that a greater amount of the flow at the near-surface layers is deviated towards the lateral branch, which that decreases the amount of sediment deviated. With regard to sediment distribution, it is found that sediment discharge in the lateral branch depends on

the main channel Froude number and reaches a minimum value for Froude numbers between 0.35 and 0.45.

Lastly, another important point that has been studied in the past regarding sediment distribution in fluvial diversions is the influence of the main channel curvature and the relative position of the diversion entrance. Rocha (2005) reports some results and conclusions drawn by Habermaas (1935) in a study to which the author of this thesis was not able to access (Figure 2.22). Experiments were performed with the lateral intake in different positions with relation to a bend in the main channel, namely, in a straight section (a); in the inner bank of a bend, at the beginning (b) and at the end (c) of it; in the outer bank of a bend, at the end (d), in the middle (e) and near the beginning (f); just before the beginning of the bend (g). In the cases (a) to (d), almost all the sediment discharge is captured by the lateral branch. However, when the diversion is located in the outer bank of the bend and near its beginning, the almost all the sediment tends to follow the main channel. The interpretation of this fact is that with this kind of geometry, the diversion plays the role of the main and straight channel, whereas the main channel is the branch that is exiting laterally in the final configuration. Brink (2004) carried out an experimental and numerical study focusing on the location of a lateral intake along the outer bank of a river bend, highlighting some conclusions about the optimal location of the diversion as a function of the total bend angle and the ratio between the curvature radius and the channel width. A deep analysis of velocity field along the bend was performed in order to evaluate the optimal location of the diversion in terms of higher diverted discharge ratio. The presence of the diversion was found not to influence on the secondary flow structure caused by the curvature in the main channel.

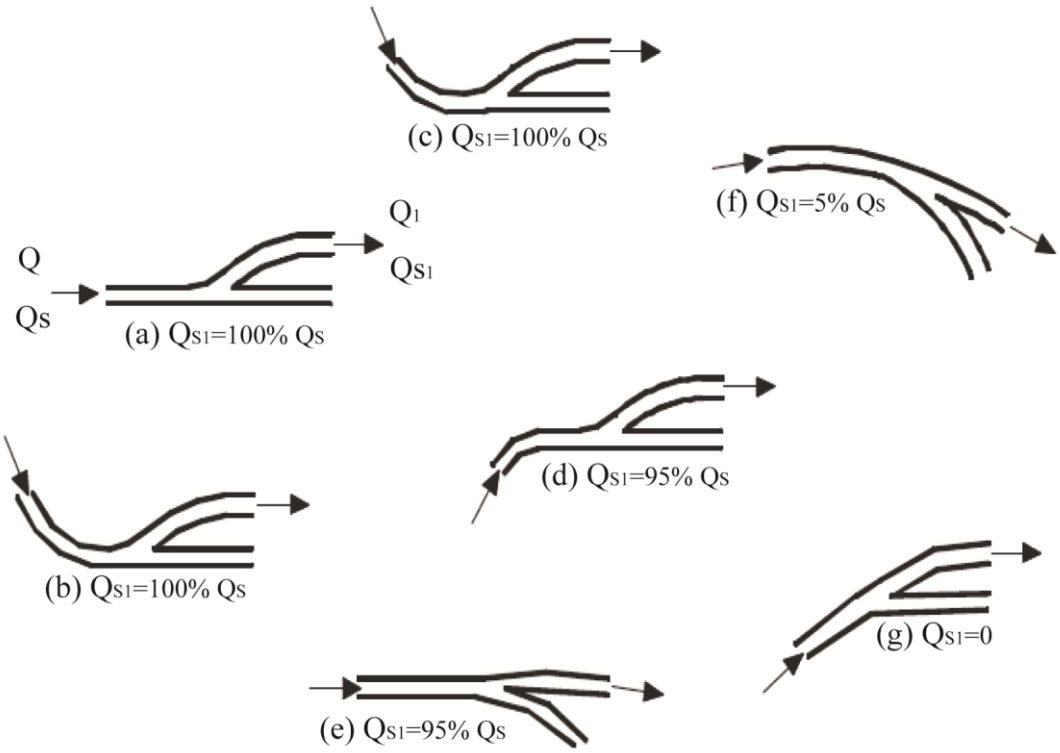

Figure 2.22. Proportion of sediment deviated into the diversion for different positions and orientations of the lateral branch in relation to main cannel geometry (adapted from Rocha (2005))

2.2.7 Sediment control at lateral intakes

Considering the problems associated to the disproportionate sediment distribution that are found in many situations due to the points commented in the previous section, several methods have been applied in the past to try to solve or minimize the entrance and subsequent deposition of sediment in lateral intakes. Although an appropriate location of the diversion with relation to main channel geometry has been proved to decrease the amount of sediment that is deviated (Brink, 2004; Rocha, 2005), in some situations this alternative is not possible and additional structures are needed.

Probably the most extended of this strategies is the use of submerged vanes (Odgaard, 2009). The main point on which this measure is based, consists in generating a secondary flow that enhances sediment transport depending on the interest in a certain situation. The flow characteristics around a submerged vane are a consequence of over-pressure at the front wall that faces the incoming flow and sub-pressure behind the vane. The consequence of this pressure field is a helical flow that extends downstream for a certain distance. These patterns have been studied in detail, both experimentally (Marelius and Sinha. 1998; Flokstra, 2007) and numerically (Sinha and Marelius, 2000; Flokstra, 2007). Submerged

vanes are usually built with a height of one third of the design water depth and forming an angle of around 15º to 20º with the longitudinal direction of the flow. On the other hand, Gupta et al. (2007) report the influence of the angle between the vertical and the end of the vane that faces the flow, on the strength of the vortex generated by the vane. An angle of 40º is concluded to be optimal.

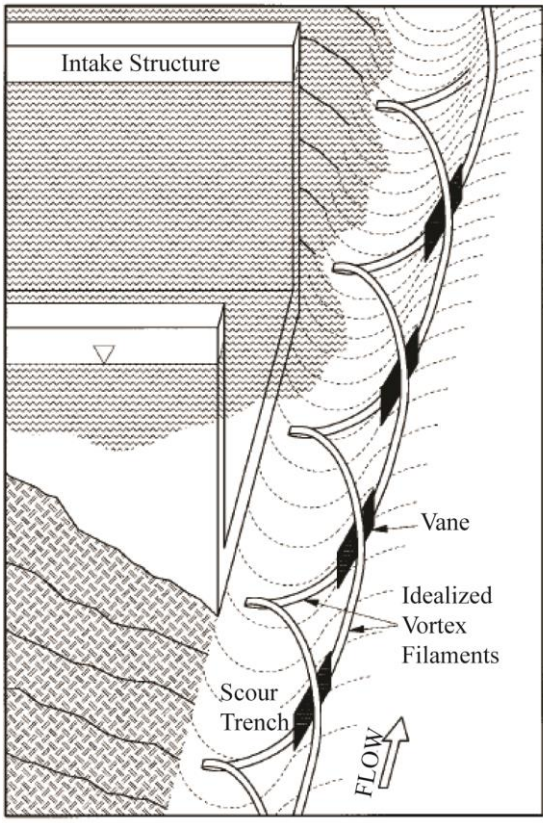

Figure 2.23. Scheme of the helical flow and subsequent transversal slope caused by submerged vanes located next to a lateral intake

Submerged vanes were originally applied extensively in river bends in order to minimize the scour problems in the outer bank of a bend, in those cases in which meander migration supposed a danger for human interests. The applied solution consisted in locating a series of submerged vanes oriented forming a certain angle with the main flow direction. In this way a secondary flow was generated that counteracted the natural secondary flow that is caused by the higher centrifugal force that acts on the faster near-surface layers of the flow. Associated with the secondary flow generated by the vanes, there is a transversal sediment transport that is interesting for engineering purposes. In the case of river bends, this sediment transport achieves in some way to balance the erosion that is caused by the centrifugal force over the outer bank. The results from a monitoring process of a river bend where submerged vanes were introduced can be found for example in Odgaard and Mosconi (1987).

When applied in lateral intakes, the objective of the submerged vanes is to generate a transversal slope that decreases the bed levels in the bank where the diversion is located, in such a way that bed load transport is less accessible for the diversion and the amount of sediment deviated is reduced (Figure 2.23). Odgaard and Spoljaric (1986) developed a conceptual model based on momentum equations applied to the vane, in order to evaluate the transversal component of the velocity induced by the vane and the subsequent transversal slope. Odgaard and Wang (1991a) provide a series of figures as a result of their

theoretical development, that allow to evaluate the increase or decrease of bed level provoked by the vanes, under different conditions of number of vanes, vane submergence and Froude number. Bed topography evolution has also been tested in the laboratory (Odgaard and Spoljaric, 1987; Odgaard and Wang, 1991b) and the measured transversal slopes show good agreement with the predicted values. A laboratory analysis specifically focused on submerged vanes performance on a lateral intake was carried out by Barkdoll et al. (1999). Two vane arrangements were tested, one with three rows of vanes parallel to the main channel axis and the other with three rows forming an oblique direction moving away from the intake side. The use of vanes reduce the sediment transport into the diversion between 30% and 40% and the sediment deposited at the intake entrance decreases around 50%. On the other hand Yonesi et al. (2009) tested the effects of different longitudinal distances between the vanes were tested (3*H*, 4*H*, and 6*H*, where *H* is the vane height over bed level) and two different oblique arrangements in relation to planimetric distribution of the vanes (Figure 2.24). The result was a redirection of the river thalweg towards the entrance of the diversion with the consequent reduction of sediment transport entering the lateral branch.

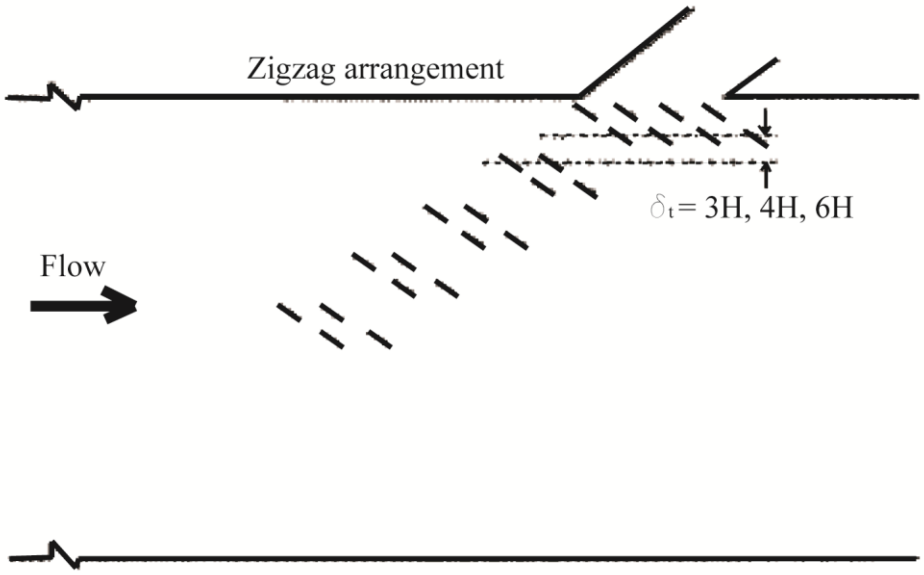

Figure 2.24. Zigzag vane arrangement proposed and tested by Yonesi et al (2008) with different transversal spacing between vane groups (Figure obtained from Yonesi et al., 2008)

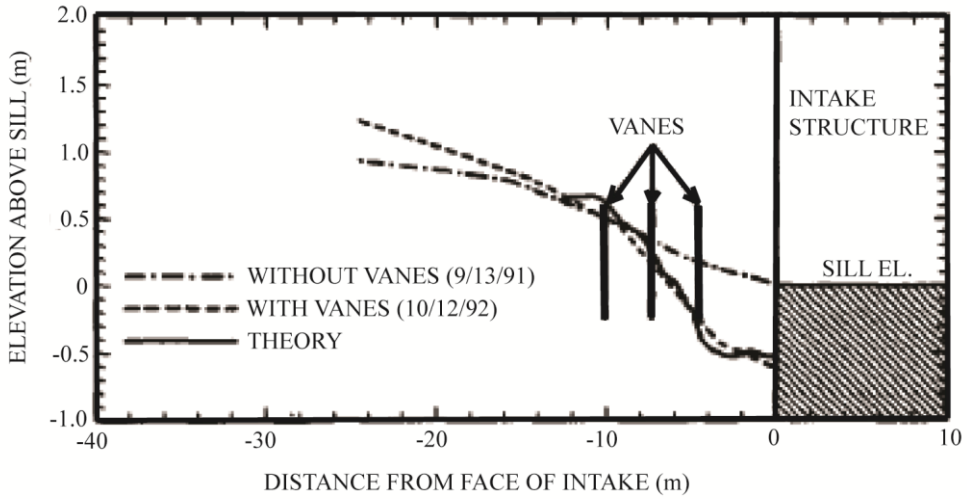

Figure 2.25. Bed profiles in Cedar River at Duane Arnold Energy Center intake structure before and after the installation of vanes (Figure obtained from Wang et al. 1996)

Field observations about cases of application of submerged vanes in real lateral intakes are also found in literature. Wang et al. (1996) studied the effect of the introduction of submerged vanes each next to two power plant water intake structures of the Cedar River (Iowa, USA) and the Rock River (Illinois, USA). In both cases an important redirection of the river thalweg was caused, generating a decrease of between 1 and 2m next to the intake inlet (Figure 2.25). A similar situation was studied by Nakato et al. (1990) concerning to another power plant river intake where vanes were introduced to solve previous sedimentation problems at the inlet. Taking into account the results of an experimental analysis in a laboratory model, two rows of submerged vanes were introduced parallel to the river longitudinal axis and next to the intake entrance. Their performance was monitored during three years and found to be excellent, with bed level decrease of around 1.5m and a significant reduction of sediment discharge in the lateral branch. Similar situations are reported by Odgaard (2009) in sand-river situations as several intakes in the Missouri River (Missouri, USA), Waikato River (New Zealand), Huntly Power Station in the Waikato River (New Zealand) and Conesville Staion in the Muskingum River (Ohio, USA). Submerged vanes were also introduced in the gravel-bed Kosi River (Nepal), with a satisfactory performance.

Apart from submerged vanes, other structures have been used as part of the sediment control mechanisms introduced to solve deposition problems related to lateral intakes. Nakato and Ogden (1998) recommended the use of a skimming wall for intakes on the

Missouri River. The skimming wall consists in a wall starting from the diversion-side bank, that forms a small angle with it for a certain length and then goes parallel to the bank. This strategy was suggested combined with the introduction of submerged vanes. The use of a skimming wall was tested in the laboratory by Barkdoll et al. (1999). The height of the wall needs to be not too low so that most of the sediment is prevented from entering the diversion, nor too high so that a hydraulic jump is avoided, a fact that would enhance turbulence and sediment resuspension at the entrance of the intake. Other kinds of sediment excluders can be found in Ordoñez et al. (1974).

Chapter 3: Experimental analysis of sediment transport in a 90-degree diversion

3.1 Introduction

As mentioned in the previous chapters, bifurcations are fluvial systems that have an important effect on aspects such as field irrigation, navigability and land management. From a fluid mechanics' point of view, the water flow that takes place in these systems is complicated and highly 3-dimensional. This has consequences related to sediment transport and the amount of material that is delivered into each of the downstream branches. Therefore, on a large time scale, these flow patterns determine stability conditions for bifurcations, that is, circumstances in which one of the branches tends to be predominant over the other. The abandonment of one of the distributaries can be a problem for the population when the river plays a crucial role in its daily activities (Bateman et al., 2009).

Bifurcations can be found individually or as part of a braided net, a more complex system in which they interact with confluences and other bifurcations (Bertoldi et al., 2006). Another aspect to be considered is the river granulometry which determines the time scale relationship between bank and bifurcation evolution processes (Miori et al., 2006) and discharge variations (Miori et al., 2008). These points have to be taken into account when applying hypotheses to these kinds of fluvial systems.

According to geometry between the different reaches that originate from the junction, diversions can be distinguished as bifurcations in which one of the downstream branches is parallel to the upstream reach, whereas the other branch exits laterally forming a certain angle with the former. This geometry can be found in many natural systems but also in artificial lateral intakes as the ones used for irrigation or power plants. Flow patterns in fluvial diversions differ from those in systems with a different geometry and this fact has consequences on the sediment transport that takes place there.

3.2 Experimental setup and procedure

The experiments were performed in a physical model located in the Fluvial Morphodynamics Laboratory of the Sediment Transport Research Group (GITS) in BarcelonaTech. The model consists of a 9-meter long and 20-centimeter wide flume (main channel) with a lateral branch connected 6 meters from the inlet. It is 2.5 meters long and 20 centimeters wide, as is the main channel. The lateral walls of the model are 35 centimeters high, providing enough space for a sufficiently thick sediment layer (15

centimeters) at the bottom and the water depth associated to discharges applied during the experiments. The model is constructed with methacrylate, and U-shaped metallic elements are placed regularly at the top of the channel in order to avoid deformation of the walls under water pressure. A schematic plant view of the model is displayed in Figure 3.1, showing the model and the recirculation circuit.

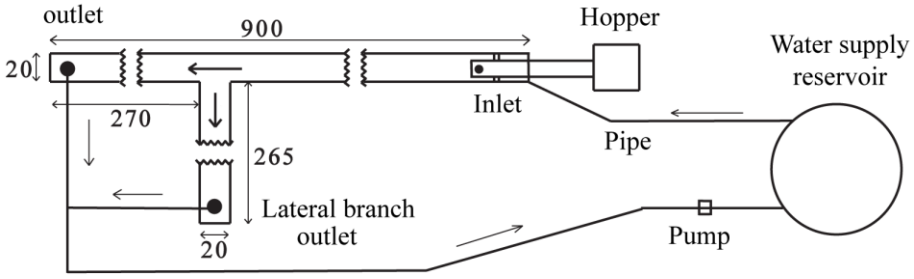

Figure 3.1. Plant view of the experimental model (distances in cm)

Water discharge is supplied from an 8-cubic-meter tank through a pipe that is able to provide up to 10 l/s to the experimental model. The recirculation circuit is schematized in Figure 3.1. At a short distance from the water inlet, a sieve is located to reduce flow turbulence. Experiments reported in this paper correspond to total discharges running from 3.5 to 6 l/s.

Sand of 0.25mm in diameter (σ=0,08mm) is used for the experiments. The sediment size distribution is described in detail in Figure 3.3 and Table 3.1. It is supplied by an Arquimedes screw hopper of variable rotation speed (Figure 3.2). Some previous experiments were performed to calibrate the relationship between its frequency and solid discharge. In the experiments carried out so far, solid discharge has been kept constant and equal to 5.5 g/s, which corresponds to the lower part of the frequency range available. Hopper capacity is about 35 litres, which correspond to approximately 70 kilograms of sand and four hours of experimentation. Sand is supplied just downstream from the turbulence dissipater.

Figure 3.2. Arquimedes screw hopper used to feed the model with sediment. The model inlet is under the hopper engine and follows a direction parallel to the

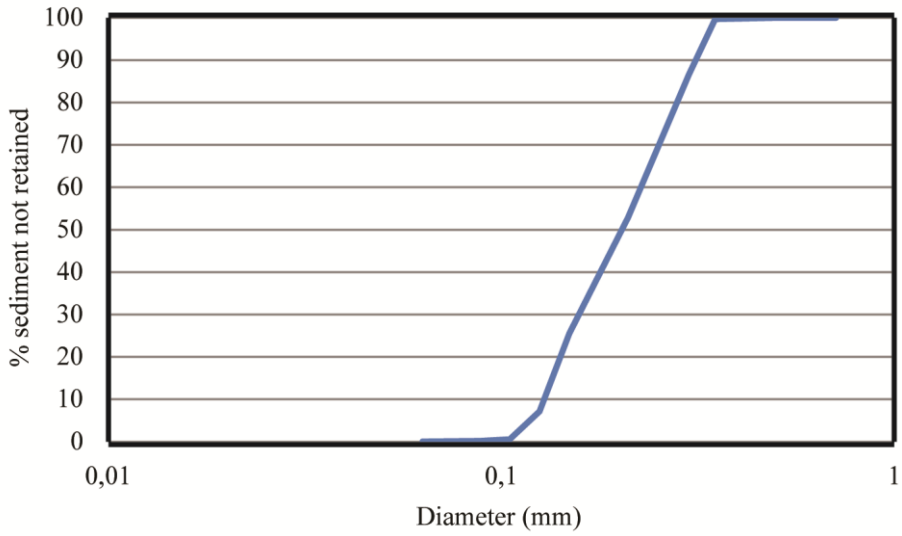

Figure 3.3. Granulometry of the sediment used in the experiments

Table 3.1. Size distribution of the sediment used during the experimental work

Sieve (mm)	Weight retained (g)	% Interval	% accumulated
0.710	0.020	0.010	0.010
0.595	0.027	0.014	0.024
0.500	0.668	0.336	0.360
0.350	26.006	13.093	13.453
0.300	66.983	33.723	47.175
0.210	54.242	27.308	74.484
0.149	36.515	18.384	92.867
0.125	13.070	6.580	99.447
0.105	0.738	0.372	99.819
0,088	0.240	0.121	99.940
0,063	0.050	0.025	99.965
Rest	0.070	0.035	100.00

Both water and sediment travel through the model and are measured at the end of each branch. Water discharge is measured by the volumetric method using a 132-liter can and timing how long it takes to fill it with water from the corresponding outlet. During the measurement, the top of the can is partially covered in order to properly identify the exact moment when the water overflows. Its volume is suitable for the applied discharges because it is high enough for the time error not to imply a significant discharge error and small enough to be emptied quickly by hand.

Solid discharge is measured using a sieve that captures sediment of 0.063mm in diameter (Figure 3.4). It is placed at the water outlet during a certain period of time, which depends on the amount of sediment that flows through each branch during a particular experiment. Trials are performed in order to check that sand is uniform enough and no material passes through the sieve. Sediment is removed from the sieve, put into plastic glasses and weighed, therefore obtaining the weight corresponding to humid sand. During the first experiment, 50 plastic glasses filled with sand coming from the model were dried during several days by heavy-light exposure and found to have a humidity (ratio between water weight and total weight) of around 20 percent. Deviations from this value were not important when translated into solid discharge error, so this value was used for estimating water content in all the subsequent samples.

Figure 3.4. Outlet of the lateral branch: settling tank and sieve for solid discharge measurements

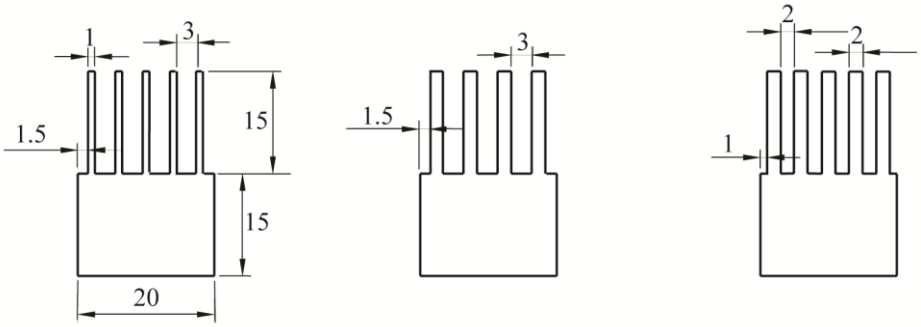

Figure 3.5. Different types of tooth-shaped methacrylate pieces used as boundary conditions at the end of the main channel and the lateral branch (lengths in cm.)

Boundary conditions at the end of both branches consist of tooth-shaped methacrylate pieces with different width (Figure 3.5 and Figure 3.6). Depending on the combination of pieces introduced at the end of the model, the opposition to the flow is different in each branch and different discharge ratios can be established for a constant total discharge. However, this system did not work as well as expected and the effect of changing the chosen designs was not significant, so all the experiments exposed in this study have been carried out with the same combination. The discharge ratio is only a consequence of total discharge, the hydrodynamics established in the diversion and the bed topography related

to it. On the other hand, an L-shaped methacrylate piece was placed in front of the tooth-shaped piece in order to avoid local scour in this area.

Each experiment lasts from 12 to 24 hours depending on the discharge and the time it takes to reach equilibrium. Therefore, because of the hopper capacity and in order to rest, experiments have to be carried out over several days. Moreover, the sand that is introduced into the hopper must be dry, otherwise it sticks together and the screw generates a cave at the lower part of the hopper preventing the sediment from going out, and causing a non-uniform solid discharge. Consequently, sand is collected at the outlet of each branch by two reservoirs where it falls to the bottom. At the end of every experiment day, sand is removed and spread over a wood sheet illuminated by several spotlights. The time to dry it is a limiting factor in the duration of the experiments.

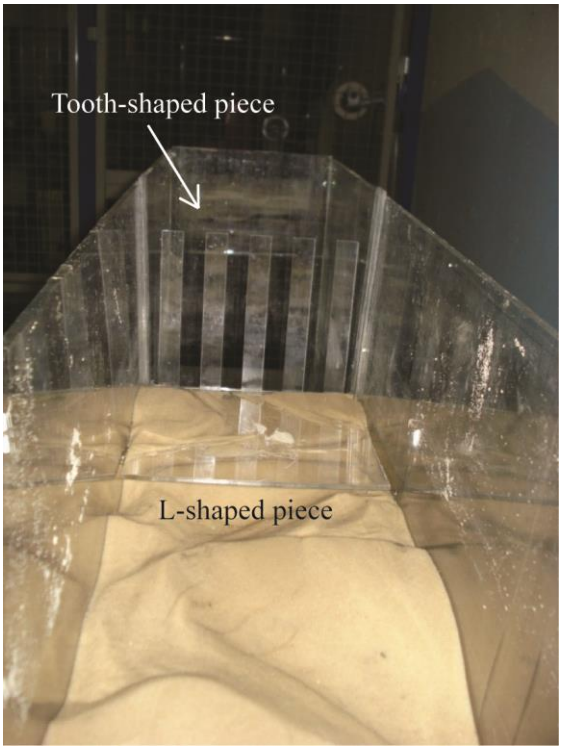

Figure 3.6. Image of the tooth-shaped methacrylate piece used as boundary conditions at the outlet of the branches. The L-shaped piece is introduced to avoid local scour at the front of the tooth-shaped piece.

When the experiment is restarted, special attention has to be paid in order not to modify bed conditions from the previous day. As discussed below, in some conditions a depression is formed in the main channel downstream from the diversion. If water is introduced into the model and water flows over the border of this depression, even slowly, there is a stability problem in its lateral slopes and the bed topography is modified in this area. Hence, before restarting the experiment we introduce water slowly into just the depression, in such a way that water penetrates into the pores of the lateral slopes. Once it is filled, water discharge is introduced gradually through the inlet. This procedure has been checked visually several times, and it was found that, if carried out carefully, it causes no alteration of bed topography in the diversion area.

As mentioned in the introduction of the thesis, the model has a special piece at the diversion that connects the lateral branch to the rest of the model (Figure 1.11). This piece is interchangeable so that by changing it the lateral branch can be oriented in different

directions We have constructed pieces for setting the lateral branch at an angle of 30º, 60º and 90º in relation to the main channel. Moreover, each of these pieces can be set at different heights, establishing a step of a certain height over the main channel. However, these two variables have not been changed in the present study, the angle of the diversion has been kept to 90º and no step has been applied artificially between the lateral branch and the main channel.

Each experiment is started from a flat bed condition and evolution is left until equilibrium is reached. Periodical measurements of water and solid discharge at the inlet and both outlets are taken every hour, as well as bed and water surface heights every 25cm, using transparent rulers attached to the walls of the model. The first measurement is started 10 minutes after the beginning of the experiment and each set of measures lasts around 30 minutes, so there are 30 minutes between measurements to check other elements of the model or start the data process.

Equilibrium is identified when water and solid discharge flowing through both branches is constant in time and their addition is equal to water and solid discharges introduced at the inlet. Another aspect taken into account for equilibrium identification is bed topography at the diversion area. Bed heights at several points are used as a reference for this purpose. Some of these variables, especially solid discharge, oscillate significantly in time, so the constancy refers to their average value during a specific period of time.

Once equilibrium is achieved, some videos of laser projections over different vertical planes are taken in order to identify the main flow patterns. Laser light is reflected in the particles that go through the plane so that their trajectories can be identified. Despite the turbulence and irregularities of the flow, some characteristics can be identified as described later. Furthermore, bed heights in the diversion area are measured when there is no water in the model in points forming a grid of 2cm x 2cm, in order to get an approximate bathymetry of the zone.

3.3 Results

First of all, a qualitative description of the system evolution is provided (Figure 3.7). At the beginning of all the experiments, an erosion hole is formed next to the downstream wall of the lateral branch (1) due to the secondary flow caused by flow curvature and pressure distribution in this area. At the same time, sediment is deposited in the recirculation area next to the opposite wall (2).

The erosion hole of the lateral branch expands progressively to the area of the main channel just downstream from the diversion and forms a large depression with no local bed forms in it (3). Bathymetry in this zone becomes deeper than in the lateral branch. Simultaneously, bed level in the lateral branch keeps rising as a consequence of the excess sediment that is introduced into it. According to Lane, sediment balance slope has to increase in order to enhance sediment transport and therefore, accretion must occur in the upstream part of the branch.

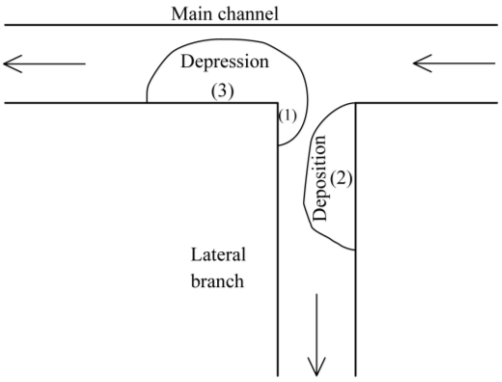

Figure 3.7. Scheme of the erosion and deposition areas observed in the vicinity of the diversion

Once the depression starts to form, different behaviors have been observed depending on the experiment conditions. For high total discharges, the system evolves so that the depression in the main channel increases its depth until a certain point of equilibrium is reached. In these conditions, the vast majority of sediment (over 90%) is deviated into the lateral branch, although water discharge is higher in the main channel. On the other hand, for low total discharges the depression is progressively filled with sediment until it disappears and the system reaches a state of equilibrium, where bed topography has uniform characteristics all along the main channel. In this situation, solid discharge is higher in the main channel than in the lateral branch and the system reaches an equilibrium at which water discharge in the lateral branch is very low.

3.3.1 Water discharge

In Figure 3.8, time evolution of the water discharge ratio between the main channel and lateral branch downstream from the diversion is shown for the different total water discharges.

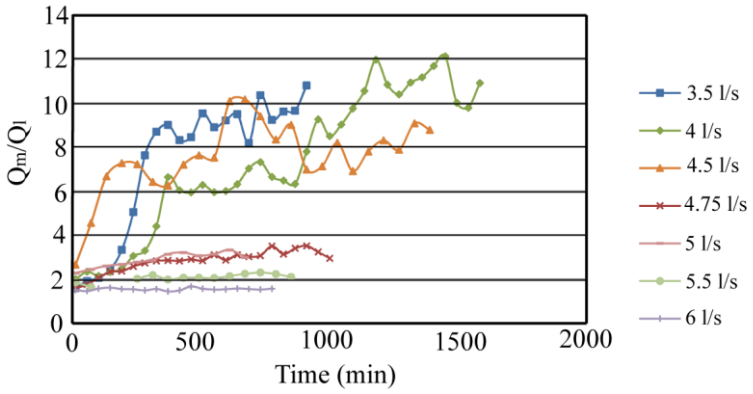

Figure 3.8. Time evolution of water discharge ratio (Q_m: main channel discharge downstream the diversion; Q_l: lateral branch discharge)

We can see how the system reaches a more unbalanced configuration for lower discharges according to the water discharge ratio. In the experiments with 3.5 l/s, 4 l/s and 4.5 l/s, the depression was not present in the equilibrium. We can observe a significant separation between these experiments and those with a higher discharge, suggesting that the presence of the depression encourages the deviation of a higher proportion of water discharge toward the lateral branch. In Table 3.2, we can see the discharge values corresponding to equilibrium states for the different experiments. We also see how, for a high discharge, an increase of upstream value implies the same increase in lateral branch discharge without modifying the amount of flow that goes straight into the main channel.

Table 3.2. Water discharge distribution in the equilibrium state for varying total discharge

Total discharge (l/s)	Main channel (Q_m, l/s)	Lateral branch (Q_l, l/s)	Discharge ratio (Q_m/Q_l)	Solid discharge ratio (Q_{sm}/Q_{sl})
3.5	3.18	0.32	9.93	1.75
4	3.66	0.34	10.76	2.46
4.5	4.03	0.47	8.57	1.25
4.75	3.64	1,11	3.28	0.08
5	3.79	1.21	3.13	0.09
5.5	3.79	1.71	2.22	0.08
6	3.66	2.34	1.56	0.09

Finally, in Figure 3.9 the water discharge ratio corresponding to a state of equilibrium is plotted versus the total discharge introduced from upstream. A sudden decrease in this ratio, corresponding to an increase in the lateral branch discharge, can be observed for a value of 4.5 – 4.75 l/s of total discharge.

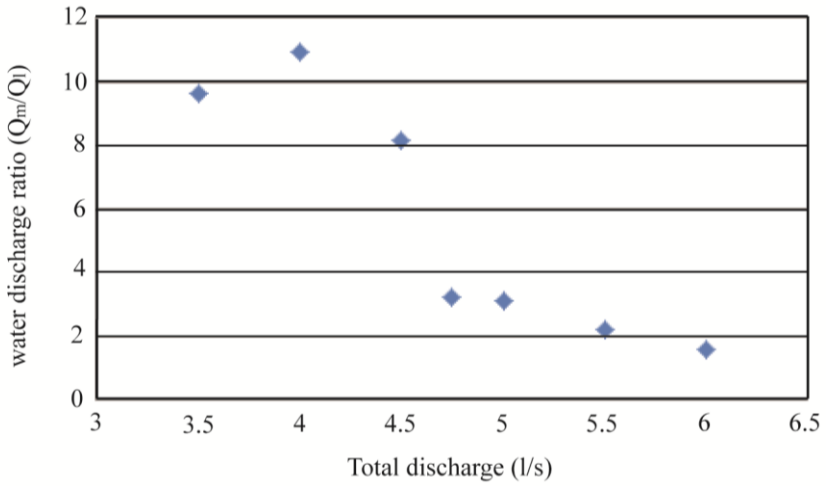

Figure 3.9. Equilibrium water discharge ratios plotted against total water discharge

3.3.2 Sediment discharge

Regarding solid discharge, Figure 3.10 illustrates a significantly different behavior between high and low discharges. In the first case, most of the sediment deviates into the lateral branch, giving rise to low solid discharge ratios of around 0.1. On the other hand, low discharges lead to situations where solid discharge in the main channel is higher than in the lateral branch, although these situations are less unbalanced and solid discharge ratios keep between 1.5 and 2.5. However, it is interesting to highlight that at the beginning of these experiments there is a phase during which the solid discharge ratio is less than one, that is, solid discharge is higher in the lateral branch. As shown below, this phase corresponds to the transitory formation of the depression in the main channel downstream from the diversion.

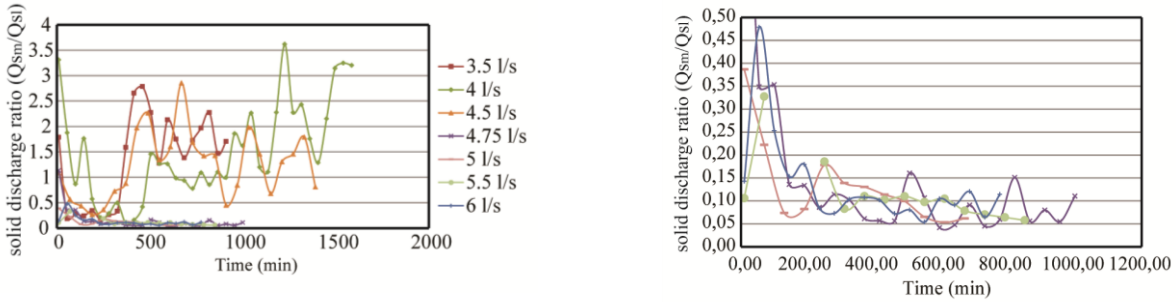

Figure 3.10. Time evolution of solid discharge ratio (Qs_m: main channel solid discharge; Qs_l: lateral branch solid discharge). The figure on the right shows a detail of the high discharge experiments

It should be observed that the important oscillations reflected in the measured values of this ratio are due to the variability of solid discharge caused by migrating bed forms. Therefore, ratio values corresponding to equilibrium are obtained by averaging solid discharges over an

appropriate period of time during which the mean value is nearly constant. These values are plotted against total discharge in Figure 3.11.

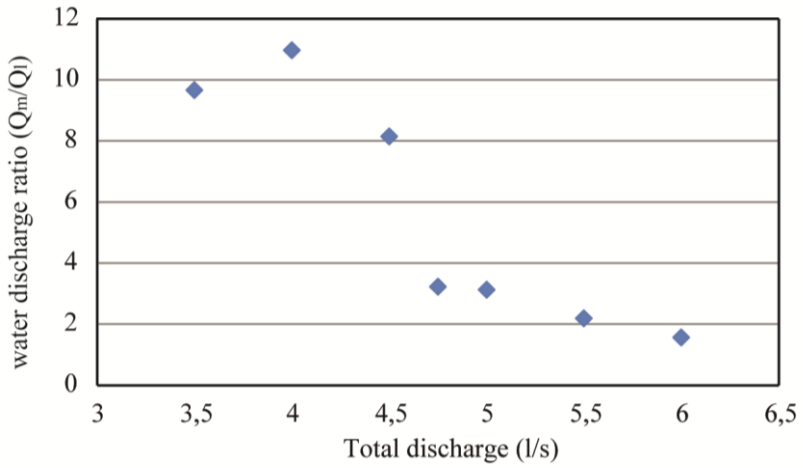

Figure 3.11. Equilibrium solid discharge ratios plotted against total water discharge

It is also interesting to calculate sediment concentration in both branches, calculated as the ratio between solid and water discharge (Table 3.3). The obtained results show that, although there is always a higher concentration in the lateral branch, those experiments in which the depression remains at equilibrium present a significantly higher concentration ratio between the lateral branch and main channel concentrations. The decrease in the concentration ratio that is observed for the experiments with depression as discharge rises is associated with the increase in deviated water discharge that does not correspond with a further increase in sediment deviation.

Table 3.3. Concentration values (solid discharge over liquid discharge) in both branches and at equilibrium

Total discharge (l/s)	Main channel (vol.sed/vol.water $*10^{-4}$)	Lateral branch (vol.sed/vol.water $*10^{-4}$)	Concentration ratio (C_l/C_m)
3.5	3.79	20.90	5.57
4	2.59	11.91	4.87
4.5	1.95	13.85	7.85
4.75	0.48	17.33	42.33
5	0.34	13.47	43.77
5.5	0.37	10.84	30.59
6	0.42	6.71	16.52

3.3.3 Bed erosion downstream from the diversion

As mentioned above, a wide and deep depression develops progressively in the area downstream from the diversion in the first part of all the experiments (Figure 3.7), disappearing only in those with low water discharge. The evolution of this depression is described in terms of bed height measurements at the lateral gage which is closer to the diversion and attached to the wall of the

lateral branch side (Figure 3.12). This point corresponds approximately to the maximum depression depth.

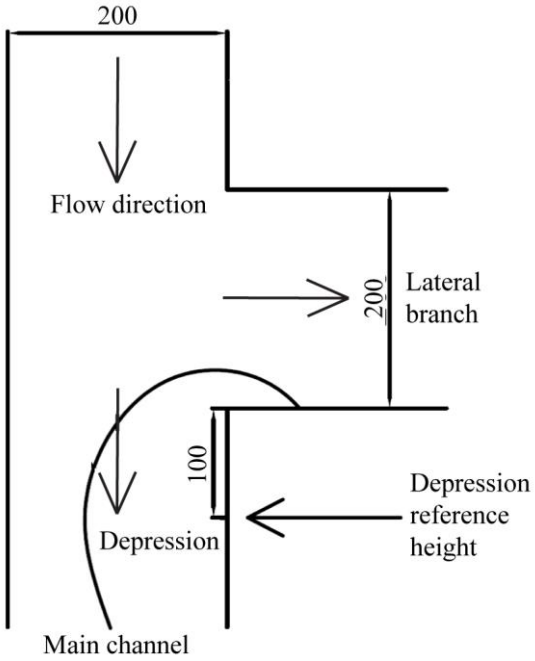

Figure 3.12. Scheme of the diversion area with the point where the reference depth of the depression (Figure 3.13) is measured

Figure 3.13 shows the time evolution of the main channel depression depth in all the experiments carried out in this study. A different behavior is appreciated below and above a total discharge of 4.5 l/s. In the first case, after a phase during which the bed deepens, the hole is filled again until equilibrium. In this state, there is no discontinuity in bed topography along the main channel between upstream and downstream the diversion so that bed forms migrate through the diversion area without interruption. Over this value, the depression remains until equilibrium is reached and its depth increases with increasing total discharge. For values higher than 6l/s and the present thickness of the sediment layer, the depression reaches the methacrylate base of the model and results are no longer valid.

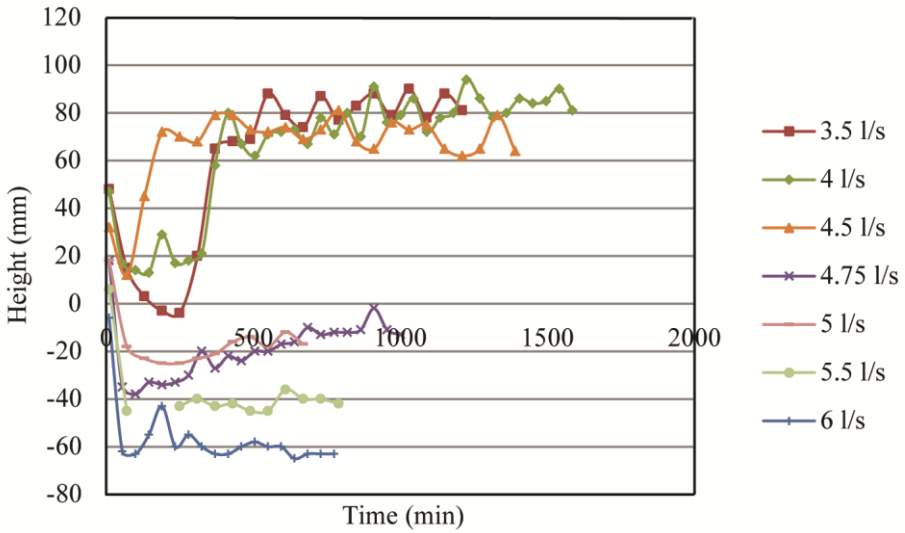

Figure 3.13. Time evolution of bed height at control point 33 (close to the depression's deepest point)

Figure 3.14 shows how the previous comments are reflected in the bathymetry corresponding to the state of equilibrium for 4.5l/s (without depression) and 5.5l/s (with depression). The depression area is observed downstream from the diversion for 5.5 l/s, with higher depths next to the wall of the lateral branch side, while for 4.5l/s the bed forms keep traveling downstream without interruption. In this case, only a small erosion area is observed next to the right wall of the lateral branch, caused by flow impact against this wall and subsequent secondary flow. Another remarkable difference between both bathymetries is that the deposition area in the lateral branch is considerably larger for 4.5 l/s, leading to lower discharges through this branch.

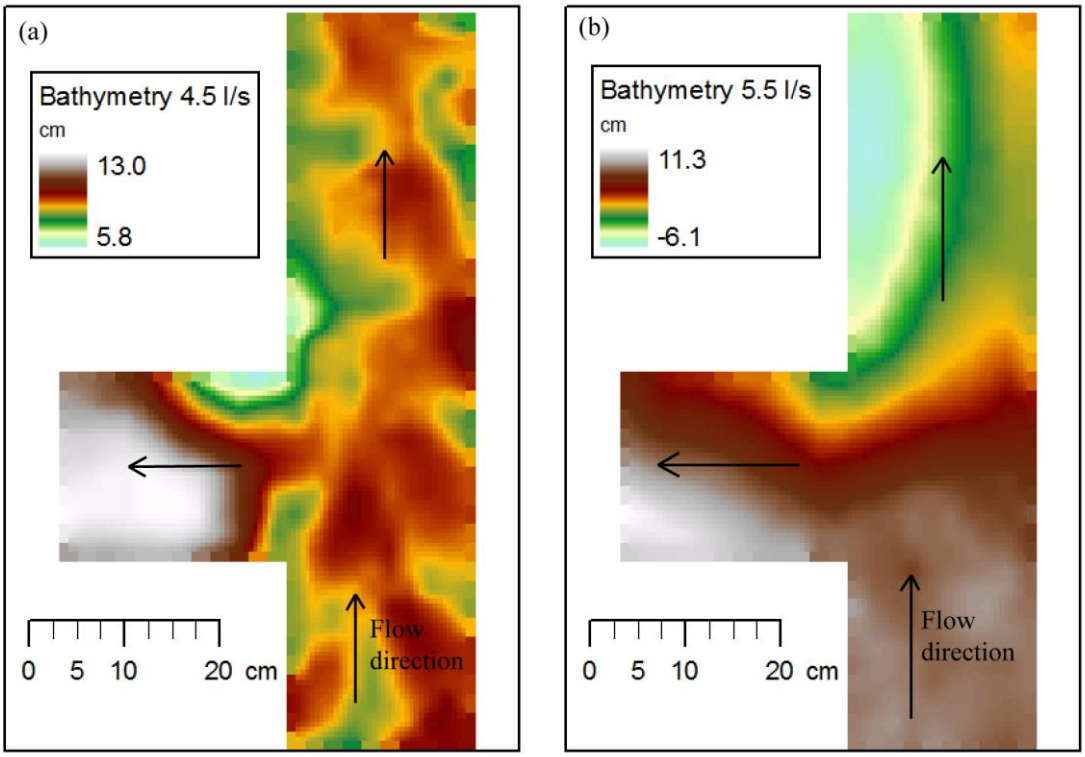

Figure 3.14. Bed topography in the diversion area for 4.5l/s (a) and 5.5l/s (b). Measures were taken once the equilibrium had been achieved

3.4 Discussion

When comparing the results referring to sediment discharge and the depression observed in the main channel, it can be observed that those cases in which the depression remains in equilibrium coincide with those with a higher sediment discharge through the lateral branch than the main channel (Figure 3.15). This fact suggests a relationship between both observed patterns, the appearance of the depression and the deviation of sediment into the lateral branch. If we look closely at the results of the experiments with low discharge, we can see that there is a certain lag between the moment when the depression starts to fill up and the beginning of the decrease in lateral sediment discharge, suggesting that the depression and mainly the hydrodynamics related to it are the cause for the sediment deviation and not the opposite.

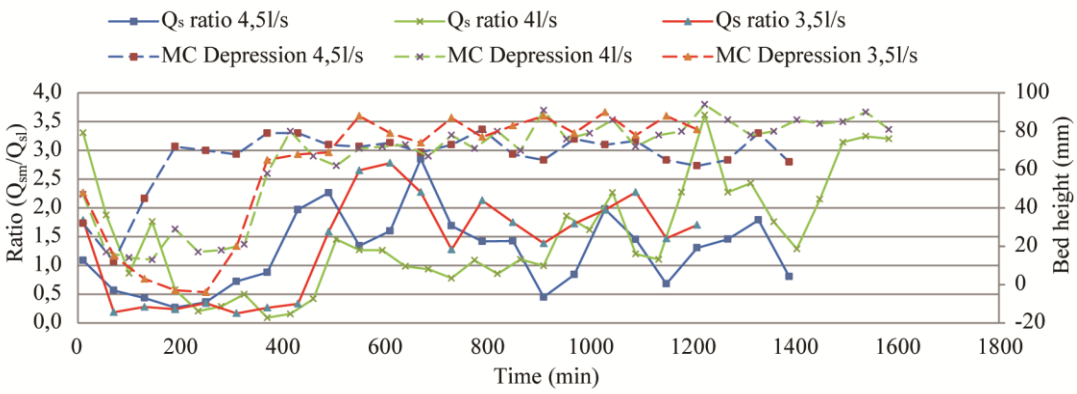

Figure 3.15. Comparison of time evolution for solid discharge ratio and bed height in the main channel for those experiments in which the depression is not present in the equilibrium configuration (3.5l/s; 4l/s; 4.5l/s)

Preliminary visual observations of suspended sediment movement help to recognize flow patterns in the diversion area, although the situation is considerably chaotic, with a high variability in space and time. Thus, in those situations when the depression is present, either at the equilibrium of high discharges or the transitory of lower ones, a permanent high bed point remains approximately in front of the entrance of the lateral branch. At this point, migrating bed forms coming from upstream disappear and do not move into the depression. At the downstream face of this high point (upstream slope of the depression), a horizontal axis vortex is formed parallel to the lateral branch and similar to those that appear downstream from the bed dunes due to pressure distribution, which stops the sediment from traveling as bed load. The position of this vortex in regards to the lateral branch causes a stretching phenomenon in such a way that sediment coming from upstream is sharply deviated and transported into the intake (Figure 3.16). Observations carried out with a laser projected in vertical planes show the movement of sediment particles in concentric circumferences (Figure 3.17). Although the flow is highly turbulent, an increasing trend in vortex size is observed in videos as the laser projection plane approaches the intake side.

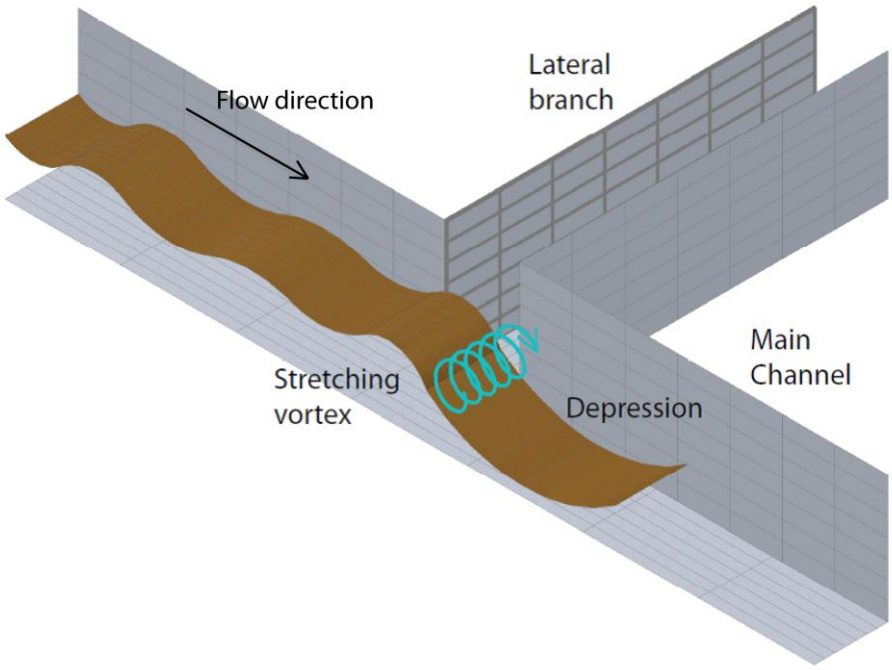

Figure 3.16. Horizontal axis vortex and stretching phenomenon formed at the depression downstream from the diversion

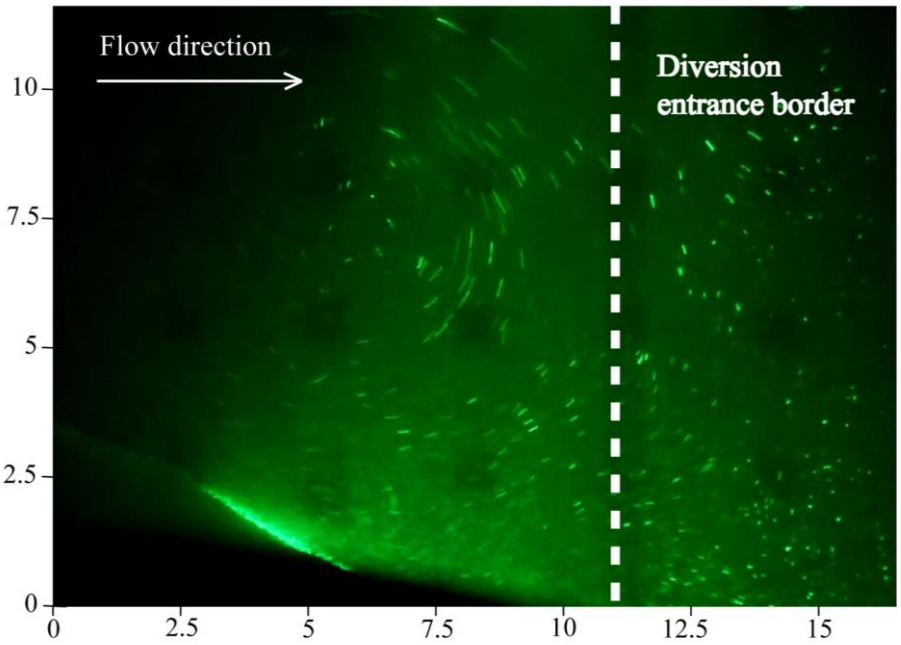

Figure 3.17. Laser image of the stretching vortex formed in front of the entrance of the lateral branch (axes correspond to scale in centimeters in the laser plane of projection)

The previously mentioned mechanism is able to deviate most of the sediment into the lateral branch. However, some of the solid discharge traveling next to the wall opposite the diversion changes its direction, but not enough to enter the branch, and falls into the depression. In this zone, vertical axis vortexes are formed intermittently, resuspending sediment and making it available for the upper layers of the flow. Depending on the moment and the point of

resuspension, some of this sediment is carried back to the diversion area and mixes with the flow that enters the lateral branch and some joins the main flow that continues into the main channel.

Sediment balance in the depression is determined by the input, represented by the part of upstream solid discharge which is not sufficiently deviated by the horizontal vortex and its related stretching phenomenon, and the output, corresponding to the sediment that is resuspended by the vertical axis vortexes formed around the central part of the depression. A preliminary interpretation indicated that vertical vortexes are related to the angular momentum associated with the flow that goes into the lateral branch. High discharges in the lateral branch imply the formation of stronger and more frequent vortexes in the depression, causing a higher resuspension. Therefore, bed depth increases, as well as the slope in the upstream face of the depression, making it easier for the sediment to fall into it without deviating toward the intake. The equilibrium depth of the depression is the one in which both mechanisms balance each other out. As higher total discharges imply higher discharges in the lateral branch (Table 3.2), they also entail deeper and larger depressions (Figure 3.13).

The high entrance of sediment into the lateral branch exceeds its transport capacity, and deposition occurs with the corresponding increase in bed slope. Therefore, bed height at the beginning of the lateral branch rises, blocking its entrance and diminishing its discharge. The system evolves until equilibrium is reached between bed slope, water and solid discharge. For a low total discharge (Figure 3.18), during the first part of the experiment the discharge through the lateral branch is high enough to develop the depression in the main channel, although smaller than in the high discharge cases (A). However, sediment deposition in the recirculation area causes the blockage of the lateral branch, provoking a refilling of the depression (B) and changes the hydrodynamic patterns in such a way that the amount of sediment that is deviated decreases and becomes lower than in the main channel (C). The system then adjusts with some erosion in the lateral branch to balance the sediment deficit caused by the horizontal vortex disappearance and stretching phenomenon. However, the final discharge deviated is not high enough to develop erosion in the main channel in the same way as in the first stages of the experiments.

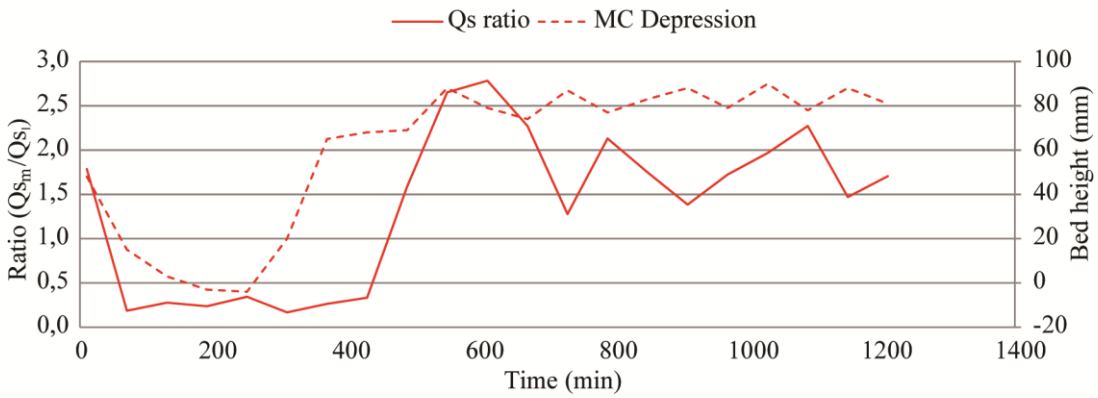

Figure 3.18. Time evolution of solid discharge ratio and depression bed height in the experiment with 3.5l/s of total discharge. (A: formation of the depression; B: refilling of the depression; C: decrease in lateral branch solid discharge)

Lastly, some comments on the formation of the depression should be made. According to the results, the depression is maintained while water discharge through the lateral branch and the corresponding angular momentum associated with flow are high enough to generate a secondary flow that erodes the depression area. Our preliminary interpretation was based on the relation of the occurrence of the pit to the angular momentum associated to the lateral branch flow. Figure 3.20 shows the evolution of lateral angular momentum flow in time, which was calculated as:

$$L_{lb} = \rho v^2 Sd = \rho \left[\frac{Q_l}{0.5 B y_{lb}} \right]^2 \left(B y_{lb} \right) \left(h_{lb} - \frac{y_{lb}}{3} \right) \qquad (3.1)$$

Where ρ is water density, Q_l is water discharge through the lateral branch, B is branch width, y_{lb} is maximum water depth at the entrance of the lateral branch and h_{lb} is water surface height over the reference level used to calculate angular momentum (level zero adopted in the experiments). Section geometry has been simplified considering bed topography, assuming it has a triangular shape (Figure 3.19).

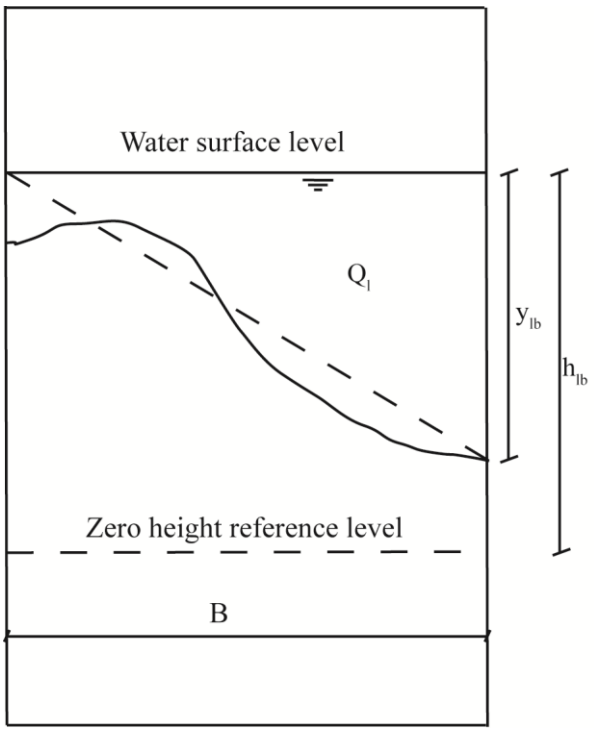

Figure 3.19. Scheme of the variables used in the calculation of the angular momentum

The discontinuous line separates the scenarios with and without depression, based on the moment when this pattern disappears in the experiments with low discharges (3.5l/s, 4l/s and 4.5l/s). Therefore, there seems to be a threshold value for lateral angular momentum, above which the secondary flow generated by the deviated flow is able to maintain the depression.

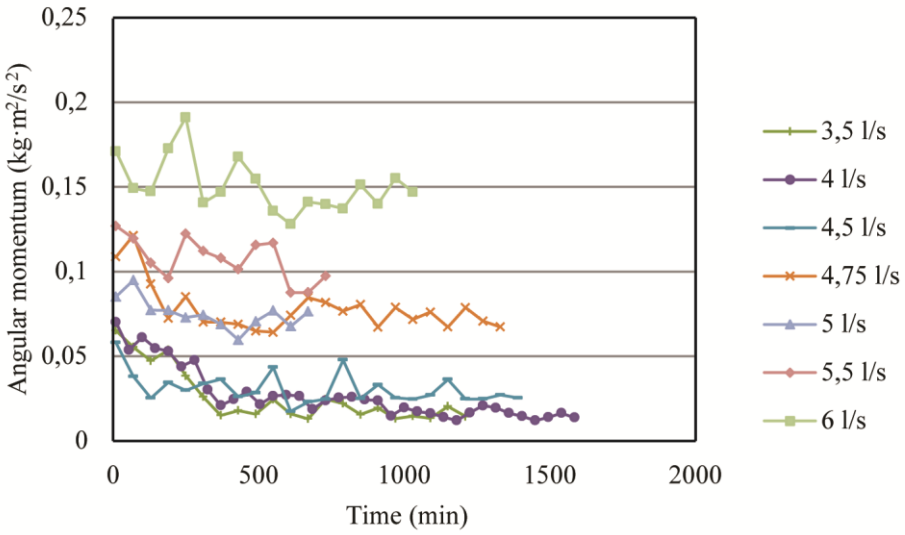

Figure 3.20. Angular momentum evolution in the lateral branch. Discontinuous line separates the situations with (above) and without (below) depression.

3.5 Summary

An experimental analysis has been carried out in order to study the influence of total incoming discharge on the water and sediment discharge ratios between the two branches of a 90-degree diversion. Different runs have been performed following the system evolution until reaching a

state of equilibrium, measuring water and sediment discharge through each of the branches as well as bed evolution along the entire model. The solid discharge introduced was kept around 5g/s whereas the range of total water discharge applied in the different experiments goes from 3.5l/s to 6l/s.

In the range of discharges analyzed, a remarkably different behavior has been observed between discharges above and below a certain threshold value, according to the bed topography and sediment discharge ratio. In our experiments, this threshold value has been found to be 4.75l/s.

The equilibrium of high discharges is characterized by the formation of a large depression in the main channel downstream from the diversion, the deviation of most of the sediment into the lateral branch (around 90% of total discharge introduced) and a relatively balanced water discharge ratio (around 60-70% of the total discharge goes through the main branch).

The equilibrium of low discharges is characterized by a continuous bed topography in the main channel between upstream and downstream, a higher sediment discharge in the main channel (around 70% of the total discharge introduced), and a very low water discharge in the lateral branch (around 10% of total discharge).

Observations suggest a relationship between the hydrodynamics patterns that occur in the diversion and depression area and the sediment deviation observed for high discharges. Visual and laser observations show the formation of a vortex next to the upstream slope of the depression and in front of the entrance to the lateral branch. The vortex blocks the movement of sediment particles and the associated stretching phenomenon absorbs them into the diversion.

Formation of the depression seems to be related to the amount of flow deviated into the lateral branch through an angular momentum balance, as the significant decrease of lateral branch discharge corresponds to the disappearance of the depression for lower discharges.

To sum up, this study highlights that the evolution of diversion systems is ruled by an interaction between diverted water discharge, bathymetry patterns and 3-dimensional flow patterns that imply a certain sediment deviation.

Chapter 4: Flow energy balance in a 90-degree diversion

4.1 Introduction

One of the main conclusions of the experimental results commented in the previous chapter is that in those runs in which the total discharge upstream from the diversion is higher than a threshold value, a vortex with its axis parallel to the lateral branch is formed in front of the entrance of the diversion and a large scour hole occurs in the first part of the main channel downstream from the diversion. This pattern influences on the turbulent characteristics that are observed in the diversion area. Therefore, the turbulence increase associated to the vortex occurrence is expected to cause a significant decrease in the energy levels downstream from the diversion, compared to those found upstream. This variation should be considered in those cases in which the pit is formed.

The theoretical models about bifurcations found in the literature include an equation of water level compatibility at the point from which both branches diverge (Wang et al. 1995, Bolla Pittaluga et al. 2003). On the other hand, uniform flow is considered in the branches downstream from the diversion. Assuming these hypotheses, eventual energy losses associated with the 3-dimensional patterns that may appear in the diversion area are neglected. Considering the observations commented in the previous chapter, this approach may be inappropriate for the study of flow in lateral intakes with an angle of 90º.

The objective of this chapter is to carry out an energy balance between upstream and downstream from the diversion. The experimental data obtained during the laboratory experiments are used to perform further calculations of the energy levels and energy losses associated with the local vorticity are calculated. The model is finally tested against the experimental data.

4.2 Further experimental results

During the experimental work, water discharge and sediment discharge evolution were measured in both branches and in the main channel upstream from the diversion. Moreover, bed and water surface levels were measured along the whole model and therefore, water depths at the last section of the upstream main channel and at the first section of each branch can be calculated, as well as flow velocities in these sections. Therefore, energy height (energy per unit weight) can be calculated as:

$$H = z + y + \frac{v^2}{2g} \qquad (4.1)$$

Where H is energy height, z is bed level, y is water depth, g is gravity acceleration and v is flow velocity, which is calculated in each section and each time considering the measured values of discharge and water depth. The water depth at a certain section is calculated as the average value amongst the two values measured at both side walls.

Figure 4.1 shows the energy height at the end of the main channel just upstream the diversion and at the beginning of each branch, calculated from the experimental data corresponding to sections A, B and E (Figure 4.3). Results for a discharge of 4.5l/s (below the threshold value) and 6 l/s (above the threshold value) are shown, highlighting that in both situations there is an energy loss in the flow that deviates towards the lateral branch, but only in the second case, this energy decrease in the flow that follows the main channel is observed. We associate the energy loss in the lateral branch to the effect of the walls, the sudden bed height increase and the vorticity patterns that are present in this area. On the other hand, the fact that the energy loss in the main channel appears only in the experiments with high discharge, that is, those in which the depression and the subsequent vortex are present, suggest that this flow structure has an important effect, and should be considered in a hypothetic energy balance involving the diversion area. The energy difference corresponds to the amount that the vortex needs to stay active. It should be noted that the energy height loss is around 1cm, which represents a significantly higher loss than that associated to the general energy slope of the main channel (between 1.5 and 2mm).

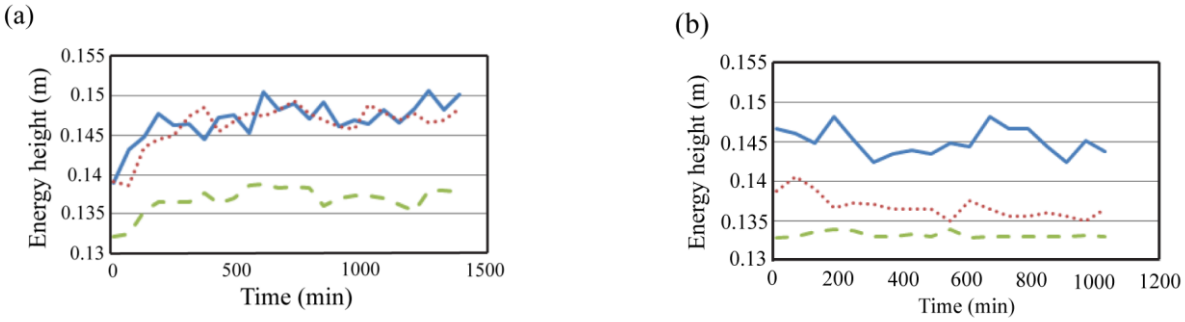

Figure 4.1. Energy height evolution in time upstream the diversion (continuous line), at the beginning of the main channel (dotted line) and at the beginning of the lateral branch (dashed line), for the experiments with 4.5l/s (a) and 6l/s (b)

4.3 Theoretical approach

In this section, we explain the reasoning for setting out an energy balance of the form shown in equation (4.2), where ΔP is the difference between the powers associated to the incoming and outgoing discharges and L_{vort} is the energy loss rate related to the vortex (measured as energy per unit time). The objective is to develop a simplified model that considers the main vorticity

patterns and to check its consistency with the experimental observations, which could be an important piece of models to describe flow and sediment distributions in diversions.

$$\Delta P = L_{vort} \tag{4.2}$$

Flow in the diversion area is 3-dimensional (Neary & Sotiropoulos, 1999; Khan et al., 2000; Omidbeigi et al., 2009), with several secondary flows taking place in both branches. In the lateral branch, near surface water hits against the right wall and descends towards the bottom generating a counter-clockwise secondary flow with a horizontal axis (Figure 4.2, V1). This pattern has an important effect on sediment resuspension at the base of this wall. Sediment lifted in this zone is partially deposited in the recirculation area of the opposite wall (R1), where low velocities enhance sedimentation of the material.

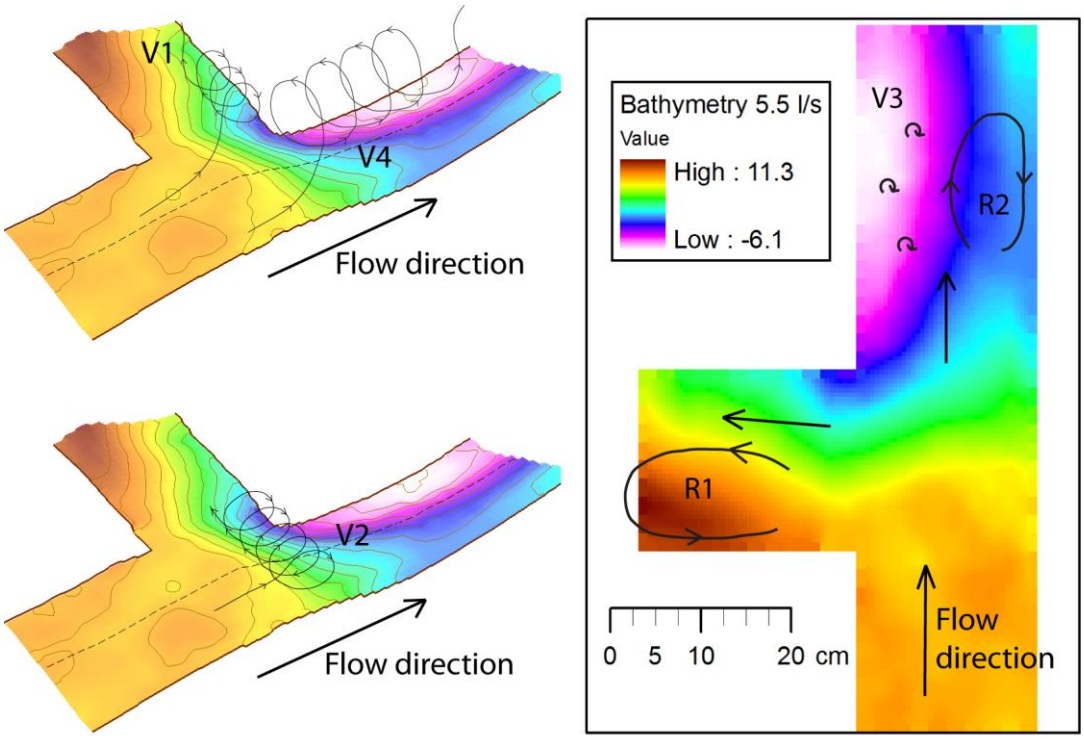

Figure 4.2. Secondary flows observed in the diversion area (vortexes and recirculation areas)

In the area downstream the diversion of the main channel, the situation is a bit more complicated. In the experiments carried out in this study, some flow patterns have been observed that seem to be related to the development of the depression. Firstly, small vertical axis vortexes appear intermittently in the deeper area (V3). Secondly, as mentioned above, the existence of the depression is related to the development of a vortex in front of the entrance of the diversion (V2). On the other hand, due to the existence of the diversion, streamlines curve towards the intake side wall and generate a helicoidal secondary flow (counter-clockwise in the model case, with the lateral intake on the left side, V4). In addition to this, in some conditions when diverted discharge is large enough and streamlines curve more sharply, a recirculation area (R2) is

observed next to the wall opposite the diversion (Bulle, 1926; Neary & Sotiropoulos, 1999). This recirculation area transports part of the sediment resuspended from the depression zone back to the vortex and subsequently adds more solid discharge to the lateral branch.

Visual and laser observations show that the most active vortexes are V1 and V2, and the turbulence and vorticity related to them may play a relevant role in the energy balance in the diversion area. We will then assume that energy loss between upstream and downstream from the diversion is only due to these vortexes, neglecting the contribution of the rest of secondary flows and bed roughness. The rate of decrease of turbulent energy associated with a vortex structure is found experimentally to be of the order of u^3/l, in those situations in which inertia forces are appreciable. Batchelor (1953) and Bateman et al. (2005) use the same idea to evaluate the power of the vortex in the scour hole process. Therefore, energy loss (per unit mass and time) can be expressed as:

$$\frac{du^2}{dt} = -A\frac{u^3}{l} \tag{4.3}$$

Where A is a number of order unity (non-dimensional), and u and l are respectively characteristic velocity and length of the vortex.

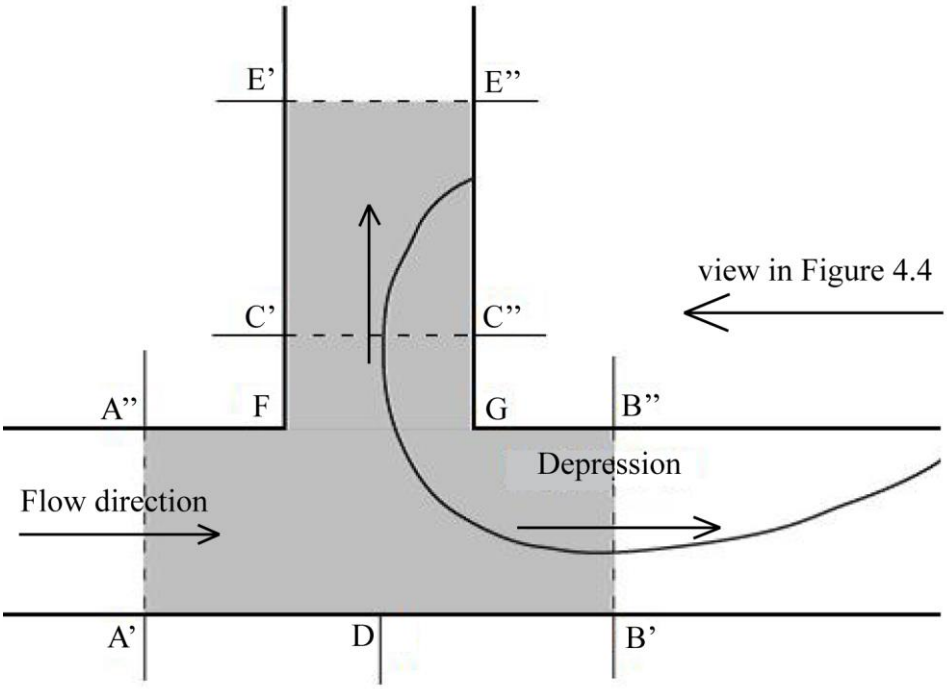

Figure 4.3. Points and sections used for the calculations of the energy balance in the control volume involving the diversion (colored in grey)

These parameters have been calculated as a function of the data collected during the experiments. Regarding vortex V1, its characteristic length is considered as equal to the difference of bed heights between point A'' and point C'' (Figure 4.3), and the characteristic velocity is calculated as:

$$l_1 = z_{A''} - z_{C''} \tag{4.4}$$

$$u_1 = \frac{Q_l}{y_D\left(B\frac{Q_l}{Q}\right)} \tag{4.5}$$

That is, considering that the ratio between the width of the deviated flow and total width is equal to the ratio of deviated and total discharges. In the longitudinal direction of the lateral branch, this vortex is considered to occupy the stretch between the entrance of the diversion and the point where the bed attains the height of point A'' (Figure 4.4, L_1).

$$L_1 = \overline{C''G} + \left(z_{A''} - z_{C''}\right)\cdot\frac{\overline{C''E''}}{\left(z_{E''} - z_{C''}\right)} \tag{4.6}$$

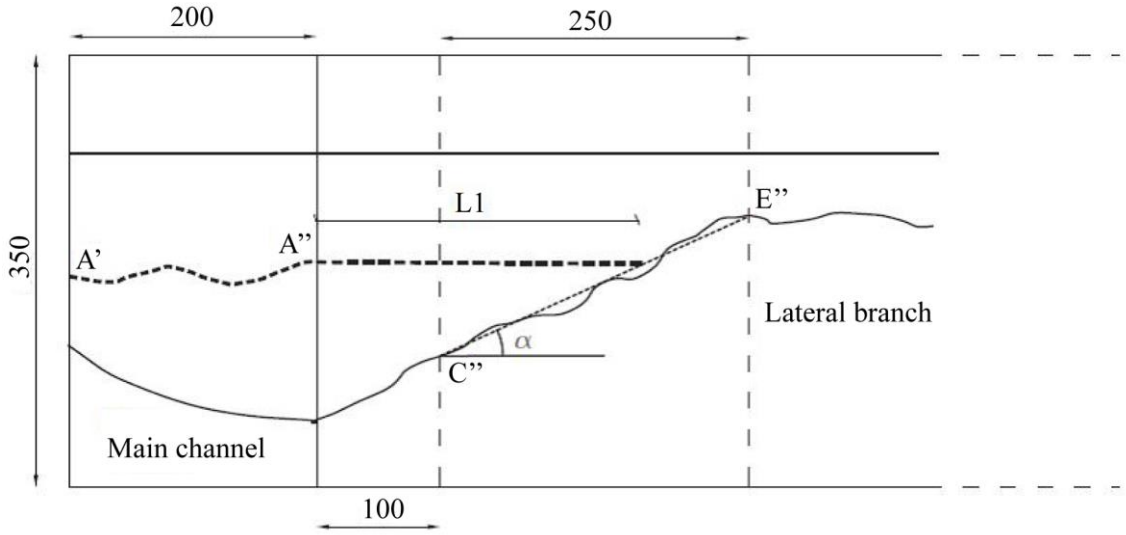

Figure 4.4. Scheme of the calculation of the dimensions of vortex V1. Dashed line between A' and A'' represents the transversal profile of section A and the projection of point A'' over the line between C'' and E''.

Therefore, the vortex V1 is considered to be a cylinder of average diameter l_1, the mass involved in it can be expressed as:

$$m_1 = \rho\pi\frac{l_1^2}{4}L_1 \tag{4.7}$$

On the other hand, the vortex V2 is considered to be located between point D (in front of the diversion entrance) and section B (the first control section in the main channel and downstream the diversion). In those situations in which the depression is present, point D coincides approximately with the high point starting from which the bed level deepens. On the other hand, section B corresponds to the deepest part of the depression. The characteristic length of the vortex is considered to be the water depth at section B, taken as the average value of the measurements on both sides (B' and B'').

$$l_2 = y_B = \frac{y_{B'} + y_{B''}}{2} \tag{4.8}$$

This hypothesis differs from the one assumed for vortex V1, where bed height difference between points A'' and C'' has been considered. This difference is based on visual and laser observations and is due to the fact that V1 is more confined in the erosion hole schematized in Figure 4.4, whereas in the case of V2 vorticity patterns seem to be extended to a larger fraction of the water depth.

Regarding characteristic velocity, it is calculated as:

$$u_2 = \frac{Q_m}{By_D} \tag{4.9}$$

Where Q_m is water discharge in the main channel, B is channel width and y_D is water depth at point D (Figure 4.3). It is assumed that water discharge in the main channel in this point flows through an effective section with the total channel width and a water depth equal to the one measured at point D.

The vortex V2 is considered to be a cylinder with an average diameter of l_2 and to occupy the whole width of the main channel, so that the mass of water involved is:

$$m_2 = \rho\pi \frac{l_2^{\,2}}{4} B \tag{4.10}$$

Power associated with the flow that enters the control volume at section A and exits at sections B and E, are respectively:

$$P_A = \rho g Q_T H_A \tag{4.11}$$

$$P_B = \rho g Q_m H_B \tag{4.12}$$

$$P_E = \rho g Q_l H_E \tag{4.13}$$

Where ρ is water density, g is gravity, Q_T , Q_m and Q_l are total, main channel and lateral branch discharges, and H_A, H_B and H_E are the energies per unit weight at sections A, B and E respectively, which are calculated as:

$$H_A = z_A + y_A + \frac{Q_T^{\,2}}{\left(By_A\right)^2 2g} \tag{4.14}$$

$$H_B = z_B + y_B + \frac{Q_m^{\,2}}{\left(By_B\right)^2 2g} \tag{4.15}$$

$$H_E = z_E + y_E + \frac{Q_l^{\,2}}{\left(By_E\right)^2 2g} \tag{4.16}$$

Where z_A , z_B and z_E are bed heights at the corresponding points.

The quotient $\frac{du^2}{dt}$ has dimensions of power per unit of mass. Therefore, the energy balance can be written as:

$$P_A - P_B - P_E = A\left(\frac{u_1^3}{l_1}m_1 + \frac{u_2^3}{l_2}m_2\right) \tag{4.17}$$

With these considerations, an expression for the coefficient 'A' can be determined, as a function of the flow conditions at a certain moment:

$$A = \frac{4\left(P_A - P_B - P_E\right)}{\rho\pi\left(u_1^3 l_1 L_1 + u_2^3 l_2 B\right)} \tag{4.18}$$

Froude and Reynolds numbers at the entrance and both exits of the diversion are shown in Table A.1 (Appendix A). On the other hand, the values of the variables used for the calculation of coefficient 'A' are detailed in Table A.2 (Appendix A), corresponding to the last five measurements of each experiment.

4.4 Results

The starting point for the calculations of the diversion energy balance is the set of experimental data that are available from the laboratory work (Herrero et al., 2011). Discharge through each branch and bed and water surface heights at points introduced in the theoretical approach, have been measured every 60 minutes until reaching equilibrium. This steady situation has been identified as that in which the addition of water and sediment discharges through both branches is equal to the total values introduced at the inlet of the model, and bed heights at sections A, B, C, D and E are approximately constant. As in the initial condition the channel bed is set horizontally and the system has to evolve until sediment and water discharge are in equilibrium, experiments with low discharges are longer than the ones with high discharges.

Starting from these data, power associated with the flow at sections A, B and E is calculated for each time (every 60 minutes), as well as the parameters that characterize vortexes 1 and 2, the ones that we suggest that are involved in the energy balance (Figure 4.2). Thus, equation (4.18) is used to calculate coefficient A for each time and to analyse its evolution (Figure 4.5).

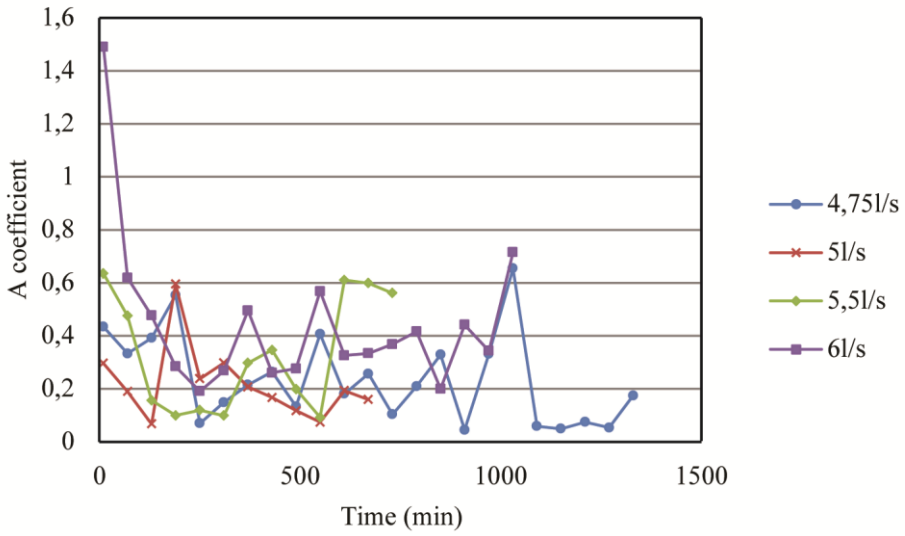

Figure 4.5. Evolution of coefficient A in time based on calculations starting from the experimental data. Each line corresponds to a different total water discharge.

In experiments with discharges below 4.5l/s, depression is not present at equilibrium state, nor are the vortex structures related to it (V2 in Figure 4.2). Therefore, calculations of the vortexes' characteristic lengths as a function of bed heights are no longer valid and have not been taken into account.

However, in experiments with discharges above this threshold value these oscillations disappear and the A values keep relatively constant between 0 and 1. Values corresponding to equilibrium for discharges between 4.75l/s and 6l/s have been calculated as the average of the last five hours of experiment. These results are shown in Figure 4.6 and Table 4.1.

Table 4.1. Average values for coefficient A corresponding to the state of equilibrium

Q_T (l/s)	A
4,75	0,084
5	0,145
5,5	0,415
6	0,424

4.5 Discussion

There are several points that explain the fact that the values are lower than unity. Firstly, characteristic velocities, u_1 and u_2 are calculated as the ones of the water flowing over the upper part of the vortexes, which corresponds to the velocity at the external part of the vortex and, therefore, represents an upper limit for the characteristic value.

Concerning the characteristic length of the main channel vortex (V2), as mentioned above the water depth at section B represents an upper limit for the characteristic value. If we estimate that the vortex arrives only at a height equal to half the water depth at point D, y_D, considering the

experimental values obtained in the laboratory analysis, the relation between the "real" and the considered characteristic length would be:

$$l_c = 0.83 l_2 \qquad (4.19)$$

On the other hand, vortex V1 has been considered to be a cylinder of radius $l_1/2$ and height H_1, and l_1 is defined by equation (4.6). However, Figure 4.4 shows clearly that the mass involved in this vortex is significantly lower than the mass of the mentioned cylinder. Actually, it could be considered that the vortex covers only half of this cylinder, whereas the other half is under the bed. This fact implies that the first summand of the denominator of equation (4.18) is multiplied by a factor 2.

An increase in 'A' values is observed as discharge becomes higher. We interpret that this trend could be related to several factors. A possible reason would be an increase in the "real" characteristic length of vortex V2, compared to the assumed value, that is, water depth at section B. However, no realistic delimitation of this vortex could be done with the available methods, accurate enough to identify a significant trend in vortex diameter.

On the other hand, other possible mechanisms not considered in equation (4.18) could have an increasing influence in energy losses as total discharge raises. Turbulence increases as total discharge becomes higher, and coefficient 'A' raises so that vortexes V1 and V2 have to counteract the fact that these new energy losses are not considered. These turbulent patterns include vortexes V3 and other more complicated and chaotic structures that have not been identified and do not appear in Figure 4.2.

However, we believe that the main reason for the increasing trend in the values of coefficient '*A*' is that the vortex becomes more stable as the power associated to the incoming flow is higher. This fact causes that 'A' values get closer to unity and improves the suitability of equation (4.3) for quantifying the energy losses associated to the vortex that appears in the diversion. A similar application can be found in Bateman et al. (2005), referring to the vortexes that form in a flow around a pier.

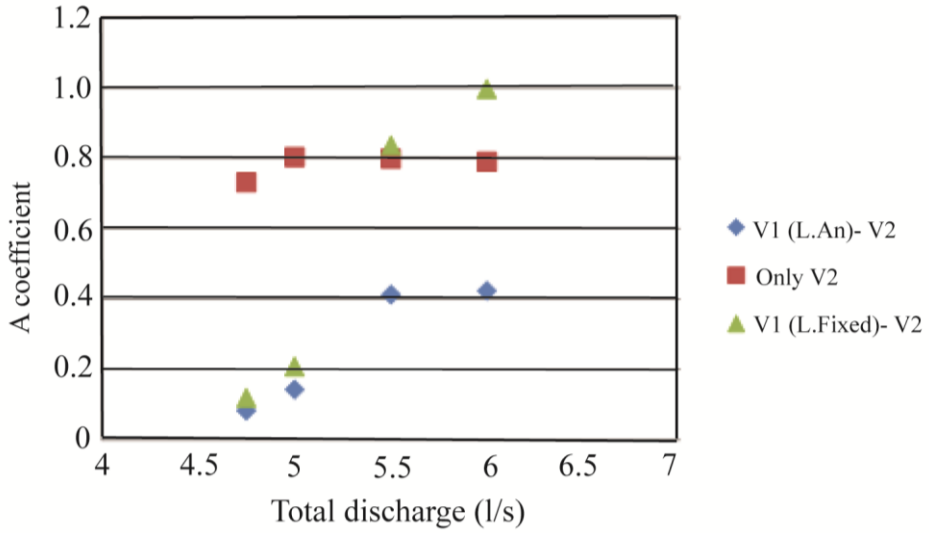

Figure 4.6. Values of coefficient A that correspond to the state of equilibrium (calculated averaging the values for the last 5 hours of experiment), considering either the analytically-computed or a fixed height for V1, or without considering this vortex.

A sensitivity test has been carried out in order to analyse the evaluation of energy losses associated with vortex structures of the diversion (Figure 4.6). Firstly, energy loss expression in vortex V1 has been modified, making L_1 independent of bed topography and setting it equal to the distance between the entrance of the diversion and section C, that is, 0.1m. This implies a reduction in the mass of water involved in the vortex, so that there is an increase in the values of 'A' necessary to generate the same energy losses in the system. In a second modification of the energy balance, contribution of vortex V1 to energy losses has been completely neglected. Similar consequences are observed in this case, with an even more significant increase in 'A' values. However, the increasing trend of 'A' values as discharge rises is observed for the three ways to evaluate the energy balance.

4.6 Summary

In this chapter, a theoretical analysis is developed to establish the energy balance over a control volume that involves the diversion area. We consider incoming and exiting power associated with the flow and energy losses due to the main vorticity patterns.

Vortex energy losses computed from the experimental data are significantly higher (one order of magnitude) than those associated to bed roughness. They are calculated using Equation (4.3) which introduces coefficient '*A*', an order unity parameter.

The proposed balance equation is tested against the experimental data collected in a previous study (Herrero et al., 2011) and values are obtained for coefficient 'A'. Characteristic values for vortex length and velocity are proposed as a function of the

experimental data. '*A*' values lower than unity are obtained, which is associated with the fact that the proposed expressions for characteristic length and velocity are upper limits for the "real" values.

An increasing trend is observed as total discharge rises, which we associate to the fact that the vortex is more stable as the incoming flow energy becomes higher. On the other hand, another factor that can influence in the mentioned pattern is the appearance of new turbulent structures that have not been taken into account in the hypothesis made to calculate 'A' (equation (4.18)).

The values close to unity obtained for coefficient 'A', reinforce the correlation between the energy lost in the bifurcation with the energy needed to keep the vortex in motion. This good correlation allows to affirm that the visualized vortex shows a hydrodynamic behaviour which can be described by equation (4.3).

Lastly, alternative calculations of coefficient 'A' have been carried out, first changing the expression of parameter L_1 for a fixed value and secondly neglecting the contribution of this vortex to energy losses. The increase of 'A' values when compared to the ones obtained with equation (4.18) are due to the larger amount of mass involved in this case.

To sum up, we consider that this balance equation is an important tool to understand and describe water and sediment distribution in a 90º diversion, and could be applied in an analytical model to quantify these magnitudes.

Chapter 5: Theoretical model for flow and sediment transport in fluvial diversions

5.1 Introduction

As highlighted in chapter 2 previous theoretical models on fluvial diversions focus on the relation between water discharge ratio and different variables as Froude number in the main channel or water depth ratio between the main channel and the lateral branch (Ramamurthy and Satish 1988, Ramamurthy et al. 1990, Lama et al. 2002). Therefore, to the authors knowledge no theoretical model has been developed to evaluate the relationship between flow and sediment distribution in fluvial diversions.

On the other hand, Wang et al. (1995) and Bolla Pittaluga et al. (2003), carried out an experimental approach to study morphological evolution of fluvial bifurcations in the case of Y-shaped systems. However, the different geometry and subsequent flow patterns that occur, make it difficult to apply the mentioned models to lateral intakes.

The objective of this chapter is to develop a theoretical model that relates the sediment discharge distribution and water discharge distribution, that is coherent with the patterns observed in both experimental and field studies. Starting from the experimental data explained in chapter 3, some further calculations are performed in order to evaluate in which conditions the vortex and the scour hole that appear in the main channel occur, as they have proved to be determinant to the local sediment transport processes in the diversion area. Then, a nodal equation is developed relating water and sediment discharge ratios between both branches, considering separately suspended sediment distribution and bed load distribution. Later, the results obtained from this equation are compared with the data obtained in the laboratory and a discussion of the main results and the assumed hypothesis is carried out. Finally, the nodal equation is linked with the energy balance equation developed in chapter 4 and other equations to set out a system of equations that describe the equilibrium state of a fluvial diversion and a summary with the general conclusions of the chapter is shown.

5.2 Experimental data

Despite the experimental work has been widely described in chapter 3, some further calculations were performed during the development of the conceptual model in order to characterize and find the origin of some of the patterns highlighted in the mentioned chapter.

5.2.1 Bed morphology evolution

As mentioned above, bed morphology is highly related to hydrodynamic characteristics which, in turn, condition the bed load sediment distribution absolutely. Considering the importance of this point for the establishment of a nodal equation that describes solid discharge distribution, a further analysis of the experimental data is carried out herein, in order to determine those conditions in which the mentioned scour patterns are formed in the first stretch of the main channel. Some preliminary considerations are made about this point in chapter 3, and the influence of angular momentum associated with the flow through the lateral branch is tested using the experimental data. However, further development of this reasoning is carried out next in order to relate the occurrence of the scour pit to some dimensionless parameter that allows a wide application of the results obtained herein.

A similar situation in which there is a determinant interaction between bed morphology and flow patterns occurs in river confluences (De Serres 1999, Bradbrook 2000). Several aspects affect these connected characteristics, as the angle of the tributaries, the symmetry of the confluence, the discordance or bed level difference between the joining rivers (Biron 1996, De Serres 1999, Leite Ribeiro et al. 2012) and the momentum flux ratio of the two associated flows (Rhoads and Sukhodolov 2001, Miyawaki et al. 2010). Symmetric confluences are characterized by the development of two opposed helical secondary flows similar to those that occur in meanders. This phenomenon is accompanied by the formation of a scour hole in the central part of the downstream channel. The geometric asymmetry of the system or a higher discharge in one of the tributaries can modify these patterns, in such way that one of the helical flows become predominant, even destroying the other one, and the scour hole is displaced towards the river bank opposite the tributary with a higher discharge. Depending on the momentum flux ratio and mainly in those situations in which one of the tributaries forms a certain lateral angle with both the other tributary and the downstream channel, flow separation occurs next to the downstream corner of the confluence and a bar is often formed in this area (Miyawaki et al. 2010).

Inspired by the situation described above that takes place in confluences and considering that the geometry of the system is the same for all the experiments of the laboratory analysis on which the model we present is based, the ratio between the momentum flux associated with the discharges of each branch is analysed as well as its possible influence on the bed morphology of the bifurcation. This momentum flux ratio is defined as:

$$M_r = \frac{\rho Q_l v_l}{\rho Q_m v_m} \quad (5.1)$$

The values of the momentum flux ratios corresponding to equilibrium have been calculated for each experiment. The flow velocity in the lateral branch, v_l, corresponds with the data in the first control section of this branch (section C in Figure 5.2), whereas v_m is obtained dividing the main channel discharge (Q_m) by the channel width and the water depth in point D (Figure 5.2), that is, upstream from the depression area. This measure is adopted in order to avoid considering the part of the water depth inside the scour hole in those cases in which it is present, because it does not contribute to the main channel momentum flux that appears in M_r. The equilibrium values of M_r are shown in Figure 5.1 and Table 5.1. The results highlight a significant increase in momentum flux ratios for those situations in which the depression is present.

Table 5.1. Values of the momentum flux ratio between the main channel and the lateral branch

Q_T (l/s)	Q_l (l/s)	v_l (m/s)	Q_m (l/s)	v_m (m/s)	M_r (-)	Scour hole
3,5	0,323	0,072	3,20	0,452	0,016	No
4	0,336	0,073	3,65	0,400	0,017	No
4,5	0,485	0,096	4,05	0,405	0,028	No
4,75	1,148	0,131	3,72	0,414	0,097	Yes
5	1,228	0,125	3,87	0,372	0,107	Yes
5,5	1,740	0,137	3,84	0,269	0,231	Yes
6	2,387	0,144	3,71	0,208	0,444	Yes

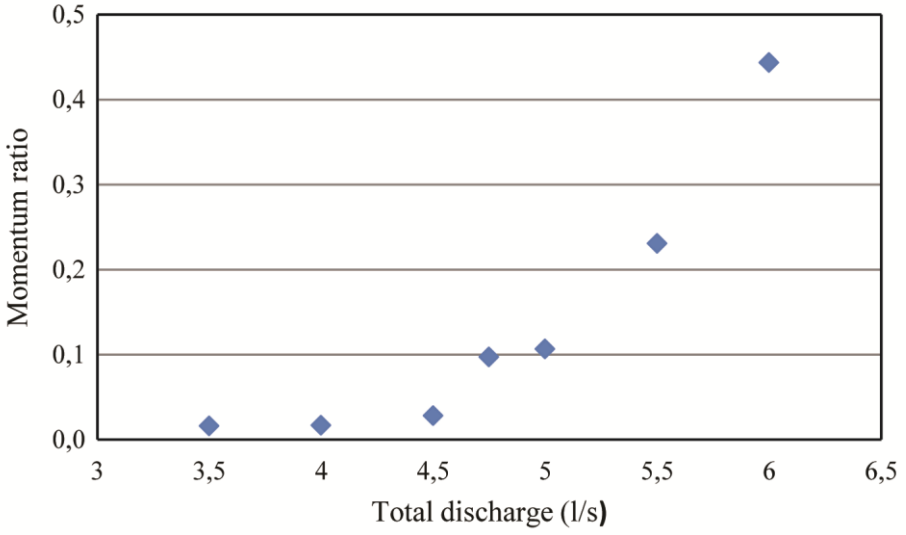

Figure 5.1. Values of the momentum flux ratio between the lateral branch and the main channel

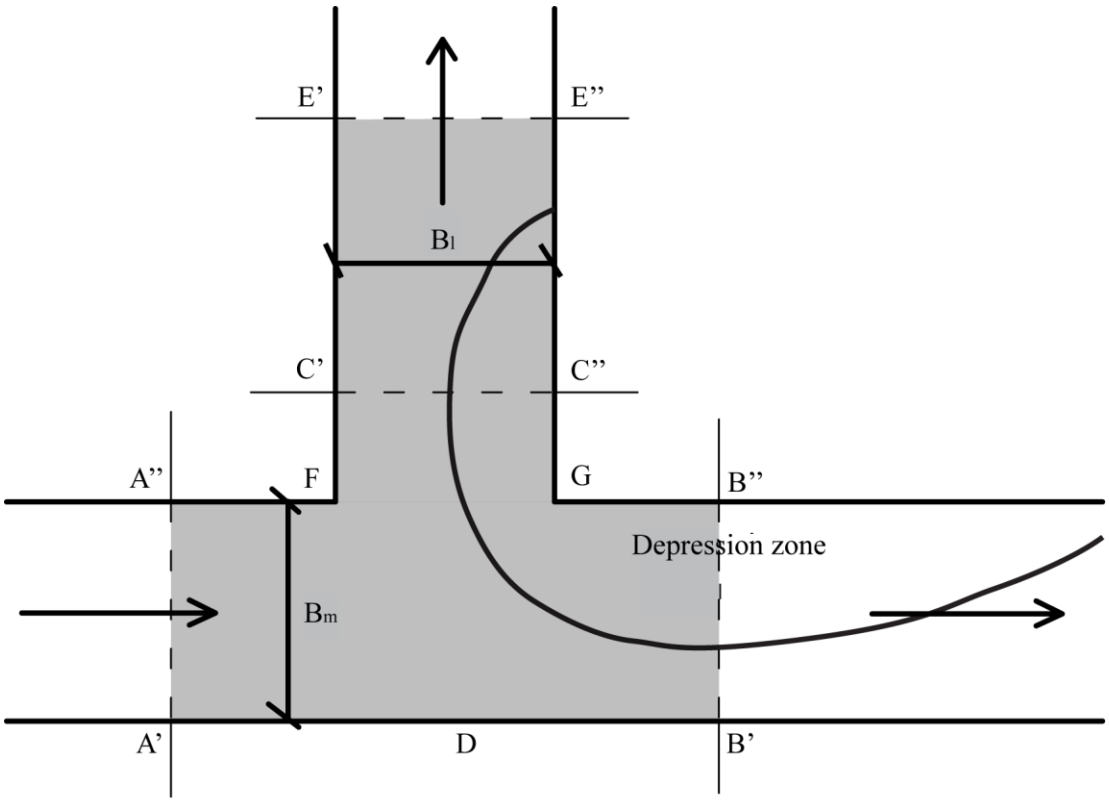

Figure 5.2. Position of the measurement points in the diversion area and location of the depression zone of the main channel downstream from the diversion

It is also interesting to study the evolution of the momentum flux ratio in time, for the runs in which the system evolves into a state of equilibrium with no scour hole in the main channel. In these tests, there is an initial phase during which the vortex and the subsequent pit occur, so studying the time interval during which the scour hole disappears can be useful in determining the flow conditions that allow or prevent the presence of the scour hole. Figure 5.3 shows the time evolution of the bed level for point B'' in Figure 5.2. It is possible to see how the runs with 3.5l/s, 4l/s and 4.5l/s present an initial period during which scour occurs and after that sediment deposition raises the bed level until equilibrium is reached, where bed bathymetry is continuous along the main channel, and no depression area is present downstream from the diversion. Table 5.2 shows the measurement instants before and after the disappearance of the depression and the values of M_r at these moments for the three runs mentioned above, calculated with the corresponding flow conditions. During the three periods of time exposed, the system goes through a situation that provokes the disappearance of the depression. If the momentum flux ratio governs this behavior, there must be a certain value of M_r within the three intervals of this parameter that separates those situations with or without the depression and subsequent vortex.

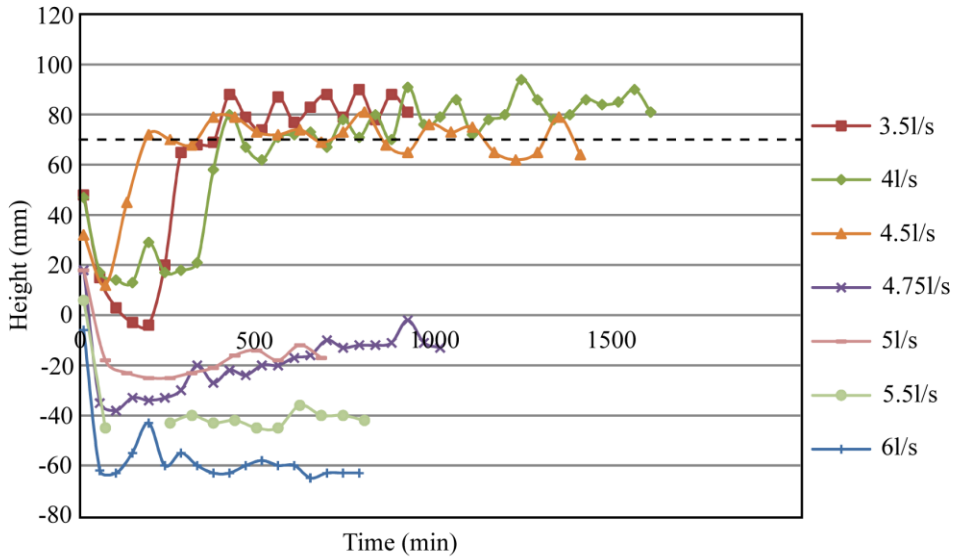

Figure 5.3. Bed level evolution of the control point B'' (Figure 5.2) for the different total discharges. The dashed line indicates the bed level in the initial condition.

Table 5.2. Times and momentum flux ratio values before and after the depression is filled in the experiments with low total discharges (in which no depression occurs at the equilibrium state)

Q_T (l/s)	t before (min)	t after (min)	M_r before	M_r after
3.5	250	310	0,133	0,035
4	325	370	0,040	0,022
4.5	70	130	0,068	0,030

In regards to the results that appear in Table 5.2, it can be proposed that the scour area occurs in those flow conditions with a momentum flux ratio higher than 0.04, whereas in situations with lower values of M_r the system tends to deposit sediment in this zone favouring the disappearance of the scour hole. Therefore, our interpretation of these results is that in the experiments with low total discharges, the lateral branch "needs" to increase its slope in order to transport sediment with the lower lateral branch discharge that is present in this situation. This slope increase is attained through deposition at the entrance of the lateral branch, a fact that complicates the inflow of water and therefore provokes a decrease in lateral branch discharge and, subsequently, in the momentum flux ratio. In the experiments with a low total discharge, M_r decreases to low enough values so that the main channel vortex and the pit are no longer sustainable.

5.3 Nodal equation development

The objective of this section is to show the steps carried out to develop an equation that relates solid discharge ratio, r_s (ratio between solid discharge at the main channel, Q_{sm},

and solid discharge in the lateral branch, Q_{sl}), and water discharge ratio, r_Q (ratio between water discharge at the main channel, Q_m, and water discharge in the lateral branch, Q_l). For this purpose, suspended transport and bed load are considered separately, and different conceptual hypotheses are assumed to obtain analogous ratios for both modes of sediment transport.

With such decomposition of sediment transport, the solid discharge ratio can be expressed as follows:

$$r_s = \frac{Q_{sm}}{Q_{sl}} = \frac{Q_{ssm} + Q_{sbm}}{Q_{ssl} + Q_{sbl}} \tag{5.2}$$

Where 's' and '*b*' second subscripts, refer to suspended and bed sediment transport. Defining r_{ss} and r_{sb} respectively as the ratios between suspended sediment discharge and bed sediment discharge in the main and the lateral branches, and applying the mass continuity equation to relate both types of sediment discharge downstream from the diversion with the total value entering from upstream, equation (5.2) can be rearranged and written as:

$$r_s = \frac{\frac{r_{ss}}{r_{ss}+1} Q_{sst} + \frac{r_{sb}}{r_{sb}+1} Q_{sbt}}{\frac{1}{r_{ss}+1} Q_{sst} + \frac{1}{r_{sb}+1} Q_{sbt}} \tag{5.3}$$

Where Q_{sst} and Q_{sbt} are respectively suspended and bed sediment discharges in the main channel and upstream from the diversion, which can be calculated as a function of the corresponding flow conditions. Applying mass continuity to obtain equation (5.3), it is considered that all the sediment that travels as bed load when entering the diversion area, does so when exiting it following one of the branches, and the analogous reasoning applies to suspended transport. Therefore, no net resuspension or deposition is considered in the diversion area.

In the following subsections, expressions for r_{ss} and r_{sb} are developed separately.

5.3.1 Suspended sediment discharge ratio

Adopting a simplified approach, we assume that suspended sediment moves with the water flow velocity field, that is, neglecting its inertia. Moreover, a certain pressure difference is considered between the opposite side of the main channel and the entrance of the lateral branch. This pressure gradient causes a lateral acceleration that can be written as:

$$a_l = \frac{\Delta p}{\rho_w b} \tag{5.4}$$

Where Δp is the pressure difference between both sides of the main channel in the diversion area, b is main channel width and ρ_w is water density.

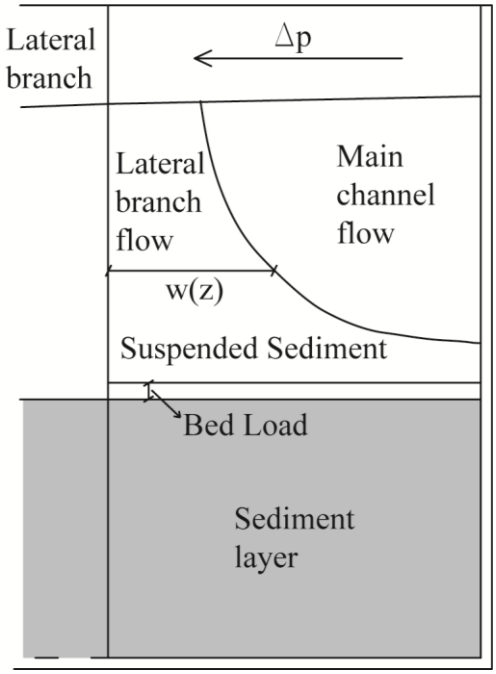

Figure 5.4. Vertical schematic view of the diversion area with the "captured width" or flow separation surface between the flow deviated towards the lateral branch and the flow that follows the main channel.

Assuming a logarithmic profile for the velocities in the incoming flow and supposing that this longitudinal velocity component keeps constant as the flow crosses the diversion area, a "captured width", *w*, referring to the part of the flow that is deviated towards the lateral branch, can be defined as a function of depth:

$$\frac{u(z)}{u_*} = \frac{1}{\kappa}\ln\left(\frac{z}{z_0}\right) \tag{5.5}$$

$$w(z) = \frac{1}{2}\frac{\Delta p}{\rho b}\frac{\kappa^2 b^2}{u_*^2 \ln^2\left(z/z_0\right)} \tag{5.6}$$

Where *z* is the vertical coordinate, κ is von Karman constant, u_* is shear velocity at the end of the upstream main channel and z_0 is bed roughness length associated with the incoming flow. The captured width dependence on depth is schematized in Figure 5.4.

Taking this into account, water and solid discharges through the main channel and the lateral branch can be computed with the following equations:

$$Q_l = \int_0^H u(z)\,w(z)\,dz \tag{5.7}$$

$$Q_m = \int_0^H u(z)\left[b - w(z)\right]dz \tag{5.8}$$

$$Q_{ssl} = \int_0^H u(z)\,w(z)\,C(z)\,dz \tag{5.9}$$

$$Q_{ssm} = \int_0^H u(z)\,w(z)\left[b - w(z)\right]dz \tag{5.10}$$

Where $u(z)$ is the main channel longitudinal flow velocity, H is water depth in section A (Figure 5.2) and $C(z)$ is the volume suspended sediment concentration profile, which will be assumed as described by the Rouse profile:

$$\frac{C}{C_b} = \left[\frac{(H-z)/z}{(H-\delta)/\delta}\right]^{Z_R} \tag{5.11}$$

Equation (5.11) involves C_b, suspended sediment concentration at a near-bed reference height, δ, and the exponent $Z_R = v_s/(\kappa u_*)$, being v_s the sediment fall velocity.

Introducing equations (5.5), (5.6) and (5.11) into equations (5.7)-(5.10) and rearranging terms, the following expression can be obtained for the suspended sediment discharge ratio, as a function of the water discharge ratio:

$$r_{ss} = \frac{Q_{sst}}{Q}\frac{I_1}{I_2}\left(r_Q + 1\right) - 1 \tag{5.12}$$

Where Q is total incoming discharge, and I_1, I_2 are two integrals defined as follows:

$$I_1 = \int_\delta^H \frac{1}{\ln(z/z_0)}\,dz \tag{5.13}$$

$$I_2 = \int_\delta^H \frac{C(z)}{\ln(z/z_0)}\,dz \tag{5.14}$$

The lower limit 'δ' that appears in the integrals of equations (5.13) and (5.14) corresponds with a height chosen very close to the bed to integrate the mass conservation equation for suspended sediment and obtain the Rouse profile for the suspended sediment concentration.

Table 5.3. Values of suspended sediment discharge ratio and variables used for the calculations

Q (l/s)	Q_{sst} ($\cdot 10^{-6}$ m^3/s)	I_1 ($\cdot 10^{-6}$)	I_2 ($\cdot 10^{-3}$)	r_Q	r_{ss}
3.5	0.930	1.207	5.655	9.650	12.259
4	0.932	1.209	6.622	10.953	14.270
4.5	0.885	0.978	7.544	8.131	12.857
4.75	1.090	1.269	7.410	3.212	4.643
5	0.946	1.116	7.357	3.114	4.134
5.5	0.843	1.030	7.698	2.182	2.648
6	0.922	1.071	0.851	1.554	2.115

5.3.2 Bed sediment discharge ratio

As mentioned above, two different situations occur in the main channel downstream from the diversion, consisting of the formation or not of a depression area in the first stretch of this branch. This pattern is determinant for solid discharge distribution and especially for the sediment transported as bed load.

With the help of dark sediment that has been used as a tracer, visual observations carried out during the experimental study highlight the fact that, in those situations in which the depression is present, practically all the bed load sediment is deviated towards the lateral branch. Therefore a zero value is assigned for r_{sb} in these cases. This statement is based on the observations carried out by Herrero et al. (2011) and has the limitations of the experimental conditions present in their analysis.

For those situations in which there is no depression in the main channel, bed load sediment is supposed to move parallel to bed shear stress, forming an angle δ with the main channel direction which can be computed as:

$$\tan\beta = \frac{v_*}{u_*} \tag{5.15}$$

where u_* and v_* are, respectively, the shear velocity components in the longitudinal (main channel) and transversal (lateral branch) directions. We assume that these components are related to the flow variables in the main channel and in the lateral branch respectively. Therefore, considering a logarithmic profile for flow velocities in both branches, u_* and v_* can be written as:

$$u_* = \frac{\kappa Q_m}{D_m B_m \left(\ln \frac{D_m}{z_0} - 1 \right)} \tag{5.16}$$

$$v_* = \frac{\kappa Q_l}{D_l B_l \left(\ln \frac{D_l}{z_0} - 1 \right)} \tag{5.17}$$

where D_m and D_l are the water depths in the main channel and the lateral branch respectively and B_m and B_l are the channel widths in each branch.

Considering the geometry of the diversion (Figure 5.2), the ratio for bed sediment discharges can be written as a function of the bed load transport direction as follows:

$$r_{sb} = \frac{B_m}{B_l \tan \beta} - 1 \tag{5.18}$$

In the case of the model used for this experimental analysis the width ratio B_m / B_l is equal to unity.

Table 5.4. Values of bed sediment discharge ratio and variables used for the calculations

Q (l/s)	Q_m (l/s)	Q_l (l/s)	D_m (m)	D_l (m)	u_*	v_*	r_{sb}
3.5	3.20	0.32	0.0374	0.0096	0.027	0.014	0.939
4	3.65	0.34	0.0443	0.0124	0.026	0.011	0.636
4.5	4.05	0.48	0.0512	0.0126	0.024	0.015	0.596
4.75	3.72	0.11	0.0504	0.0230	0.022	0.017	0.279
5	3.87	1.23	0.0502	0.0258	0.024	0.016	0.460
5.5	3.83	1.74	0.0529	0.0376	0.022	0.015	0.476
6	3.71	2.39	0.0590	0.0481	0.019	0.015	0.230

5.4 Comparison with the experimental results

In this section, equation (5.3) and the subsequent reasoning to calculate the components of solid discharge ratios for suspended sediment and bed load are tested against the experimental data obtained during the laboratory analysis (Herrero et al. 2011).

Total solid discharge upstream from the diversion, which is measured at the model inlet, is divided into bed load and suspended sediment. Bed load solid discharge is calculated using the following equation (Wong & Parker, 2006):

$$q^* = 3.97 \left(\tau_s^* - 0.0495 \right)^{3/2} \tag{5.19}$$

Where q^* is the dimensionless solid discharge per unit width, calculated as $q_s / D\sqrt{RDg}$, being q_s the solid discharge per unit width, D the mean sediment diameter, R the sediment specific density, $(\rho_s - \rho_w)/\rho_w$, and g is gravity acceleration. On the other hand τ_s^* is the dimensionless bed shear stress associated with skin friction, calculated as:

$$\tau_s^* = 0.06 + 0.4 \left(\tau^* \right)^2 \tag{5.20}$$

Where τ^* is the total dimensionless shear stress, computed as:

$$\tau^* = \frac{\rho_w g H S}{\rho_w g R D} \tag{5.21}$$

With *H* being the water depth at section A (Figure 5.2) and *S* the energy slope, considered equal to the bed slope and obtained through linear regression applied to the bed topography of the main channel upstream from the diversion.

Suspended sediment discharge is calculated as the difference between the total solid discharge and bed load discharge, which is calculated using equation (5.19). This discharge could be calculated also starting from the flow conditions, but the former option has been preferred, considering the possibility to measure total solid discharge at the model inlet with appropriate precision.

The suspended sediment discharge ratio, r_{ss}, is calculated using equation (5.12). Q_{sst} is calculated, as mentioned above, as the difference between total solid discharge and bed sediment discharge, both computed from the experimental data corresponding to each test. *Q* is introduced as the total water discharge applied in each experiment. The integrals I_1 and I_2 are calculated using equations (5.13) and (5.14), and the Rouse concentration profile (equation (5.11)). The near-bed elevation where bottom boundary condition is applied when obtaining the Rouse profile, is calculated with the formulation by Smith and McLean (1977):

$$\delta = \alpha_0 \left(\tau_s^* - \tau_c^* \right) D + k_s \tag{5.22}$$

Where $\gamma_0 = 2.4 \cdot 10^{-3}$, $\alpha_0 = 26.3$, *D* is the sediment mean diameter, τ_s^* is the skin shear stress, τ_c^* is the critical shear stress for sediment motion and

k_s is the effective roughness height, which is related to the bed roughness length as $z_0 = k_s / 30$. On the other hand, c_b has been adjusted so that the integrated suspended sediment discharge is equal to the difference between total sediment discharge and bed sediment discharge. Table 5.5 shows the ratio between bed and suspended sediment discharges in the different experiments.

Table 5.5. Ratios between bed and suspended sediment discharge in the flow upstream from the diversion

Q_T (l/s)	Q_{sbt} ($\cdot 10^{-6}$m^3/s)	Q_{sst} ($\cdot 10^{-6}$m^3/s)	Q_{sbt}/Q_{sst}
3.5	1.064	0.930	1.144
4	0.892	0.932	0.956
4.5	0.855	0.885	0.966
4.75	0.992	1.090	0.911
5	1.131	0.946	1.195
5.5	1.199	0.843	1.422
6	1.108	0.922	1.202

Lastly, experimental values of the water discharge ratio 'r_Q' are introduced into equation (5.12), therefore obtaining a value for r_{ss} based on the experimental results.

Regarding the bed sediment discharge ratio, the laboratory data have been applied to equations (5.15) to (5.18), to obtain values of r_{sb}. In equation (5.16), values of Q_m and D_m correspond, respectively, to the main channel discharge and the water depth at section B (Figure 5.2), the first control section of the main channel. The calculation of u_* is carried out for each set of data, corresponding to every 60 minutes. Similarly, experimental data are applied to equation (5.17) to obtain the transversal shear velocity, v_*, for each time. In this case, Q_l is introduced as the lateral branch discharge for that particular time and D_l is adopted as the water depth at section E, which is the second control section of the lateral branch. Section E is chosen instead of the first one (C), to avoid the influence of the turbulence that is formed at this point and ensure more uniform conditions.

With these considerations, equation (5.3) is used together with laboratory data to obtain values for the total solid discharge ratio. These calculated values are compared with the values obtained at the laboratory in Figure 5.5.

Table 5.6. Measured and calculated values of solid discharge ratio with the different variables used in the calculation

Q (l/s)	Q_{st} (10^{-6}m^3/s)	Q_{sst} (10^{-6}m^3/s)	Q_{sbt} (10^{-6}m^3/s)	r_{ss}	r_{sb}	r_S (calc.)	r_S (meas.)
3.5	1.99	0.93	1.06	12.26	0.94	2.22	1.75
4	1.82	0.93	0.89	14.27	0.64	2.01	2.46
4.5	1.74	0.89	0.85	12.86	0.60	1.90	1.25
4.75	2.08	1.09	0.99	4.64	0	0.76	0.08
5	2.08	0.95	1.13	4.13	0	0.58	0.09
5.5	2.04	0.84	1.20	2.65	0	0.43	0.08
6	2.03	0.92	1.11	2.11	0	0.45	0.09

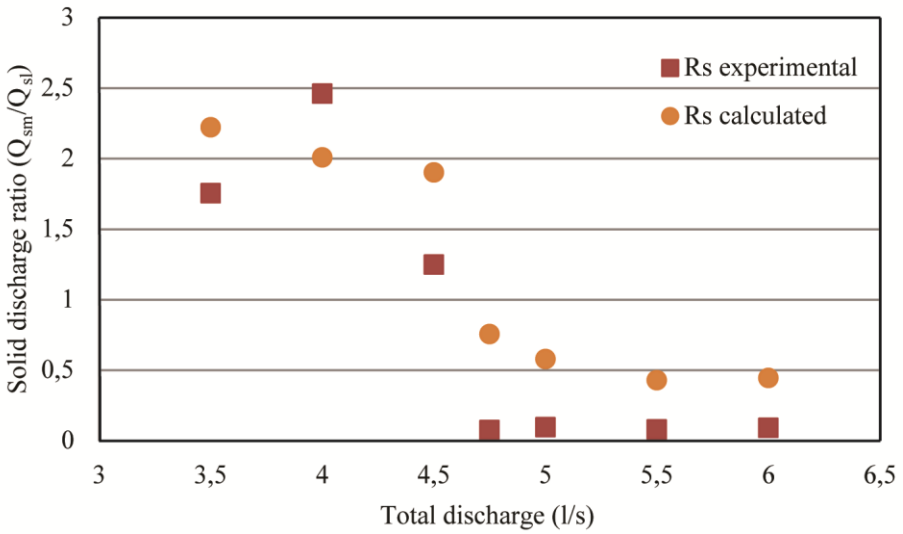

Figure 5.5. Calculated values of solid discharge ratio (Q_{sm}/Q_{sl}) compared with experimental values corresponding to equilibrium.

5.5 Discussion

The calculated results for the solid discharge ratio compare quite well to the experimental data and reasonably distinguish the high discharge behavior by which the depression is formed and most of the sediment is deviated towards the lateral branch, from the low discharge behavior where no depression is present and sediment discharge ratios are higher than one.

However, the simplified approach implies several limitations of the model that should be noted and may affect the obtained results. Firstly, the logarithmic profile is significantly altered when the flow is affected by the turbulent structures that appear in front of the entrance of the lateral branch. This fact probably affects the shape of the dividing flow surface. Through the adopted hypothesis we are assuming that these alterations compensate on average and that the diversion has a net influence in the transversal direction only.

Secondly, the influence of the vortex that is formed in the upstream part of the depression area of the main channel has only been considered to affect bed load transport, in those situations in which the scour hole is present. However, although the high turbulence that is present in this zone makes it difficult to establish general flow patterns, the upper part of the vortex goes above the bed level upstream from the depression area (point D in Figure 5.2), therefore also affecting part of the suspended sediment. This fact would affect the calculation of r_{ss} by decreasing its value (and therefore, r_s), and could be taken into account by introducing a certain height value below which all the suspended sediment (according to the Rouse concentration profile) is captured by the lateral branch. On the

other hand, another aspect related to the depression vortex which may have an influence on sediment deviation is its intermittency. The observations that were carried out during the experiments with the help of vertical laser projections highlight the fact that the vortex is not steady in time, but rather appears and disappears cyclically with a frequency in the order of few seconds. The consequence of this fact would be that there is a certain percentage of the total time during which the mechanism that deviates practically all the bed load sediment is not present, therefore increasing the value of r_{sb} and r_s. However, these effects go beyond the scope of the simplified approach exposed in this paper, and would need further and more specific experimental data to be taken into account.

Moreover, other flow patterns related to the presence of the depression influence sediment resuspension and subsequent transport. In effect, vertical vortexes occur in the depression area, which are observed to resuspend sediment towards the upper layers of the flow (Herrero et al. 2011). In addition, for low water discharge ratios (high discharge in the lateral branch) a recirculation area is formed in the first stretch of the main channel next to the wall opposite the diversion. The sediment lifted by the vertical vortexes is observed to enter this area and go back towards the diversion, mixing with the flow that enters to the lateral branch and, therefore, decreasing the value of r_s.

On the other hand, assuming that suspended sediment moves with the flow when calculating the corresponding solid discharge ratio, sediment inertia is being neglected. Considering the higher sediment density in relation to water, the trajectories of sediment particles are expected to be less curved than those of the water flow. Therefore, this hypothesis underpredicts solid discharge ratio, as more sediment is in fact traveling into the main channel.

Another simplification of the model refers to the bed load sediment direction in those cases in which no depression is present in the main channel, which is calculated using equation (5.15). Shear velocities have been expressed as a function of equilibrium flow variables of the main channel and the lateral branch through equations (5.16) and (5.17). In the final model that is presented below, these variables refer to uniform flow conditions which are not found until a certain distance downstream from the diversion along any of the two branches. Further analysis and more precise measurements are required to properly characterize the shear stress direction in mobile bed conditions where the bathymetry is complex. However, we consider that the assumed hypothesis is a reasonable starting point for this simplified conceptual model.

Finally, the experimental data on which this conceptual model is based do not allow taking into account the influence of other variables that may have a significant impact. On one hand, the ratio between the width of the main channel and that of the lateral branch is expected to affect the dimensions of the depression area and the associated vortex. In effect, the narrow geometry of the laboratory model used here, when present, causes the depression area to extend over the whole width of the main channel, therefore affecting all the bed load transport and decreasing the values of r_s. For wider main channels or diversions with a larger width ratio (B_m / B_l), the area that is affected by the flow patterns caused by the lateral intake, would probably not extend to the opposite channel wall, part of the bed load would not be affected by the depression area and the related vortex, and the hypothesis that in this case sets r_{sb} values to unity would no longer be valid.

On the other hand, the diversion angle is another variable that probably affects the flow patterns that steer sediment discharge distribution. Although the reasoning exposed so far could also be applied to different orientations of the lateral branch, the complexity of the flow suggest the necessity of further experiments to analyze the influence of the diversion angle on the bathymetry evolution in different discharge conditions, which has been shown to have a determinant influence on the solid discharge distribution. Future studies are expected to be carried out to understand the influence of this angle, as well as the behavior of submerged vanes as a measure to modify sediment distribution and avoid deposition at the lateral intakes entrance (Odgaard, 2009).

5.6 Simplified conceptual model

In this section, equation (5.3) and the subsequent expressions for its components are joined with other equations in order to establish a model that describes diversion equilibrium conditions. The following hypotheses are devised:

1) Water discharge and water depth in the main channel and the lateral branch correspond to uniform flow conditions
2) Sediment transport in both branches is considered to move as bed load and equal the transport capacity associated with the flow conditions and can be calculated by some of the well-known sediment transport formulas. Water depth is used to calculate the Shields parameter and separation is carried out between skin and bed form associated roughness
3) Mass conservation for water and sediment in the diversion area with no erosion or deposition of sediment (equilibrium conditions)

4) The vortex associated with the depression area causes energy losses that have to be taken into account in those cases in which the depression is present. These energy losses are expressed as (Batchelor et al. 1953):

$$\Delta E = \alpha \frac{u_c^3}{l_c} \tag{5.23}$$

Where α is a proportionality constant that can be considered equal to unity (Herrero et al. 2012), u_c is the characteristic velocity of the vortex and l_c is its characteristic length. This approach was applied to the experimental data in Herrero et al. 2011 to carry out an energy balance involving the inflow and the outflow from the diversion, the results of which are detailed in Herrero et al. 2012.

5) Sediment discharge distribution is related to water discharge distribution through equation (5.3)

Therefore, adopting a logarithmic profile to describe the uniform flow and using the Wong and Parker (2006) equation to compute the sediment transport, a system of eight equations could be set out as follows:

$$Q_j = B_j H_j \left(g H_j S_j\right)^{1/2} \left(\frac{1}{\kappa}\right) \ln\left(\frac{H_j}{z_0}\right) \qquad (j = m,l) \tag{5.24}$$

$$Q_{sj} = B_j D \left(gRD\right)^{1/2} \cdot 3.97 \left(\frac{H_j S_j}{RD} - \theta_c\right)^{3/2} \qquad (j = m,l) \tag{5.25}$$

$$Q_t = Q_m + Q_l \tag{5.26}$$

$$Q_{st} = Q_{sm} + Q_{sl} \tag{5.27}$$

$$z_{0m} + L_m S_m + H_m + \alpha \frac{Q_m^3}{B_m^3 H_m^4} = z_{0l} + L_l S_l + H_l \tag{5.28}$$

$$r_s = \frac{\frac{r_{ss}}{r_{ss}+1} Q_{sst} + \frac{r_{sb}}{r_{sb}+1} Q_{sbt}}{\frac{1}{r_{ss}+1} Q_{sst} + \frac{1}{r_{sb}+1} Q_{sbt}} \tag{5.29}$$

Where r_{ss} is calculated using equations (5.11) to (5.14) and r_{sb} with equations (5.15) to (5.18).

On the other hand, Q and Q_s are imposed and flow conditions upstream from the diversion can be calculated by obtaining the slope, the water depth and the bed load and suspended sediment discharges (Q_{sst} and Q_{sbt}) which are introduced in equation (5.29).

To sum up, in those situations when there is no depression area in the main channel, this equations system has to be applied without considering the vortex energy losses in

equation (5.28) and writing r_{sb} in equation (5.29) as stated by equation (5.15). On the other hand, when the depression is present equation (5.28) is applied with all its terms and r_{sb} is equalled to zero. Considering the analysis shown in subsection 5.2.1, both situations are distinguished by the value of the momentum flux ratio which, in turn, depends on Q_l, H_l, Q_m and H_m, that are unknowns of the system. Therefore, the equations system has to be solved iteratively in order to find a solution that is coherent with the hypotheses assumed when choosing the form of equations (5.28) and (5.29).

5.7 Summary

Based on a previous experimental study (Herrero et al. 2011), an equation to relate solid discharge distribution to water discharge distribution in fluvial diversions is developed. Suspended sediment and bed load sediment are treated separately for this purpose. The distribution of suspended sediment has been determined by assuming a logarithmic profile for the velocities of the incoming flow, a certain lateral acceleration associated with a transversal pressure difference and a sediment concentration depth profile as predicted by the Rouse equation.

On the other hand, the distribution of bed load has been observed to highly depend on the bed morphology patterns generated in the diversion area. Specifically, in some cases a vortex is formed in the main channel downstream from the diversion that entails the formation of a scour hole. In these situations, the vortex captures practically all the bed load sediment and directs it towards the lateral branch. Therefore, the equation that describes bed sediment distribution has two forms, which are applied depending on the situation (with or without the depression). A further analysis of the experimental data has been carried out in order to determine the flow conditions that are compatible with the presence of the depression. The conclusion is that there is a threshold value for the ratio of the momentum flux associated with the flow to each branch that separates the situations with and without the scour hole and subsequently determines the suitable description of the ratio of bed sediment discharge.

The resulting equation for the total solid discharge ratio has been tested against the experimental data and the results obtained are quite satisfactory. The decreasing trend of r_s with total water discharge is reproduced, specifically for those cases in which the depression is present and the vast majority of the sediment is deviated towards the lateral branch.

This equation presents several limitations that can affect its applicability. The 3-dimensional flow patterns that are present in the diversion area can modify the amount of water captured by the lateral branch, with respect to that which derives from the hypothesis applied herein. Moreover, bed sediment direction in the diversion area is assumed to be a function of longitudinal and transversal shear velocities, which are calculated using flow variables that correspond to a downstream location inside the main channel and the lateral branch. Finally, the influence of other variables like the diversion angle or the ratio between the main channel and lateral branch widths is not taken into account and may have impact on the results.

This equation is joined with uniform flow equations and sediment transport equations through each branch, water and solid discharge continuity equations between upstream and downstream from the diversion and the energy balance equation along both branches. The result is a system of eight equations that may be solved to obtain the water discharge, the solid discharge, the water depth and the slope of the lateral branch and the main channel.

Further work is necessary to expand on the several aspects that limit the applicability of this model. However, we consider that to be a promising and constructive starting point in an area that significantly lacks experimental and conceptual analysis.

Chapter 6: Conclusions

Initially, an experimental study was conducted on the analysis of flow and sediment distribution in a 90-degree diversion. The motivation behind the study was a real case corresponding to the lower reach of the delta of the Patía River in Colombia. Due to a man-made structure the river course avulsed to a separate channel, consequently forming a bifurcation. . During the next several years the new bifurcation evolved in such a way that the main course of the river shifted from the old to the new one, generating a social, economic and ecological problem in the area. Despite being inspired by this particular case, the aim of this study is not to reproduce the specific conditions of the Patía river, but to understand the general physics of the phenomena that rule the behavior of flow and sediment transport in fluvial diversions or bifurcations in which, similar to that of the Patía River, one of the downstream branches exits laterally and forms a certain angle with the main channel.

From a solid transport point of view, fluvial diversions or lateral intakes are characterized by a significant trend of sediment to deviate towards the lateral branch. This phenomenon is known as the Bulle effect, in honor of Henri Bulle, the German scientist who carried out the first experiments on this topic.

A new facility was built in the Fluvial Morphodynamics Laboratory at BarcelonaTech University, consisting of a 9-meter long and 20-centimeter wide main channel, and a 2.75-meter long and 20-centimeter wide lateral branch that is connected to the former orthogonally, at a point placed 6.2 meters downstream from the model inlet. The sediment used for the experiments consists of sand with a mean diameter of 0.25mm, which is introduced at the required discharge by an Arquimedes-screw hopper. Different water discharges ranging from 3.5l/s to 6l/s were introduced at the model inlet and a constant solid discharge of 5.5g/s was kept throughout the different tests.

The adopted approach intended to shed some light on several aspects on which the current literature is limited. First of all, models of fluvial diversions considering sediment transport are quite meager and only include experimental studies. Conclusions obtained from numerical analyses are only indirect and drawn from fixed-bed conditions. Furtehermore, the existing experimental reports do not describe the system evolution from an initial state to final equilibrium. Moreover, the duration of the experiments cast some doubts over the attainment of such state of equilibrium. Lastly, no description is available of the influence of bed morphology evolution and the flow patterns that are in turn related to the local sediment transport in the diversion area.

The protocol and methodology of the experiments were developed considering the previous points. Each test was started from an initial flat-bed condition. Water discharge and solid discharge were measured every 60 minutes, as well as bed level and water surface height along the whole model. The experiment was maintained until the system reached equilibrium, which was identified when water and solid discharge at the end of the branches were approximately constant, as well as the bed level at several reference points in the diversion area. At the end of each experiment, bed bathymetry was measured in detail in the diversion area and flow patterns were observed with the help of laser projections on planes parallel and perpendicular to the main channel direction.

The experimental results confirm the sediment's tendency to deviate towards the lateral branch reported in previous studies and field observations, which is known as the Bulle effect. However, in our experiments, this effect was observed to be much more significant for the experiments with a high total water discharge, in our case above 4.75l/s. In such instances, around 90 percent of the sediment arriving from upstream follows through the lateral branch, whereas only between 25 and 40 percent of the water discharge does so. On the other hand, for low water discharge experiments there is an initial phase during which most of the sediment is deviated but the system evolves towards a state in which only around 30 to 40 percent of the solid discharge is captured by the lateral branch. Regarding water discharge ratio, the situation is much more dramatic, as only around 10 percent of the total flow follows the lateral branch.

The conditions with a high solid discharge in the lateral branch coincide with the presence of two remarkable patterns in the diversion area. On one hand, an erosion pit is formed in the first stretch of the main channel and downstream the diversion, with a maximum bed level difference in relation to the upstream bed bathymetry equivalent to 2 to 3 times the water depth. On the other hand, a vortex is observed in front of the entrance of the diversion presenting a horizontal axis parallel to the lateral branch direction. This stretching vortex is observed to cause an abrupt change in the direction of the bed load sediment and is interpreted as the main cause of the high solid discharge in the lateral branch. Both the stretching vortex and the erosion pit are connected between them, in such a way that the pit is formed due to the alteration of the flow velocity field in the diversion area and, as the erosion continues, the increase in space causes the vortex to become enlarged which, in turn, enhances the eroding process. Measurements of the bed height at a reference point in the pit area were compared to the measurements of the solid discharge ratio for the experiments with a low total water discharge, showing that the disappearance

of the depression area is always followed by the decrease in the solid discharge in the lateral branch. Therefore, the experimental results highlight that the vortex and the associated erosion pit play a crucial role on the sediment discharge distribution.

The experimental results were analyzed in order to define the conditions that allow the presence of the vortex and the pit. Inspired by the influence of the flow momentum ratio between two converging tributaries on the bathymetry of the convergence area, the ratio between the momentum associated with the lateral branch flow and that related to the main channel flow was calculated and compared to the bed morphology evolution in the depression area. Momentum ratios corresponding to the different states of equilibrium showed an increasing trend as the total water discharge upstream the diversion rose. Special attention was paid to the phase in which the pit disappears during the experiments with low total discharge. Momentum ratio values before and after the pit's disappearance were compared and a value of 0.04 was proposed as a threshold that separates the states in which the depression is present (above the threshold value) from those where the bed bathymetry is continuous along the main channel (below the threshold value).

We interpret the observations as follows: in the first phase of the experiments the momentum ratio is always above the threshold value and the vortex and the depression are formed, causing most of the sediment to deviate toward the lateral branch. Due to excess sediment feeding, deposition occurs at the first stretch of the lateral branch, causing a raise of the bed level that partially blocks the entrance of this branch. Subsequently, the water discharge in the lateral branch and the momentum ratio both decrease. As deposition occurs, lateral branch slope progressively increases until the feeding sediment equals the transport capacity. If the blockage of the lateral branch is such that the momentum ratio falls below the threshold value, the vortex and the pit both disappear, solid discharge in the lateral branch decreases and the system evolves to a state of equilibrium in which the bed bathymetry is continuous along the main channel. On the other hand, if, the momentum ratio is still above the threshold value once the sediment feeding of the lateral branch has reached an equilibrium with the transport capacity, the system evolves towards a state of equilibrium in which the vortex and the depression are present.

With regard to the experimental results and the subsequent conclusions, a theoretical analysis was carried out in order to develop a conceptual model of the equilibrium configuration of fluvial diversion. Previous models for Y-shaped bifurcations developed by Wang et al. (1995) and Bolla Pittaluga et al. (2003) were taken as a basis. These models include the equations of uniform flow and transport capacity along each branch, water

discharge and solid discharge continuity equations, water surface compatibility at the diversion and a nodal equation that relates solid discharge distribution to water discharge distribution. The variables involved are water depth, channel slope, water discharge and solid discharge in each branch, therefore setting a system of eight equations with eight variables that can be solved. However, the diversions' characteristics present some particularities that make the application of these models unsuitable. On one hand, water surface compatibility at the diversion implies the assumption of no local energy losses in the bifurcation area; and, energy balance in the system only takes into account the energy losses associated with friction along the branches. However, the 3-dimensional flow patterns characteristic of a diversion and the previously mentioned vortex in particular highlight that in some conditions, local energy losses may be important and should be taken into account. Energy heights calculated starting from the experimental results confirm this point, as they are in the order of 1cm, approximately ten times higher than those associated with bed friction in the equivalent channel stretch. On the other hand, the nodal equation describing sediment distribution at the diversion should differ from that of the Y-shaped bifurcations, considering the difference in the physical phenomena involved. Therefore, the analytical work carried out in this thesis aims to deal with these two limitations and propose an alternative approach to these points.

Concerning the water surface compatibility equation, the model proposed herein substitutes it for an energy balance equation along the branches that takes into account the energy losses associated with the vortex in those situations in which it is present. These energy losses are calculated as proportional to the cube of the characteristic velocity of the vortex and inversely proportional to its characteristic length, an approach that has proved to be successful when applied to vorticity associated to bridge piers (Bateman et al., 2005). The characteristic velocity is considered to be the velocity of the flow that follows the main channel calculated from the main channel discharge and the water depth in the section upstream from the depression. The characteristic length is considered to be the bed level difference between the section upstream from the depression and the section at the point of maximum depth. This energy balance was tested against the experimental data and the proportionality constant was found to be of order 1. An increasing trend is observed in its values as total water discharge rises, which is interpreted as a consequence of the increase in the vortex stability.

With regards to the nodal equation describing solid discharge distribution, suspended sediment is considered separately from bed load sediment. Suspended sediment is assumed

to move following the flow velocity field and its distribution has been determined by assuming a logarithmic profile for the velocities of the incoming flow, a certain lateral acceleration associated with a transversal pressure difference and a sediment concentration depth profile as predicted by the Rouse equation. Alternatively, concerning bed load distribution, two possible cases are considered. In those situations in which the vortex and the pit are present, all the bed load discharge is considered to deviate towards the lateral branch. Oppositely, when the vortex and the depression are not present due to the flow conditions, the ratio of bed load discharge is obtained by assuming a flow direction of the sediment which is calculated from the shear velocities associated with the main channel flow and the lateral branch flow.

As a result, a system of eight equations and eight variables is obtained. It should be noted that the two equations proposed herein present a different version depending on the momentum ratio between the lateral branch and the main channel, which in turn depend on the unknowns of the problem. Therefore, the system must be solved iteratively assuming conditions with or without the existence of the vortex and checking if the hypothesis is consistent with the adopted hypothesis.

The model presents several limitations that can affect its applicability. The 3-dimensional flow patterns that are present in the diversion area can modify the amount of water captured by the lateral branch, with respect to that which is derived from the hypothesis applied herein. Moreover, bed sediment direction in the diversion area is assumed to be a function of longitudinal and transversal shear velocities, which are calculated using flow variables that correspond to a downstream location inside the main channel and the lateral branch. Finally, the influence of other variables like the diversion angle or the ratio between the main channel and lateral branch widths is not taken into account and may have an impact on the results. However, we consider that the experimental results presented in this thesis partially palliate the lack of data on movable-bed experiments in diversions and cast some light upon several patterns governing the morphology evolution of this kind of systems. Moreover, the conceptual model developed herein represents, despite its limitations, a good starting point for the theoretical analysis of fluvial diversions, which could be improved with the performance of additional experiments focused on the influence of variables, such as the diversion angle or the width ratio.

Bibliography

Ashmore, P. E. (1991). How do gravel-bed rivers braid?, *Can. J. Earth Sci*., 28, 326-341.

Ashmore, P. E. (2001). Braiding phenomena: statics and kinetics. In: Mosley, M.P. (Ed.), Gravel-Bed Rivers V. New Zealand Hydrological Society, Wellington, pp. 95-121.

Barkdoll, B. D., Hagen, B. L. and Odgaard, A. J. (1998). Experimental comparison of dividing open-channel with duct flow in T-junction. *Journal of Hydraulic Engineering*, ASCE,124 (1), 92-95.

Barkdoll, B. D., Ettema, R. and Odgaard, A. J. (1999). Sediment control at lateral diversions: Limits and enhancements to vane use. *Journal of Hydraulic Engineering*, 125 (8), 862-870.

Batchelor, G.K. (1953). The theory of homogeneous turbulence. *Cambridge Science Classics*.

Bateman, A., Fernández, M., Parker, G. 'Morphodynamic model to predict temporal evolution of local scour in bridge piers', in *Proceedings of RCEM 2005*, pp. 911-920.

Bateman, A., Medina, V, Mujal, A., Díaz, A. and Puig, C. (2009). The impressive case of the uncontrolled diversion of the Patía River at its delta and the social and environmental consequences, in *Proceedings of RCEM 2009*, pp. 395-401.

Bertoldi, W., Pasetto, A., Zanoni, L. and Tubino, M. (2005). Experimental observations on channel bifurcations evolving to an equilibrium state. In *Proceedings of RCEM 2005*, pp. 409-419.

Bertoldi, W. and Tubino, M. (2005). Bed and bank evolution of bifurcating channels, *Water Resources Research*, 41, W07001, doi:10.1029/2004WR003333.

Bertoldi, W. Miori, S., Salvaro, M., Zanoni, L. and Tubino, M. (2006). Morphological descriptionof river bifurcations in gravel-bed braided networks. In *Proceedings of River Flow 2006*, pp. 1311-1318.

Bertoldi, W. and Tubino, M. (2007). River bifurcations: Experimental observations on equilibrium configurations, *Water Resources Research*, 43, W10437, doi:10.1029/2007WR005907.

Biron, P., Best, J. L. and Roy, A. G. (1996). Effects of bed discordance on flow dynamics at open channel confluences. *Journal of Hydraulic Engineering*, ASCE, 122 (12), 676-682.

Bolla Pittaluga, M., Repetto, R., Tubino, M. (2003). Channel bifurcation in braided rivers: Equilibrium configurations and stability. *Water Resources Research* 39 (3), 1046, doi:10.1029/2001WR001112.

Bradbrook, K. F., Lane, S. N., Richards, K. S. (2000). Numerical simulation of three-dimensional time-averaged flow structure at river channel confluences. *Water Resources Research*, 36 (9), 2731-2746.

Brink, C. J. (2004). Bend diversion to minimize sediment intake. *Master thesis*, University of Stellenbosch.

Bulle, H. (1926). Untersuchungen über die Geschiebeableitung bei der Spaltung von Wasserläufen. *VDI Verlag,* Berlin.

Burge, L. M. (2006). Stability, morphology and surface grain size patterns of channel bifurcation in gravel-cobble bedded anabranching rivers, *Earth Surf. Prcesses Landforms*, 31, 1211-1226.

Colombini, M., Seminara, G. and Tubino, M. (1987). Finite amplitude alternate bars, *Journal of Fluid Mechanics*, *181*, 213-232.

De Heer, A. and Mosselman, E. (2004). Flow structure and bedload distribution at alluvial diversions. In *Proceedings of River Flow 2004*, pp. 801-806.

De Serres, B., Roy, A. G., Biron, P. M. and Best, J. L. (1999). Three-dimensional structure of flow at a confluence of river channels with discordant beds. *Geomorphology*, 26 (1999), 313-335.

Federici, B. and Paola, C. (2003). Dynamics of bifurcations in noncohesive sediments, *Water Resources Research*, 39(6), 1162, doi:10.1029/2002WR001434.

Flokstra, C. (2006). Modelling of submerged vanes. *Journal of Hydraulic Research*, 44 (5), 591-602.

Frings, R. M. and Kleinhans, M. G. (2008). Complex variations in sediment transport at three large river bifurcations during discharge waves in the river Rhine. *Sedimentology* (2008) 55, 1145-1171.

Gupta, U. P., Sharma, N. and Ojha, C. S. P. (2007). Performance evaluation of tapered vane. *Journal of Hydraulic Research*, 45 (4), 472-477.

Habermaas, F. (1935). Geschiebeeinwanderung in werkkanäle und deren verhinderung. *Wasserkraft und Wirtschaft* 30: 97-103 (in German).

Herrero, A., Bateman, A. and Medina, V. (2011). Experimental analysis of flow and sediment transport in a 90-degrees diversion. In *Proceedings of RCEM 2011*, pp. 1537-1547.

Herrero, A., Bateman, A. and Medina, V. (2012). Sediment transport in a 90-degree diversion: experimental and conceptual approach. In *Proceedings of River Flow 2012*, pp. 649-656.

Hirose, K., Hasegawa, K. and Meguro, H. (2003). Experiments and analysis on mainstream alternation in a bifurcated channel in mountain rivers. In *Proceedings of RCEM 2003*, pp. 571-583.

Hsu, C-C., Tang, C-J., Lee, W-J. and Shieh, M-Y. (2002). Subcritical 90º equal-width open-channel dividing flow. *Journal of Hydraulic Engineering*, ASCE, 128 (7), 716-720.

Ikeda, S., Parker, G., Sawai, K. (1981). Bend theory of river meanders. Part 1: Linear development. *Journal of Fluid Mechanics* 112, 363-377.

Islam, G. M. T., Kabir, M. R. and Nishat, A. (2006). Nodal point relation for the distribution of sediments at channel bifurcation, *Journal of Hydraulic Engineering*, ASCE, 132 (10), 1105-1109.

Kasthuri, B. and Pundarikhanthan, N. V. (1987). Discussion on separation zone at open channel junction. *Journal of Hydraulic Engineering*, ASCE, 113 (4), 543-548.

Khan, A. A., Cadavid, R. and Wang, S. S. Y. Simulation of channel confluence and bifurcation using the CCHE2D model. In *Proc. Instn. Civ. Engrs Water & Mar. Engng, 2000*, 142, June, 97-102.

Kleinhans, M., Jagers, B., Mosselman, E. and Sloff, K. (2006). Effect of upstream meanders on bifurcation stability and sediment division in 1D, 2D and 3D models. In *Proceedings of River Flow 2006*, pp. 1355-1362.

Kleinhans, M. G., Wilbers, A. W. E. and ten Brinke, W. B. M. (2007). Opposite hysteresis of sand and gravel transport upstream and downstream of a bifurcation during a flood in the River Rhine, the Netherlands. *Netherlands Journal of Geosciences*, 86 (3), 273-285.

Kleinhans, M. G., Jagers, H. R. A., Mosselman, E, Sloff, C. J. (2008). Bifurcation dynamics and avulsion duration in meandering rivers by one-dimensional and three-dimensional models, *Water Resources Research*, 44, W08454, doi:10.1029/2007WR005912.

Kobayashi, K., Hasegawa, K. and Moriya, K. (2005). Hydraulic properties of a bifurcated channel system with different bed slopes under sub-critical flow. In *Proceedings of RCEM 2005*, pp. 389-394.

Lama, S. K., Kuroki, M. and Hasegawa, K. (2002). Study of flow bifurcation at the 30º open channel junction when the width ratio of branch channel to main channel is large. *Annual Journal of Hydraulic Engineering*, JSCE, Vol.46, 2002, February.

Leite Ribeiro, M., Blanckaert, K., Roy, A. G. and Schleiss, A. J. (2012). Flow and sediment dynamics in channel confluences. *Journal of Geophysical Research*, 117, F01035, doi:10.1029/2011JF002171.

Li, C. W. and Zeng, C. (2009). 3D numerical modeling of flow divisions at open channel junctions with or without vegetation. *Advances in Water Resources*, 32 (1), 49-60.

Marelius, F. and Sinha, S. K. (1998). Experimental investigation of flow past submerged vanes. *Journal of Hydraulic Engineering*, ASCE, 124 (5), 542-545.

Miori, S., Repetto, R. and Tubino, M. (2005). Morphological evolution of bifurcations in gravel-bed rivers with erodible banks. In *Proceedings of RCEM 2005*, pp. 421-430.

Miori, S., Repetto, R. and Tubino, M. (2006). Unsteadiness effects on the morphological behavior of gravel-bed river bifurcations. In *Proceedings of River Flow 2006*, pp. 1283-1291.

Miori, S., Bertoldi, W., Casarin, A. and Tubino, M. (2008). Influence of discharge fluctuations on the morphodynamics of river bifurcations. In *Proceedings of River Flow 2008*, pp. 1463-1470.

Miyawaki, S., Constantinescu, G., Rhoads, B. and Sukhodolov, A. (2010). Changes in three-dimensional flow structure at a river confluence with changes in momentum ratio. In *Proceedings of River Flow 2010*, pp. 225-232.

Moghadam, M. K., Bajestan, M. S. and Sedghi, H. (2010). Sediment entry investigation at the 30 degree water intake installed at a trapezoidal channel. *World Applied Sciences Journal*, 2010, 11 (1): 82-88.

Nakato, T., Kennedy, J. F., and Bauerly, D. (1990). Pump-station intake-shoaling control with submerged vanes. *Journal of Hydraulic Engineering*, ASCE, 116(1), 110-128.

Nakato, T. and Ogden, F. L. (1998). Sediment control at water intakes along sand-bed rivers. *Journal of Hydraulic Engineering*, ASCE, 124 (6), 589-596.

Neary, V. S., Sotiropoulos, F. (1996). Numerical investigation of laminar flows through 90-degree diversions of rectangular cross-section. *Comp. and Fluids*, 25(2), 95-118.

Neary, V. S., Sotiropoulos, F., Odgaard, A. J. (1999). Three-dimensional numerical model of lateral-intake inflows. *Journal of Hydraulic Engineering*, ASCE, 125 (2), 126-140.

Odgaard, A. J. (2009). River Training and Sediment Management with submerged vanes. *ASCE Press*.

Odgaard, A. J., and Mosconi, C. E. (1987). Streambank protection by submerged vanes," *Journal of Hydraulic Eng*ineering, ASCE, 113(4), 520-536.

Odgaard, A. J., and Spoljaric, A. (1986). Sediment control by submerged vanes. *Journal of Hydraulic Engineering*, 112(12), 1164-1181.

Odgaard, A. J. and Wang, Y. (1991a). Sediment management with submerged vanes. I: Theory. *Journal of Hydraulic Engineering*, ASCE, 117 (3), 267-283.

Odgaard, A. J. and Wang, Y. (1991a). Sediment management with submerged vanes. II: Applications. *Journal of Hydraulic Engineering*, ASCE, 117 (3), 284-302.

Omidbeigi, M. A., Ayyoubzadeh, S. A. and Safarzadeh, A. (2009). Experimental and numerical investigations of velocity field and bed shear stresses in a channel with a lateral intake. *33rd IAHR Congress: Water Engineering for a Sustainable Environment*, Vancouver, Canada, pp: 1284-1291.

Ordóñez, J. L. (1974). Sediment exclusion at river diversions. Hydraulic engineering report HEL-24. *Hydraulics and Sanitary Engineering Laboratory*, UC, Berkeley.

Pirestani, M. R., Salehi Neyshabouri, A. A. and Tabatai, M. R. M. (2007). Physical modeling of the flow in lateral intakes in curved channels. *10th International Symposium on River Sedimentation*, Moscow, Russia.

Pizardeh, B. and Shamloo, H. (2007). Investigation of characteristics of separation zones in T-junctions. *12th WSEAS Int. Conf. on applied mathematics, Cairo, Egypt, 2007*, 189-193.

Popp, M., Sallet, D. W. (1983). Experimental investigation of one and two-phase flow through a tee junction. *Proc. Int. Conf. on Physical Modeling of Multi-Phase Flow*, BHRA, Cranfield, Bedford, England, 67-88.

Ramamurthy, A. S. and Satish, M. G. (1988). Division of flow in short open channel branches. *Journal of Hydraulic Engineering*, ASCE, 114 (4), 428-438.

Ramamurthy, A. S., Tran, D. M. and Carballada, L. B. (1990). Dividing flow in open channels. *Journal of Hydraulic Engineering*, ASCE, 116 (3), 449-455.

Ramamurthy, A. S., Qu, J. and Vo, D. (2007). Numerical and experimental study of dividing open-channel flows. *Journal of Hydraulic Engineering*, ASCE, 133 (10), 1135-1144.

Rezapour, S., Moghadam, K. F. and Omid Naceni, S. T. (2009). Experimental study of flow and sedimentation at 90º open-channel diversion. *33rd IAHR Congress: Water Engineering for a Sustainable Environment*, 2979-2986.

Rhoads, B. L. and Sukhodolov (2001). Field investigation of three-dimensional flow structure at stream confluences: 1. Thermal mixing and time-averaged velocities. Water Resources Research, 37, 2393-2410, doi: 10.1029/2001WR000316.

Rocha, A. (2005). Análisis del comportamiento de los sólidos en una bifurcación. *Revista Ingeniería Civil de la Universidad Nacional de Ingeniería* (Perú), Nº3/Ed. Noviembre 2005.

Ryad, K. (1961). Analytical and experimental study of bed load distribution at alluvial diversions. *Dissertation, Delft Univ. Technol*., Waltman.

Seminara, G. and Tubino, M. (1989). Alternate bars and meandering: Free, forced and mixed interactions. In *River Meandering, Water Resour. Monogr*., vol. 12, edited by S. Ikeda and G. Parker, pp. 267 – 320, AGU, Washington, D. C.

Shettar, A. S. and Murthy, K. K. (1996). A numerical study of division of flow in open channels. *Journal of Hydraulic Research, IAHR*, 1996, 34 (5), 651-675.

Sinha, S. K. and Marelius, F. (2000). Analysis of flow past submerged vanes. Journal of Hydraulic Research, 38 (1), 65-71.

Sloff, C. J., Bernabe, M. and Baur, T. (2003). On the stability of the Pannerdense Kop river bifurcation. In *Proceedings of River Flow 2003*, pp. 1001-1011.

Sloff, C.J. and Mosselman, E. (2012). Bifurcation modeling in a meandering gravel-sand bed river. *Earth Surface Processes and Landforms* 37: 1556-1566.

Struiksma, N., Olesen, K., Flokstra, C. and Vriend, H. D. (1985). Bed deformation in curved alluvial channels, *Journal Hydraulic Research*, 23 (1), 57-79.

Van der Mark, C. F. and Mosselman, E. (2012). Effects of helical flow in one-dimensional modeling of sediment distribution at river bifurcations. *Earth Surface Processes and Landforms (2012).*

Vasquez, J.A. (2005). Two-dimensional numerical simulation of flow diversions. *17th Canadian Hydrotechnical Conference*, Edmonton, Canada.

Wang, B., Fokking, R., De Vries, M., Langerak, A., (1995). Stability of river bifurcations in 1D morphodynamics models. *Journal of Hydraulic Research*, 33 (6), 739-750.

Wang, Y., Odgaard, A. J., Melville, B. W., and Jain, S. C. (1996). Sediment control at water intakes *Journal Hydraulic Engineering*, ASCE, 122(6), 353-356.

Wong, M. and Parker, G. (2006). Reanalysis and correction of bed-load relation of Meyer-Peter and Müller using their own database. *Journal of Hydraulic Engineering*, ASCE, 132 (11), 1159-1168.

Yang, F., Chen, H. and Guo, J. (2009). Study on diversion angle effect of lateral intake flow. *33rd IAHR Congress: Water Engineering for a Sustainable Environment*, 4509-4516.

Yonesi, H. A., Omid, M. H. and Haghiabi, A. H. (2008). A study of the effects of the longitudinal arrangement of submerged vanes on sediment behavior near intake structures. *Journal of Hydraulic Research*, 46 (6), 814-819.

Zanichelli, G., Caroni, E. and Fiorotto, V. (2004). River bifurcation analysis by physical and numerical modeling. *Journal of Hydraulic Engineering*, ASCE, 130 (3), 237-242.

Zhou, J. and Zeng, C. (2009). 3-D hybrid LES-RANS model for simulation of open-channel T-diversion flows. *Water Science and Engineering*, 2009, 2(3): 13-26.

Zolezzi, G. and Seminara, G. (2001). Downstream and upstream influence in river meandering. Part one: General theory and application of over-deepening. *Journal of Fluid Mechanics*, 438, 183-211.

Zolezzi, G., Bertoldi, W., Tubino, M. (2006). Morphological analysis and prediction of channel bifurcations. In: Sambrook-Smith, G.H., Best, J.L., Bristow, C.S., and Petts, G.E. (Eds), Braided Rivers: Process, Deposits, Ecology and Management. IAS Special Publication 36, Blackwell, Oxford, UK, pp. 233-256.

Appendices

Appendix A - Tables of results

Table A.1. Froude and Reynolds numbers at the entrance and both exits of the diversion (points A, B and E)

Q (l/s)	3.5	4	4.5	4.75	5	5.5	6
Fr_A	0,776	0,678	0,628	0,680	0,719	0,738	0,674
Fr_B	0,577	0,584	0,464	0,131	0,129	0,101	0,080
Fr_E	0,586	0,403	0,558	0,540	0,474	0,383	0,362
Re_A ($*10^3$)	50,81	53,88	59,45	63,22	66,64	71,93	75,63
Re_B ($*10^3$)	44,72	49,78	51,24	32,80	33,41	30,17	26,82
Re_E ($*10^3$)	5,89	5,98	8,61	18,65	19,51	25,29	32,24

Table A.2. Data used for the calculation of coefficient "A" obtained from the experimental results

Time	1			
Q (l/s)	4,75	5	5,5	6
H_A (m)	0,143	0,141	0,148	0,147
H_B (m)	0,139	0,139	0,139	0,136
H_E (m)	0,124	0,125	0,127	0,130
P_A (w)	6,660	6,905	7,997	8,630
P_B (w)	5,058	5,204	5,180	4,917
P_E (w)	1,439	1,459	2,212	3,046
u_1 (m/s)	0,495	0,424	0,474	0,349
l_1 (m)	0,060	0,056	0,081	0,106
L_1 (m)	0,280	0,222	0,328	0,376
u_2 (m/s)	0,386	0,323	0,328	0,215
L_2	0,129	0,133	0,152	0,177
A	0,060	0,170	0,200	0,417
Time	2			
Q (l/s)	4,75	5	5,5	6
H_A (m)	0,143	0,147	0,142	0,144
H_B (m)	0,140	0,140	0,137	0,136
H_E (m)	0,124	0,126	0,130	0,130
P_A (w)	6,674	7,195	7,668	8,502
P_B (w)	5,120	5,333	5,225	5,020
P_E (m)	1,336	1,569	2,208	3,039

u_1 (m/s)	0,594	0,463	0,458	0,400
l_1 (m)	0,058	0,068	0,077	0,098
L_1 (m)	0,250	0,289	0,292	0,359
u_2 (m/s)	0,467	0,361	0,324	0,251
L_2 (m)	0,129	0,131	0,156	0,180
A	0,051	0,119	0,093	0,200
Time	3			
Q (l/s)	4,75	5	5,5	6
H_A (m)	0,140	0,146	0,149	0,142
H_B (m)	0,138	0,140	0,137	0,136
H_E (m)	0,125	0,125	0,126	0,130
P_A (w)	6,533	7,163	8,057	8,380
P_B (w)	5,069	5,256	5,199	4,988
P_E (m)	1,299	1,497	2,078	3,080
u_1 (m/s)	0,565	0,610	0,353	0,283
l_1 (m)	0,042	0,066	0,086	0,098
L_1 (m)	0,083	0,290	0,310	0,320
u_2 (m/s)	0,445	0,467	0,247	0,177
L_2 (m)	0,123	0,134	0,154	0,176
A	0,077	0,075	0,614	0,444
Time	4			
Q (l/s)	4,75	5	5,5	6
H_A (m)	0,145	0,148	0,147	0,145
H_B (m)	0,140	0,139	0,137	0,135
H_E (m)	0,124	0,126	0,127	0,130
P_A (w)	6,767	7,241	7,928	8,544
P_B (w)	5,121	5,395	5,167	4,885
P_E (m)	1,410	1,472	2,143	3,080
u_1 (m/s)	0,579	0,446	0,320	0,366
l_1 (m)	0,061	0,059	0,087	0,098
L_1 (m)	0,272	0,256	0,341	0,364
u_2 (m/s)	0,456	0,354	0,223	0,225
L_2 (m)	0,128	0,128	0,156	0,177
A	0,055	0,198	0,602	0,344
Time	5			

Q (l/s)	4,75	5	5,5	6
H_A (m)	0,144	0,145	0,147	0,144
H_B (m)	0,137	0,140	0,137	0,137
H_E (m)	0,125	0,126	0,128	0,130
P_A (w)	6,726	7,135	7,944	8,458
P_B (w)	4,944	5,288	5,107	4,925
P_E (m)	1,520	1,585	2,261	3,005
u_1 (m/s)	0,409	0,463	0,320	0,286
l_1 (m)	0,060	0,051	0,087	0,093
L_1 (m)	0,269	0,179	0,341	0,345
u_2 (m/s)	0,317	0,356	0,221	0,175
L_2 (m)	0,127	0,134	0,156	0,177
A	0,178	0,163	0,565	0,718

Appendix B - Future works

This appendix summarizes several aspects that, to the author's consideration, would be interesting topics to carry on with the line of research undertook within this thesis. Unfortunately, the lack of time made it impossible to tackle them during the period corresponding to the author's PhD studies.

Firstly, the influence of different variables in sediment distribution and bed morphology evolution could be studied using the available laboratory model. The diversion angle can be set to 30º and 60º changing the methacrylate piece that links the lateral branch to the main channel and even other angles could be tested without much difficulty constructing new diversion pieces adapted for other orientations. Considering the results obtained for a 90º diversion and the flow patterns observed, it could be foreseen that for the same water discharge distribution, solid discharge would be higher in the main channel with a lower diversion angle, due to the decrease in the momentum ratio associated with the flow between the transversal and longitudinal directions in the diversion area.

Sediment diameter could also be changed in order to study the influence of this parameter on the formation of the scour pit and the flow patterns associated with it. To the author's knowledge, no experiments with different sediment sizes in a diversion model have been performed in the past.

Although an important modification of the available facility should be made to accomplish this purpose, studying the influence of the width ratio between the lateral branch and the main channel on solid discharge distribution would be a very interesting line of research. In the conditions of the actual model, the commented stretching vortex and the depression formed at the beginning of the main channel downstream of the diversion have a dramatic influence on the sediment deviation towards the lateral branch. However, the model dimensions are such that this pit occupies the whole width of the main channel, therefore affecting all the bed load sediment coming from upstream. Varying the width ratio between both branches and specifically setting a wider main channel in relation to the lateral branch dimension, would help to delimit the scope of the pit and the influence on the solid discharge distribution.

Considering the experiments performed within this thesis, an interesting complementary test would be to reproduce one of the experiments corresponding to a total water discharge above the threshold value that is, one that causes the occurrence of the stretching vortex and the pit, fix with glue the bed sediment once the system has reached the equilibrium state and carry out clear water tests to analyze the flow patterns generated by this

bathymetry. A 3-dimensional numerical model could be used to simulate this situation and compare the calculated results with those obtained experimentally.

With regard to the analyses related to the energy balance between upstream and downstream from the diversion, a detailed measurement of the size and the velocity distribution of the vortexes that occur in the diversion area would certainly help to improve the hypotheses assumed in the current approach. Consequently, the energy balance equation included in the theoretical model could be modified to another one that would probably reproduce better what happens in reality.

Another engaging area of investigation deals with correcting measures for sediment distribution in fluvial diversions. Submerged vanes have been used for this purpose in the last decades, but a better understanding of the flow patterns involved in a diversion and the influence that the different variables have on them, would surely be useful for an optimization of the design variables of these panels. Moreover, different kind of structures could be proposed that may be more appropriate to counteract the flow characteristics that cause the deviation of the sediment. A new thesis is being started in GITS group at the moment, focused on the application of submerged vanes on fluvial diversions.

Finally, from a theoretical point of view some effort would be worth to test the conceptual model proposed herein with the obtained experimental results. This process would imply a mathematical analysis to find the optimum way to solve the system of equations in the different cases. Other hypothesis concerning the new equations proposed here could be tested, for example in relation to the characteristic velocity and the characteristic length that are involved in the energy losses associated with the vortex of the main channel in those cases in which it is present. Different velocity profiles could also be tested in the nodal equation describing the solid discharge distribution.

As a conclusion, these are only some ideas to develop the research in the topic of sediment transport in fluvial direction, an area in which the investigation carried out in the past do not correspond to its width of application.

Appendix C - Sediment resuspension due to density currents

Appendix C includes the article "Sediment resuspension due to density currents caused by temperature difference. Application to Flix reservoir (Spain)", published by the Journal of Hydraulic Research. This paper is the result of an investigation carried out for my master thesis in the Civil Engineering School at BarcelonaTech University and a posterior analysis and deepening of the results. Although it is not directly related with the general topic of the thesis, it is included in the document as an appendix, as it is part of the work performed during my PhD studies.

Sediment resuspension due to density currents caused by temperature difference. Application to Flix reservoir (Spain)

ABSTRACT

Density currents occur in lakes and sea environments when two masses of water interact giving place to a relative movement between them. Depending on initial and boundary conditions, turbulence associated with them is able to lift sediment. This fact can be a problem in places where sediment is contaminated due to industrial activities. In 2001, a pollution episode happened in the Flix reservoir (Tarragona, Spain), in which thousands of fish died and the water supply of cities like Tarragona was affected. This study analyses the possibility of a density current due to temperature difference as the explanation of this event. The previously developed one dimensional, Lagrangian model of subaqueous turbid surges BANG 1D, has been modified to incorporate temperature evolution. The obtained results show that temperature difference can generate a density current which is able to resuspend sediment although the grade of erosion highly depends on the initial velocity of the current.

Keywords: Density currents; mercury; numerical model; resuspension; temperature;

C.1 Introduction

On Christmas day in 2001, several thousands of dead fish appeared in the Ebro River, close to the Flix reservoir area in the north of Spain (Fig. C.1). As a result of this incident, a water analysis was carried out in the river and higher than normal mercury levels were detected. This fact also affected to the water supply quality of important cities like Tarragona.

The presence of a chemical factory close to the place where fish were found, provoked suspicions of a possible illegal dumping in the river, and an investigation started about the factory activities and its waste management (Fig. C.2). In spite of the fact that a sudden dumping of mercurial substances into the river seemed the most reliable explanation of the event, several points called it into question.

The main problem is related to the low solubility of mercury in water. It seems almost impossible that a mercury spillage can dissolve in such a short time and affect a water volume large enough to kill so many fish. This incongruity gave reason to search for other explanations of the event, one of which will be the main objective of this report. This hypothesis is based on the density currents phenomenon.

Density currents are usually caused by a certain sediment source that generates a gradient in suspended sediment concentration, therefore stratifying a mass of water. However, density currents associated with temperature gradients have also been reported in the past (Lemmin *et al*. 1998, Fer 2001, Fer *et al*. 2002). Therefore, under sudden temperature changes, a turbulent current could have been generated and it would have travelled along the bottom of the reservoir, resuspending sediment of the ground, therefore justifying the presence of toxic substances, such as mercury, in river water. The presence of these pollutants in reservoir sediment would be the result of progressive sedimentation of the factory waste dumping throughout all the years it has been working. These polluted sediments have been quantified in about $8 \cdot 10^8$ kg, causing another conflict related to the factory activities (Costa *et al*. 2004).

This report compiles information about different hypotheses that were suggested in relation to the incident, and a new reasoning line based on density currents has been developed as a possible justification of this contamination episode.

The result of this study reflects that temperature can be the factor that triggers a density current, as a temperature difference between two water bodies provokes that the colder falls to the bottom. However, temperature has little direct relation with the sediment resuspension ability of the current and in this sense, the initial water velocity is much more important.

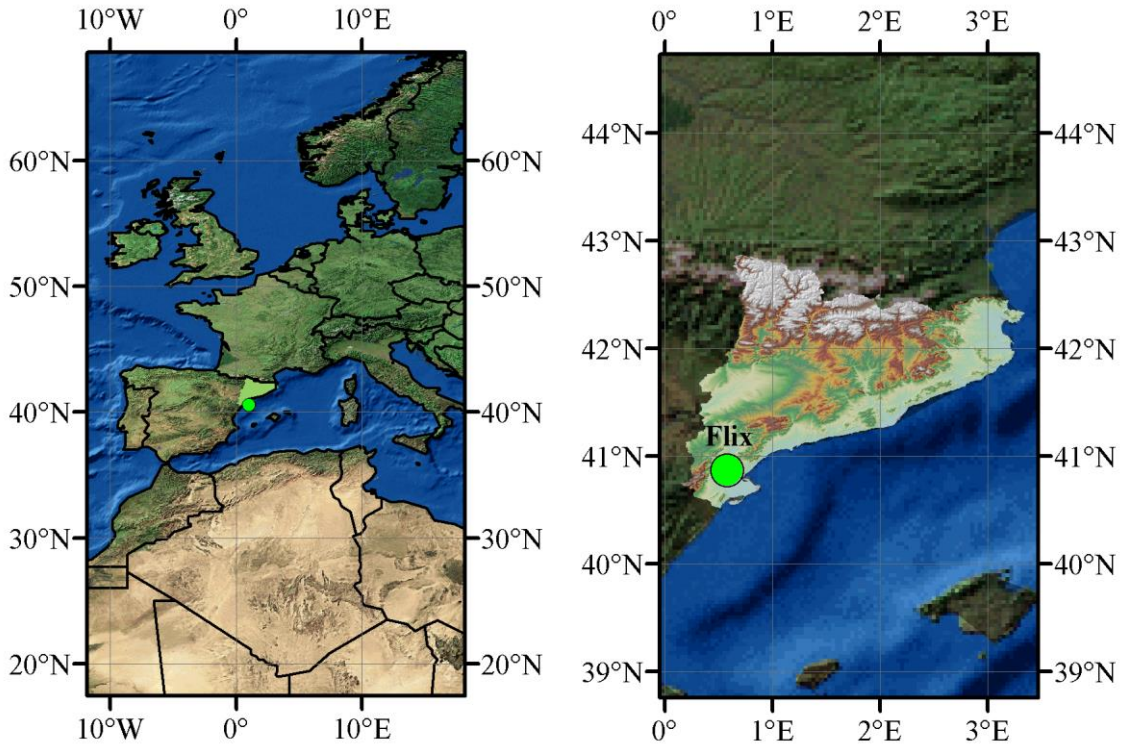

Figure C.6.1. Geographical situation of Flix reservoir (Tarragona, Spain)

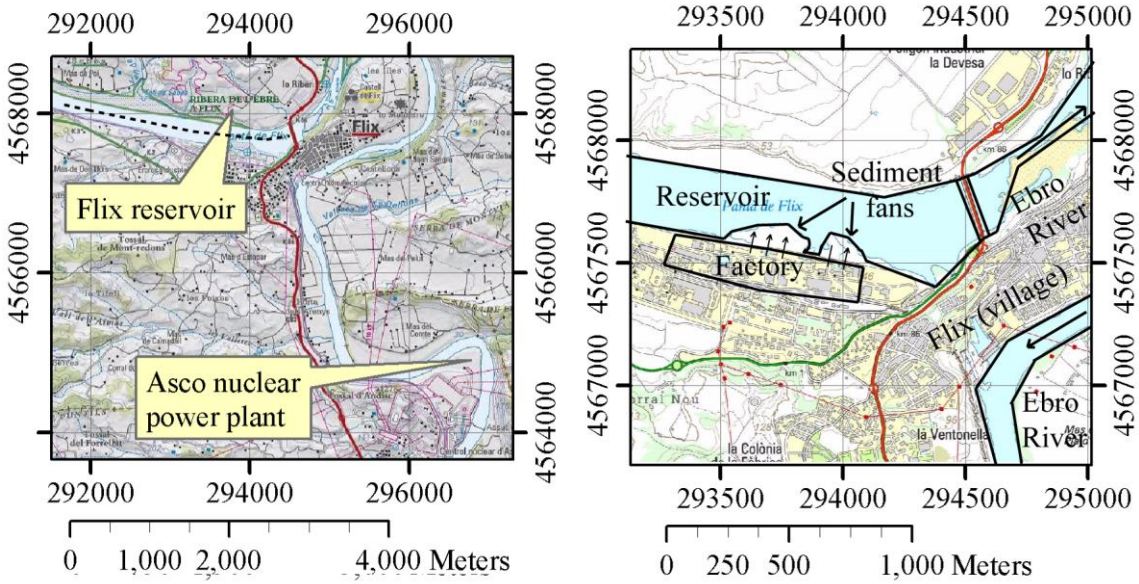

Figure C.6.2. Flix village and reservoir map and scheme of the elements involved in the event. On the left appears the location of the profile shown in Fig. 10 (dashed line)

C.2 Geographical and historical frame

Ercros present factory is located next to the town of Flix, and was built in 1908 on the bank of the Ebro River in the province of Tarragona. It is situated upstream from a mozarabic weir which was used in the early 20th-century for hydroelectric energy generation. The Flix reservoir is part of the hydroelectric compound formed also by the Mequinenza and Ribaroja reservoirs that collect water from the Segre River, an Ebro River tributary. Flix

reservoir volume is small compared with the other reservoirs (5% regarding Riba-roja and 1% regarding Mequinenza). In Table C.1 a summary of reservoirs characteristics is shown.

Table C.1. Characteristics of the reservoirs in the low Ebro River

Reservoir	Year of construction	Volume ($\cdot 10^6 m^3$)	Surface ($\cdot 10^4 m^2$)
MEQUINENZA	1966	1530	7720
RIBAROJA	1969	210	2150
FLIX	1948	11	320

During 40 years, the Flix factory was pouring chemical residuals of different types into the reservoir, which were product of the industrial processes carried out there in the first half of 20^{th} century. As no obstacle was present at that time, residuals were transported by the water flow towards the mouth of the Ebro. Since the construction of the Flix Dam in 1948, polluted sediment coming from the factory started to settle down next to the bank, forming several lobes of material with a high content of chemical products. In 1988 the factory incorporated a filter system in order to avoid the introduction of these substances into the fluvial system. Elements that can be found in Flix reservoir sediments are, in its vast majority: Al, Ca, Fe, L, Mg, Na, P, S, Si; heavy metals as Hg, Cr, Ni, Cu, Zn, As, Se, Cd, Pb, Mn, Ti; others as organo-chlorated and polichlorostyrenes or polichloro-nafthalenes; radionucleids U-238, Ra-226, Pb-210, Th-232, Cs-137, K-40).

The Flix reservoir is located 13km downstream from the Riba-roja reservoir and its volume is about 11 $10^6 m^3$. Water flow is similar to that in low velocity rivers. Regarding bed shear stresses, it is near the threshold for sediment mobilization in the factory area.

Before 1988, three sewers poured sediments previously treated in order to avoid pollutant elements from entering into the fluvial system. It can be stated that after 1988 the industrial activity in the lobes is minimal or negligible. This year a band filter was installed and liquid effluents were deviated to a sewage treatment plant, which afterwards poured the water into the reservoir. In Fig. C.3, taken from Google Earth, the formation of lobes can be appreciated next to the factory. The average reservoir width is about 278m between banks, and around 100m for the lobes. Therefore, flow constriction is remarkably high, about 36%, causing that this zone remains in an unstable equilibrium against any process which lightly raises bed shear stresses, whatever the reason for this increase.

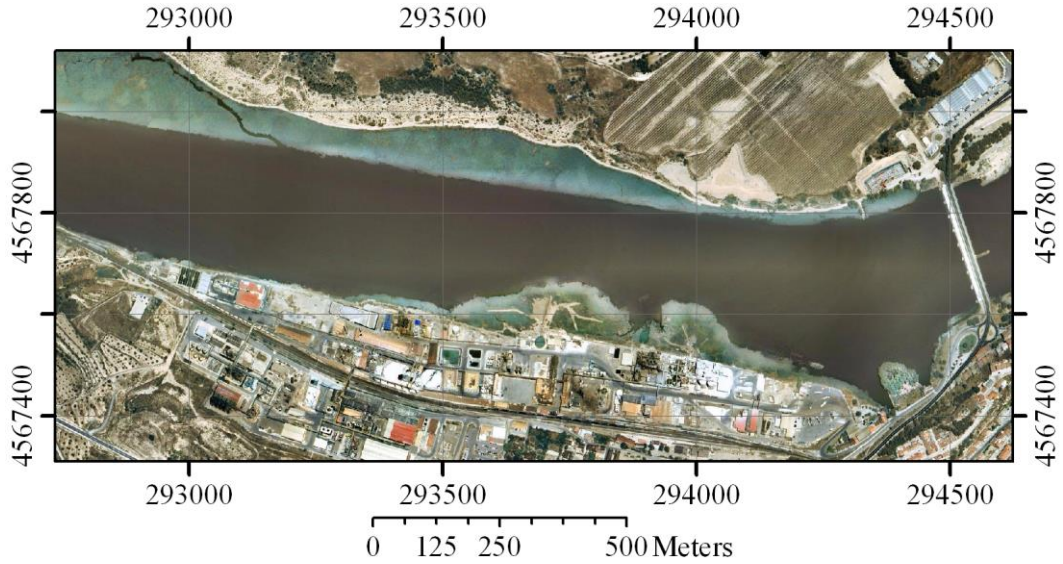

Figure C.6.3. Aerial photograph of Flix reservoir in the Ercros factory area. Lobes can be observed next to the factory.

C.3 Discussion of hypothesis

In this section we discuss several hypotheses set out in the days following the event that appeared in the newspapers. In each case, points for and against are exposed.

Hypothesis: punctual pollutant dumping

At first glance it seems the most evident explanation. In fact it is thus reflected in the first news referring to this event that appeared those days. It is logical to think that the fish's death could be provoked by the dumping of a substance that alters reservoir water composition, which constitutes the environment where these animals lived. Samples of reservoir water and dead fish were taken and analyzed by members of Veterinary School of the Universitat Autònoma of Barcelona. Once the analysis results were known and after the contamination of many important cities of Tarragona, which contributed to enlarge the social alarm, all the accusations turned to the Ercros factory, as it is the only industrial center in the area that uses mercury in its internal production chain.

Ercros factory in Flix specializes in chlorine and soda production, as well as chlorine derivatives, chlorine solvents and bicalcic phosphate. Chlorine is produced by electrolysis of watery solutions of alkaline chlorides and is used in the manufacture of agrochemicals, plastics (mainly PVC and polyurethane), general building materials and pharmaceutical products. It is also suitable for water treatment due to its highly disinfectant properties.

Chlorine is obtained through electrolysis of sodium chloride through the classical Castner-Kellner process (Newell 1903). In this process, a titanium anode is covered with platinum

or platinum oxide, and a mercury cathode which is located at the bottom of the electrolysis cell (Thomson 2000). Mercury captures sodium and forms an amalgam that falls slowly along the bottom of the cell due to a slight slope. Moreover, chlorine gas is captured at the top of the cell in order to use it for other purposes. The amalgam is led to the demercurization tower where it reacts with water injected cross-current, so that sodium and mercury are separated at the same time that soda is produced. Mercury is then led back to the electrolysis cell.

In view of the accusations set out against it, Ercros factory presented several statements that are summed up next:

Activity reduction: the company affirms that due to the low temperatures of those days, the activity was significantly reduced, fact that would imply a lower spillage of pollutant into the river.

No fish were found in the surroundings of the factory: company operators inspected and a higher accumulation of dead animals was not found.

No escape was detected that could justify fish death, although the investigation was carried out by members of the company so it is unknown how much attention to detail was paid.

Ercros affirms that in spite of the reduction of the activity in the demercurization plant, it went on working correctly, so it looks like there was not any technical problem that directly provoked a higher than normal mercury dumping.

These declarations could be called into question due to the possible company subjectivity in a matter in which it is directly affected, but there is another factor that makes this hypothesis incoherent. This fact is the great amount of mercury present in water, as well as its solubility. It seems impossible that somebody suddenly threw the amount of mercury needed for the high concentrations observed in the samples into the water and also that it could dissolve and spread all over the reservoir. Assuming a triangular-shape time distribution of the concentration, with the highest value at the moment of the fish's death and with a total duration of 10 days, the estimated amount of mercury that flowed along the Ebro River was about 400 kg.

Hypothesis: death due to freezing

The fish's death took place on Christmas day in 2001, and during the second fortnight of December of that year one of the most important cold waves of the last years in Catalonia took place. This episode of low temperatures generated a completely chaotic situation in the road and railway systems of Catalonia, due to widespread snowfalls all over Catalan

territory and low temperatures, that in many cases were a record for a long time. In Table C.2, temperatures registered in Flix area during that period are shown.

Table C.2. Flix temperatures from 14/12/2001 to 31/12/2001

	Average temperature (ºC)	Minimum temperature (ºC)	Maximum temperature (ºC)
14.12.01	5.2	-0.2	9.1
15.12.01	-1.4	-3.1	0.3
16.12.01	0.1	-4.9	5.2
17.12.01	-4.7	-6.1	-2.7
18.12.01	-2.3	-5.4	0.3
19.12.01	0.1	-3.0	4.2
20.12.01	-0.1	-2.1	2.1
21.12.01	0.1	-1.4	2.8
22.12.01	-0.5	-1.9	2.5
23.12.01	-0.6	-2.0	1.2
24.12.01	0.9	-4.4	6.7
25.12.01	-3.6	-6.9	3.4
26.12.01	2.3	-6.3	10.7
27.12.01	6.9	-0.3	12.4
28.12.01	6.2	0.8	13.1
29.12.01	3.0	-1.1	10.8
30.12.01	7.3	1.0	13.6
31.12.01	7.1	3.0	11.1

Two low temperature peaks are observed, one on the 16th and 17th, and another during the 25th and 26th. The lowest temperature corresponds to the 25th, which is exactly the day when dead fish appeared. Nevertheless, according to average temperatures, the temperature on the 17th was lower, when it remained below 0ºC during the whole day.

It may be considered that we are talking about an area where minimum temperatures in winter are usually around 5ºC and 10ºC, so the registers of this episode represent certainly extraordinary conditions.

However, species affected by this contamination incident were silures, carps and perchs, a fact that constitutes an important statement against this hypothesis, as silures are an imported specie from northern Europe, so it should be adapted to these cold conditions.

On the other hand, this explanation ignores the presence of mercury in water, although it seems logical that the high concentrations detected ($7.7\ 10^{-6}$kg m^{-3}) may have had some influence on this happening.

In spite of the fact that cold does not seem the main cause of the fish's death, it is true that low temperatures could have raised vulnerability of the fish against other aggressive factors. It is therefore a point to be taken into account.

Hypothesis: thermal shock at the outlet of the refrigeration circuit in Ascó nuclear power-station

The Ascó nuclear power-station is located close to the Flix reservoir area. The refrigeration circuit is used to lower the temperature of the station's primary and secondary circuits, and pours its water near the place where dead fish were found. This fact caused some people to believe that the difference in temperatures between the outlet and the environment, which was colder those days, could be the cause of the fish's death.

There are several factors that question the likeliness of this hypothesis. Firstly, this theory ignores the presence of mercury, although it seems that a concentration which is 25 times higher than usual, should have some incidence in the fish's death. Moreover, the area that is influenced by the outlet of the refrigeration circuit is too small to affect such a large number of fish. Furthermore, fish living in the reservoir are already used to the fact that in this point there is a sudden change of temperatures, so that although this difference may have been higher during those days, it seems to be a situation to which fish should be adapted. As it has been commented in the previous hypothesis, silures come from the north of Europe, particularly from the Rhine watershed. This area is highly industrialized, and similar situations to the one mentioned here are frequently found, so it does not seem very probable that this specie should be affected by this problem.

Hypothesis: resuspension of mercury due to a change in atmospheric pressure

The industry department of the Catalonia government asked Sarrià Chemical Institute (IQS) to elaborate a report about the case, and this gave way to a new hypothesis about the matter. This theory proposed that the presence of contaminants in the water could be due to a resuspension of sediment at the bottom of the reservoir, and that this pollutant

concentration could have killed the fish. According to this report, sediment would have been resuspended because of a sudden change in atmospheric pressure.

The ground of Flix reservoir represents a huge dumping site where all the waste of the factories that surround it, has been accumulating throughout the years. One of these factories is Ercros, and this would be the cause of the presence of mercury in the sediment. Nowadays there are between $2 \cdot 10^8$ and $3 \cdot 10^8$kg of contaminated sediment (Costa *et al.* 2004), and there is a project destined to manage and remove all this material.

The company affirms that generated dumps are legal and that the day when fish died, there was no escape and therefore no point dumping into the reservoir. This new hypothesis would be compatible with the observations as, despite that mercury comes from Ercros, which is the only factory that works with this element, it has been poured gradually throughout around 100 years, which is the age of the company. With regard to mercury losses per ton of chlorine produced ($1.3 \cdot 10^{-3}$kg ton^{-1}), and the annual production of chlorine (150000 tons), the estimated amount of mercury dumped to the environment would be of about 195 kg year^{-1}.

This way, it is also explained that mercury, despite its low solubility in water, was distributed in relatively uniform way in the reservoir, because pollutants are mixed with bottom sediment. As this sediment resuspended and mixed turbulently with water, mercury would have spread all over the reservoir, thus affecting the fish.

However, the mechanism proposed for the resuspension is a change in atmospheric pressure, which does not seem very likely because pressure at the reservoir bed is mainly due to the water column, and atmospheric pressure variations do not affect these values significantly.

On the other hand, the average atmospheric pressure of those days is shown in Table C.3. They correspond to Vinebre station, a village close to Flix.

Table C.3. Atmospheric pressure in December 2001

Date	Average atmospheric pressure ($\cdot 10^2$Pa)
20/12/2001	1020
21/12/2001	1020
22/12/2001	1013
23/12/2001	1010
24/12/2001	1015
25/12/2001	1014
26/12/2001	1010
27/12/2001	1017
28/12/2001	1020
29/12/2001	1013
30/12/2001	1008
31/12/2001	1014

These data seem to discredit definitively this hypothesis, as no strange values are observed, nor sudden exceptional pressure changes which could cause the effects indicated in the IQS report.

Hypothesis: sudden pH change

This hypothesis is described in a news article of December 30th in 2002, that is, after a year of studies about the matter, and is formulated by Roger Lloret, who is the adviser of the prosecution in the trial against Ercros, for another dumping of pollutant products in 1993.
Lloret is a chemical and agricultural engineer and interprets that the fish's death is independent of the presence of mercury in water, but could be due to other dumping carried out by Ercros. This dumping would be of hydrochloric acid and soda, and could have suddenly changed the pH of the water causing the death of the fish.

C.4 Proposal of an alternative hypothesis

As a conclusion to the previous section, none of the raised theories is completely satisfactory and coherent with the observed facts.

This leads to wonder about the need to look for another explanation more compatible with the circumstances that surrounded the event, that are summed up next:

- Great amount of mercury
- Uniform distribution of the element over a wide area of the reservoir
- Exceptionally low temperatures
- Presence of a large amount of contaminants in the sediment of the bottom of the reservoir
- Possible change in water pH

The amount of mercury observed lets us foresee that pollutant comes from the reservoir bed and mixes with water, as sediment in which it was immersed, has been resuspended. Sediment resuspension in different conditions has been studied by several authors (Ravisangar *et al*. 2001, Ravisangar *et al*. 2005, Wan and Fell 2004). The cause of this resuspension represents the main point of the hypothesis developed here and involves the existence of low temperatures. In this way, sediment could have been lifted up by a density current. As it is known, this hydraulic phenomenon is due to the interaction of two water bodies with different densities. In these circumstances, the denser water falls to the bed and generates a turbulent current which may be strong enough to lift up sediment. In the case referred to here, this density difference could be due to a difference in temperatures, but in other situations it could come from a contrast in sediment concentration. This phenomenon is known as turbidity currents (Parker *et al*. 1986, Altinakar *et al*. 1990, García and Parker 1991, García 1993, Bradford and Katopodes 1995, Bradford *et al*. 1997, Bradford and Katopodes 1999).

According to this line of reasoning, what occurred those days could be explained as follows:

During the years that the Ercros factory has been operating, the industry has generated residues with mercury as a consequence of its chlorine production process. This waste has been poured into the reservoir, according to them without breaking the law, and in any case, without having been penalized for that reason. However, even if the authorized dumping levels have not been exceeded, all the contaminant has accumulated at the reservoir bed causing that nowadays there are about $3 \cdot 10^8$kg of contaminated material. Mercury present in sediment could have suffered transformations through biological and non-biological processes, in such a way that the most harmful forms of the element would be predominant (Cathum et al., 2005).

In such conditions the event of 2001 would have occurred, in which the strange meteorological conditions, possibly helped by a punctual drainage in the specific moment from the Riba-Roja reservoir upstream from Flix reservoir, could have triggered a density current with enough strength to resuspend the sediment from the bed and, therefore, mixing mercury with water (Reddi & Bonala 1997). This mercury was later ingested by fish in a large enough concentration or amount to cause their death. Sediment and contaminants mixed with the water could have also caused a change in water pH, which would have increased fish vulnerability. However, this point has not been studied in detail.

To study the soundness of this hypothesis and to better understand the influence of the temperature in this kind of phenomenon, an analysis of the equations that describe density currents is carried out in the following section, and a new equation to introduce the temperature variable in the problem is added. Later, the results obtained with the numerical analysis are exposed.

C.5 Theoretical frame

Density current governing equations

The behavior of a density current is described by the equations of water mass continuity, sediment mass continuity, momentum and turbulent kinetic energy balance which, as developed by Pratson *et al*. (2001), are exposed next:

$$\frac{\partial h}{\partial t}+\frac{\partial \overline{u}h}{\partial x}=e_w\overline{u} \tag{1}$$

$$\frac{\partial \overline{c}h}{\partial t}+\frac{\partial \overline{uc}h}{\partial x}=W_s\left(E_s-r_0\overline{c}\right) \tag{2}$$

$$\frac{\partial \overline{u}h}{\partial t}+\frac{\partial \overline{u}^2h}{\partial x}=Rg\overline{c}hS-\frac{1}{2}Rg\frac{\partial \overline{c}h^2}{\partial x}-u_*^2 \tag{3}$$

$$\begin{aligned}\frac{\partial \overline{k}h}{\partial t}+\frac{\partial \overline{u}\overline{k}h}{\partial x}&=u_*^2\overline{u}+\frac{1}{2}\overline{u}^3e_w-\varepsilon_0h-RgW_sh\overline{c}\ldots\\ &\ldots-\frac{1}{2}Rgh\overline{cu}e_w-\frac{1}{2}RghW_s\left(E_s-r_0\overline{c}\right)\end{aligned} \tag{4}$$

The variables that describe density current evolution are h, the density current height and depth averaged velocity ($\overline{u}$), sediment concentration ($\overline{c}$) and turbulent kinetic energy ($\overline{k}$), which are a function of time ('*t*') and position ('*x*')..

Water entrainment coefficient (e_w) in water mass continuity equation depends on Richardson number (Parker 2001).

In sediment mass continuity equation, sediment fall velocity, w_s, is computed following the formulation developed by Dietrich (1982). Sediment entrainment coefficient is calculated with the expression proposed by García and Parker (1991):

$$E_s = \frac{1.3 \cdot 10^{-7} Z^5}{1 + \frac{1.3 \cdot 10^{-7}}{0.3} Z^5} \tag{5}$$

And

$$Z = \frac{u_*}{W_s} \left(\mathrm{Re_p} \right)^{0,6} \tag{6}$$

$$\mathrm{Re_p} = \frac{\left(RgD_s \right)^{1/2} D_s}{\nu} \tag{7}$$

Where u_* is shear velocity, 'R' is the relative density of the sediment, $\left(\rho_s - \rho_w \right) / \rho_w$, 'g' is the gravity acceleration , D_s is its diameter and ν is water viscosity.

This expression was obtained for values of particle Reynolds number, $\mathrm{Re_p}$, higher than 3.5. Some corrections must be introduced for finer sediment (García and Parker 1993) or in large, low-slope rivers (Wright and Parker 2004). According to the Ebro River sediment characteristics, a mean diameter of 0.1mm was adopted for the calculations, which is suitable for the use of equation (5). The term $r_0 \overline{c}$ accounts for near-bed sediment concentration and a value of 2 has been adopted for parameter r_0 (Choi and García 1996).

Equation (3) considers the momentum balance between forces of inertia, gravity, current pressure and friction. Shear velocity, u_*, is related to turbulent kinetic energy (Parker 1986, 2001) and 'S' is the longitudinal slope.

The turbulent kinetic energy equation takes into account energy changes due to density current turbulence, water entrainment, dissipation related to viscosity through coefficient 'ε_0', sediment suspension, entrained water potential energy and sediment entrainment. Further details of this set of equations can be found in Pratson *et al*. (2001) and La Rocca and Bateman (2010).

In Fig. C.4, the phenomenon is schematized and there the variables defined above appear.

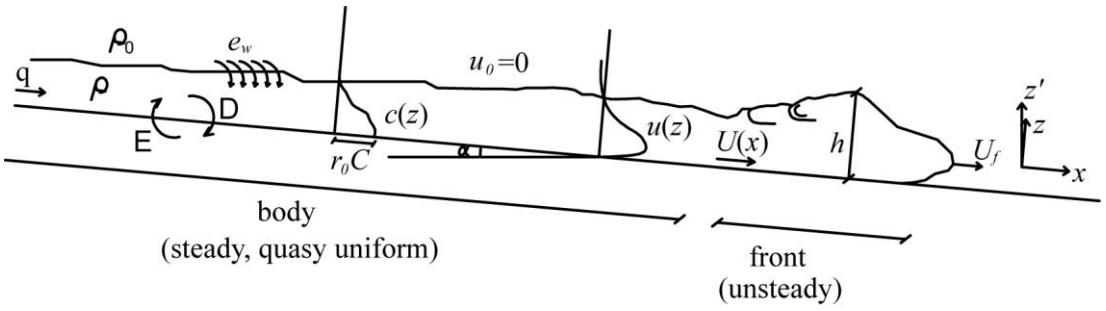

Figure C.6.4. Variables used to describe a density current

Energy balance equation due to heat flux

As mentioned above, the present study considers the possibility of a density current caused by a temperature difference between two water bodies. Therefore, an equation that takes into account processes related to temperature evolution is needed.

Considering a control volume inside a density current, Fig. C.5 shows the different aspects that cause a change in its temperature, which are the following:

- Convection: change of temperature associated to water movement
- Water entrainment through the upper part of the current
- Heat diffusion due to conduction as well as turbulent viscosity
- Turbulent kinetic energy dissipation due to viscosity

According to these criteria, the equation proposed is the following:

$$\frac{\partial(\rho chT)}{\partial t}+\frac{\partial(\rho chT\bar{u})}{\partial x}=e_w\bar{u}\rho_0 c_0 T_0+\rho_s c_s w_s\left(E_s-r_0\bar{c}\right)T^*\ldots$$
$$\ldots+\left(k+\rho c\nu_T\right)\frac{\partial}{\partial x}\left(h\frac{\partial T}{\partial x}\right)+\varepsilon_0\rho h \qquad (8)$$

Where 'ρ', 'c' and 'T', are respectively the global density, the specific heat and the temperature of the density current; 'ρ_0', 'c_0' and 'T_0' are the analogous variables for external water; and 'ρ_s', 'c_s' and 'T_s' for bed sediment. As explained later, T^*, is the temperature corresponding to sediment or density current depending on the erosion-deposition balance. Lastly, 'k' is water thermal conductivity and 'ν_T' is water turbulent viscosity.

Equation (7) left-hand side represents local and convective variation of density current internal energy, ρchT, where ρ, c, h and T are respectively the density, specific heat, depth and temperature of the density current. The product cT has a meaning of energy per mass unit. Following the ideal gas thermodynamic theory, it would be the equivalent to the internal energy per unit mass, that is, an energy associated to density current temperature. When multiplied by density the result is energy per unit volume, and adding the volume it

is finally obtained that ρchT is the internal energy per unit width and unit length in "*x*" direction, that is, the movement direction.

It could be emphasized at this point, that the above equation is an energy balance equation, similarly to turbulent kinetic energy equation. This is conceptually justified, as energy is a conservative magnitude that enables to talk about exchanges and balances, whereas temperature is not.

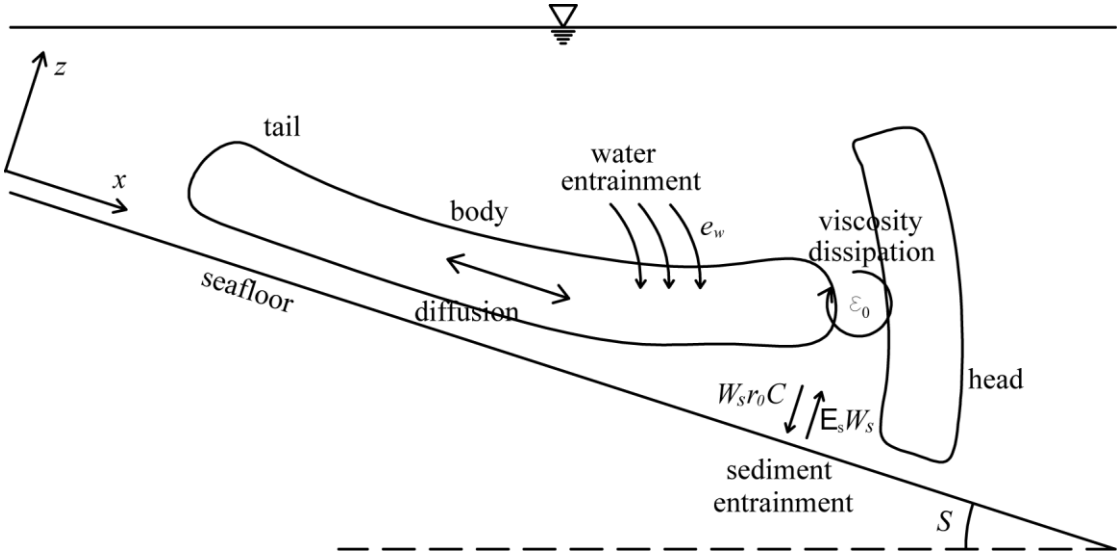

Figure C.6.5. Processes involved in temperature evolution

The first term on the right side, represents variation of energy per surface unit associated with water entrainment from the upper part of the density current, coming from the external fluid.

According to the reasoning carried out above, $c_0 T_0$ is the energy per unit mass of incoming water, where external specific heat and external water temperature are used now. These parameters are considered constants. The objective of differentiating between external and internal specific heats is that in the last one, the presence of sediment will be considered whereas the external adopts the value corresponding to clear water.

When multiplying by the external water density, which will also be considered constant, energy of the incoming water per volume unit is obtained. Similarly to the case of specific heat, external and internal densities are considered separately, in order to take into account the presence of sediment in the first one.

Returning to the continuity equation (equation 1), it can be noticed that $e_w \bar{u}$ has the meaning of an increase of density current water depth per time unit due to water entrainment. Considering that a depth increase is volume per surface unit increase, it is

concluded that product $e_w \bar{u} \rho_0 c_0 T_0$ has the meaning of variation of energy per surface unit with time.

Second term in the right side of the equation represents the energy balance due to sediment erosion and deposition at the bed. However, some remarks must be considered about temperature used here.

Sediment balance of sediment mass balance equation (equation 2) is empirical and refers to global balance, in such a way that it is not valid if the addends are separated. For that reason, when implementing the equation in the numerical analysis, cases when the balance $E_S - r_0 \bar{c}$ is either positive or negative have been considered separately. When it is positive (bed erosion) temperature *T** corresponds to sediment, while when this term is negative, the value refers to density current one. It is not an exact computation, but it is the option that adapts itself better to the origin of the expressions used.

The following term of the equation represents heat diffusive process due to conduction as well as turbulent diffusion of the current.

The first phenomenon is described with the balance of energy flux through the walls of the control volume, considering that heat flux is proportional to temperature gradient. The following expression is obtained, in terms of time variation of energy per surface unit:

$$\frac{\partial}{\partial x}\left(kh \frac{\partial T}{\partial x} \right) \tag{9}$$

Heat diffusion related to turbulence is due to water entrance in the control volume coming from adjacent ones, as a consequence of water turbulence. This water flux is added to the convective flux considered previously. However, this process cannot be treated together with convection because movement related to turbulence has velocities that are zero in their average value, due to the vortex movement, but imply a mass exchange with an associated energy exchange.

This phenomenon is controlled by turbulent viscosity, ν_T, which is related to turbulent kinetic energy and viscosity energy dissipation, ε_0, through the expression:

$$\nu_T = 0.01 \frac{\bar{k}^2}{\varepsilon_0} \tag{10}$$

In order that it has the same physical meaning than the thermal conductivity, it has to be multiplied by the density and specific heat of the current, as K has units of energy per mass unit and ε_0 of power per mass unit, and therefore ν_T is given in $m^2\ s^{-1}$. It is indeed seen that:

$$\left[\mathrm{m^2\ s^{-1}}\right]\left[\mathrm{kg\ m^{-3}}\right]\left[\mathrm{J\ kg^{-1}\ K^{-1}}\right] = \mathrm{J\ m^{-1}\ K^{-1}\ s^{-1}} = \mathrm{W\ m^{-1}\ K^{-1}} \qquad (11)$$

which are the units of thermal conductivity.

What happens in this process is that due to turbulence, water enters the considered control volume with a different temperature, the one corresponding to the adjacent volume. This water entrance involves an energy change proportional to the difference of temperatures between the two control volumes, introducing a first derivative with respect to '*x*'. Balance in the control volume will be determined by turbulence variation from one face to the other of control volume, so there is a second derivative with respect to '*x*', in a similar way to what happens with thermal conduction.

Turbulent viscosity is variable, as it depends on turbulent kinetic energy. For this reason it keeps inside the first derivative in the proposed equation:

$$\frac{\partial}{\partial x}\left[\left(\rho c \nu_T\right) h \frac{\partial T}{\partial x}\right] \qquad (12)$$

Adding the contribution of the thermal conduction process the final conductive term will be:

$$\frac{\partial}{\partial x}\left[\left(k + \rho c \nu_T\right) h \frac{\partial T}{\partial x}\right] \qquad (13)$$

Lastly, there is a term that introduces the increase of energy associated to heat dissipation due to viscosity, which is controlled by parameter ε_0. This parameter has units of energy per mass unit and time unit, so that when multiplying it by density it becomes dissipated energy per volume unit and when multiplying by water depth, the result is energy per surface unit and time unit, the same dimensions as the rest of the terms in the equation. This parameter depends on turbulent kinetic energy and water depth as shown above (Pratson *et al*. 2001).

The transformation process of the equations into their lagrangian form is shown in the next section. In the final energy balance equation due to heat flux, only processes of water and sediment entrainment were considered, for the sake of simplicity and because they were estimated as the relevant processes with influence in temperature variation within the density current.

Equations in lagrangian form

The equations set out above are in eulerian form and describe the mechanics of a density current as it travels through a control volume fixed in space.

In order to develop a finite difference numerical scheme, equations (1)-(4) and (8) are transformed into their lagrangian form, as detailed next. From this approach, equations describe the phenomenon from the material point of view, following particle movement. As an example, the case of mass continuity equation for the fluid is shown in detail, and next the complete system is exposed.

Mass continuity equation

$$\frac{\partial h}{\partial t}+\frac{\partial Uh}{\partial x}=e_w U \Rightarrow \frac{\partial h}{\partial t}+\left(U\frac{\partial h}{\partial x}+h\frac{\partial U}{\partial x}\right)=e_w U$$

$$\Rightarrow \frac{\partial h}{\partial t}+U\frac{\partial h}{\partial x}=e_w U-h\frac{\partial U}{\partial x}\Rightarrow \frac{Dh}{Dt}=e_w U-h\frac{\partial U}{\partial x}$$

System of equations in its lagrangian form

$$\frac{\mathrm{D}H}{\mathrm{D}t}=e_w U-H\frac{\partial U}{\partial x} \tag{14}$$

$$\frac{\mathrm{D}C}{\mathrm{D}t}=\frac{W_s}{h}\left(E_s-r_0 C\right)-Ce_w U \tag{15}$$

$$\frac{\mathrm{D}U}{\mathrm{D}t}=RgCS-\frac{1}{2}\frac{Rg}{H}\frac{\partial CH^2}{\partial x}-\frac{u_*^2}{H}-\frac{e_w U^2}{H} \tag{16}$$

$$\frac{\mathrm{D}K}{\mathrm{D}t}=\frac{u_*^2 U+\frac{1}{2}U^3 e_w}{H}-\varepsilon_0-RgW_s C-\frac{1}{2}RgCUe_w-\frac{1}{2}RgW_s(E_s-r_0 C)-e_w\frac{K}{H}U \tag{17}$$

$$\frac{\mathrm{D}T}{\mathrm{D}t}=\frac{e_w U}{\rho cH}\left(\rho_0 c_0 T_0-\rho cT\right)+\frac{\rho_s c_s w_s}{\rho cH}\left(E_s-r_0 C\right)T^*-\frac{T}{c}\frac{\mathrm{D}c}{\mathrm{D}t}-\frac{T}{\rho}\frac{\mathrm{D}\rho}{\mathrm{D}t} \tag{18}$$

It is necessary to put total derivatives of specific heat and density as a function of total derivatives of concentration, which is already involved in another equation, and the temperature, in such a way that the temperature total derivative can be isolated as a function of known variables.

- $\frac{\mathrm{D}\rho}{\mathrm{D}t}$ as a function of $\frac{\mathrm{D}C}{\mathrm{D}t}$ y $\frac{\mathrm{D}T}{\mathrm{D}t}$:

Concentration variable as set out in this problem is defined as the ratio between sediment volume and total volume. Therefore, the product $\rho_s C$ means mass of sediment divided by total volume. On the other hand, the ratio between water and total volumes is 1-*C* so the term $\rho_w(1-C)$ expresses mass of water divided by the total volume. It can then be concluded that density of the current (total mass/total volume) is:

$$\rho = \rho_s C + \rho_w (1 - C) \tag{19}$$

From this expression, density total time derivative can be computed:

$$\frac{\mathrm{D}\rho}{\mathrm{D}t} = (\rho_s - \rho_w)\frac{\mathrm{D}C}{\mathrm{D}t} + \frac{\mathrm{D}\rho_w}{\mathrm{D}t}(1 - C) \tag{20}$$

The density ρ_w that appears above corresponds to the water inside the density current. It should be differentiated from the rest of density variables that are involved in the problem, as ρ (total density of the current), ρ_0 (density of the external water) and ρ_s (sediment density).

This parameter, ρ_w, depends on temperature and, therefore, the derivative $\frac{\mathrm{D}\rho_w}{\mathrm{D}t}$ is a function of $\frac{\mathrm{D}T}{\mathrm{D}t}$. A simplified version of the state equation is developed in this work. In order to analyze the influence of the temperature evolution into density, a null salinity is considered. Temperature range covers from 2 to 20 ºC. The UNESCO water state equation for sea water is used (Fofonoff and Millard 1983), and a parabolic law is adjusted:

$$\rho_w = -0,064T^2 + 0,0416T + 999,92 \tag{21}$$

From now on, the following notation will be used:

$$a = -0,064$$
$$b = 0,0416$$
$$d = 999,92$$

Water density derivative can then be computed:

$$\frac{D\rho_w}{Dt} = (2aT + b)\frac{DT}{Dt} \tag{22}$$

Finally, total derivative of current total density is:

$$\frac{\mathrm{D}\rho}{\mathrm{D}t} = (\rho_s - \rho_w)\frac{\mathrm{D}C}{\mathrm{D}t} + (2aT + b)(1 - C)\frac{\mathrm{D}T}{\mathrm{D}t} \tag{23}$$

where ρ_w is described as a function of T by the parabolic law shown above.

- $\frac{\mathrm{D}c}{\mathrm{D}t}$ as a function of $\frac{\mathrm{D}C}{\mathrm{D}t}$:

As known, specific heat is defined as the energy needed to raise the temperature of a mass unit one degree. Starting from this idea, the next reasoning is followed to express specific heat as a function of sediment concentration and the specific heats of sediment and water.

The product $c_s\rho_s C$, being c_s the sediment specific heat, has units of energy divided by total volume used to heat the sediment mixed with water. Similarly, $c_w\rho_w(1-C)$ is the energy used to heat current water. The addition of these terms is the energy needed per volume unit to raise its temperature by 1ºC. If divided by density, the result is the energy per mass unit needed to produce a unit temperature increase, that is, the specific heat. Therefore, according to this reasoning, the expression of density current specific heat is:

$$c = \frac{c_s\rho_s C + c_w\rho_w(1-C)}{\rho_s C + \rho_w(1-C)} \tag{24}$$

As explained above, to develop the system of equations, the derivative $\frac{Dc}{Dt}$ must be computed:

$$\frac{\mathrm{D}c}{\mathrm{D}t} = \frac{\left[(c_w - c_s)\rho_s C(1-C)\right]\frac{\mathrm{D}\rho_w}{\mathrm{D}t} - (c_w - c_s)\rho_w\rho_s\frac{\mathrm{D}C}{\mathrm{D}t}}{\left[\rho_s C + \rho_w(1-C)\right]^2} \tag{25}$$

Water and sediment specific heats have been considered constants, thus neglecting their dependence on temperature.

Since $c_w > c_s$, if there is an increase in water density or a decrease in sediment concentration, which are processes that represent a rise in the amount of water in relation to sediment, there is an increase in total specific heat.

Both expressions for $\frac{D\rho}{Dt}$ and $\frac{Dc}{Dt}$, are introduced in Eq. 17 obtaining the following result:

$$\begin{aligned}\frac{\mathrm{D}T}{\mathrm{D}t} = {} & \frac{e_w U}{\rho c H}\left(\rho_0 c_0 T_0 - \rho c T\right) + \frac{\rho_s c_s w_s}{\rho c H}\left(E_s - r_0 C\right)T^* - \\ & -\frac{T}{c}\frac{\left[(c_w - c_s)\rho_s C(1-C)\right](2aT+b)\frac{\mathrm{D}T}{\mathrm{D}t} - (c_w - c_s)\rho_w\rho_s\frac{\mathrm{D}C}{\mathrm{D}t}}{\left[\rho_s C + \rho_w(1-C)\right]^2} - \\ & -\frac{T}{\rho}\left[(\rho_s - \rho_w)\frac{\mathrm{D}C}{\mathrm{D}t} + (1-C)(2aT+b)\frac{\mathrm{D}T}{\mathrm{D}t}\right]\end{aligned} \tag{26}$$

Numerical model

With these equations, a finite difference scheme has been applied, starting from the previous base of BANG 1D program (Pratson *et al*. 2001), to develop a new version which is named BANG 1DT. Similar models have been implemented for debris flows (Huang & Garcia 1998, Hungr 1995, Imran *et al*. 2001, Savage & Hutter 1991).

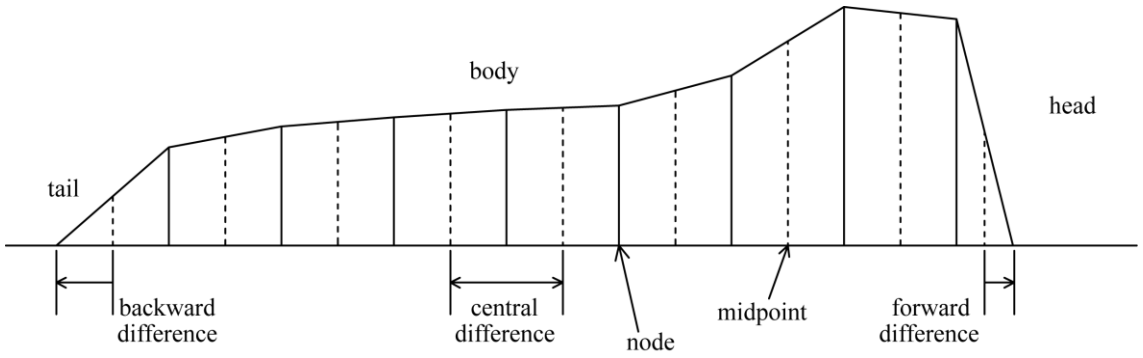

Figure C.6.6. BANG 1D solver numerical scheme

Figure C.6.6 presents a general view of model discretization. An explicit first order scheme (forward in the surge, backward in the tail) is used in flow extremes, and a second order, central difference along the body. As known, central difference discretization is second order, so it presents instabilities close to sharp gradients. Therefore, it is necessary to add an explicit damping term to smooth these oscillations. The artificial viscosity method is selected (Jameson *et al*. 1981).

Details in solution procedure can be found in Pratson *et al*. (2001) and Imran *et al*. (2001).

C.6 Results

Firstly, a qualitative study of density current behavior is carried out, with a simple geometry consisting of a variable slope that ends in a horizontal section. The study was focused on the influence of the slope, initial velocity, initial sediment and water concentrations, and initial sediment and water temperatures.

Density currents initially have a parabolic shape, as used in the previous version of the program BANG 1D (Pratson *et al*. 2001), and are located at the beginning of the longitudinal profile. The initial values for the different variables involved (depth-averaged velocity, sediment concentration, temperature) are specified for each case. Starting from this initial situation, BANG 1DT calculates the evolution of the current along the simplified profile used for the qualitative study, or along Flix reservoir bathymetry used afterwards.

Figure C.6.7 shows the evolution of the density of the current in two cases of different slopes (2º and 8º). In both cases, initial velocity, temperature and concentration are 1.0m s^{-1}, 7.0ºC and 0.05 respectively. As shown above, density is a function of temperature and sediment concentration. However, very low sediment concentrations generate density differences that are similar to the ones associated with normal temperature gradients, so in this case density evolution describes sediment concentration quite directly. Density profiles show that for higher slopes average sediment concentration decreases during the initial

phase and attains an approximately constant value until it arrives at the end of the slope. However, for low slopes density diminishes more gradually. Lower density values for high slopes are due to a higher water entrainment from the environment, increasing sediment dilution and diminishing total density, despite that the amount of sediment mixed with the current is higher. Regarding the profile shape, for higher slopes there is a significant concentration of sediment at the front of the current, showing an important resuspension activity in this area. After the change in the slope deposition occurs rapidly, especially in the case of lower slopes. This figure shows a sharper change in the velocity of the current for higher slopes after the slope break.

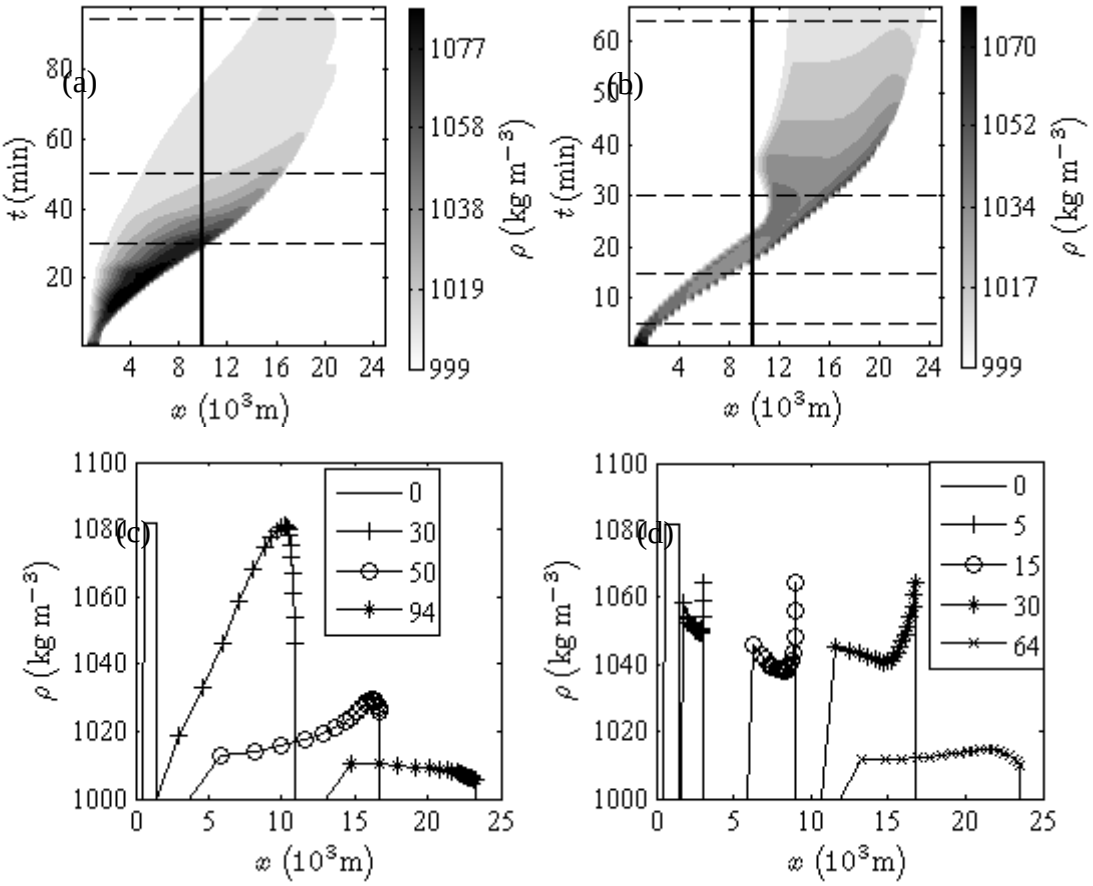

Figure C.6.7. Evolution of the density current in terms of density for a slope of 2º (a) and 8º (b). Horizontal dotted lines correspond to density profiles in different times (minutes) shown in (c) and (d) respectively. A vertical continuous line in (a) and (b) shows the location of the end of the slope.

In both low and high slopes there is a decrease in density due to deposition of sediment. As the current moves along the slope, the increase of the velocity enhances resuspension and stabilizes density values, until it arrives upon the flat section.

Figure C.6.8 shows a similar comparison but in terms of density depth. The main difference is the evolution along the horizontal section, where current increases its height for low slopes whereas for higher slopes decreases after attaining a maximum value just

after the slope change. This pattern is consistent with the decrease of the velocity of the current.

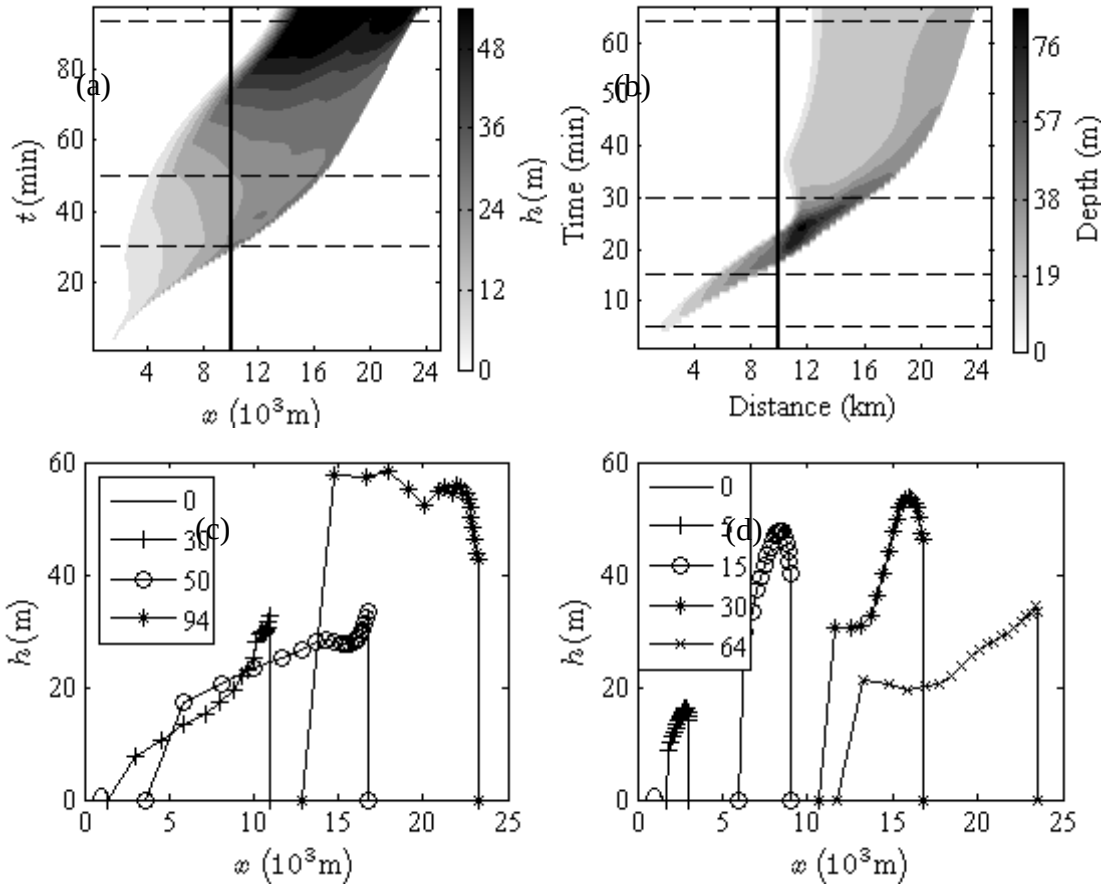

Figure C.6.8. Evolution of the density current in terms of current height for a slope of 2º (a) and 8º (b). Horizontal dotted lines correspond to height profiles in different times (minutes) shown in (c) and (d) respectively. A vertical continuous line in (a) and (b) shows the location of the end of the slope.

It is interesting to analyze the evolution of the density current in terms of Richardson number, which is calculated as:

$$\mathrm{Ri} = \frac{Rg\bar{c}h}{\bar{u}^2} \qquad (27)$$

Richardson number determines the flow regime of the density current, being supercritical when Ri<1 and subcritical when Ri>1. Richardson number also determines the entrainment of water which in turn, influences the evolution of density current depths and sediment concentration. Figure C.6.9 shows the evolution of the current in one of the qualitative study runs. The flow during the initial phase is highly supercritical, in such a way that the current increases its volume quickly. This trend stabilizes later and density current tends to critical conditions.

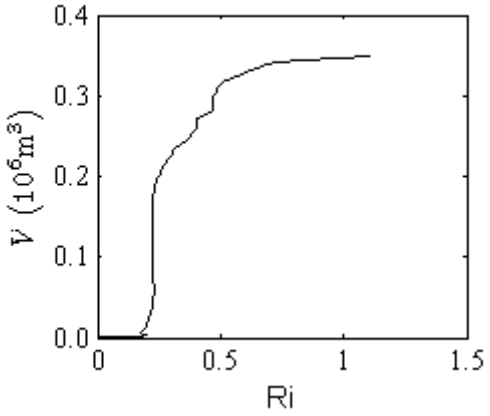

Figure C.6.9. Evolution of the density current in terms of Richardson number and total volume for initial conditions of 1.0m s^{-1}, 4ºC and with no sediment concentration, and boundary conditions of 15ºC for sediment and environment water temperature and a slope of 4º.

Next, Flix reservoir bathymetry (Fig. C.10) is introduced in BANG 1DT, and density currents of different characteristics are tested with the aim of studying the eroding effects on the reservoir bed.

Figure C.6.11 shows the amount of sediment that is mobilized per unit width by density currents with no initial sediment concentration and different velocities. The increase is significantly regular as initial velocity becomes higher, and the position of maximum erosion moves further from the initial position. These results have been used to calculate the amount of mercury mobilized in different conditions shown in Table C.4.

In Fig. C.12 and Fig. C.13 erosion-deposition profiles caused by density currents with an initial length of 1000m and different initial sediment concentrations are exposed, for initial velocities of 1 m s^{-1} and 3 m s^{-1} and different initial sediment concentrations (values of 0.0, 0.0002 and 0.001). For the case of 3m s^{-1} there is no significant difference between different initial concentrations due to the higher eroding potential of the current at these velocities and the three lines collapse in one single line.

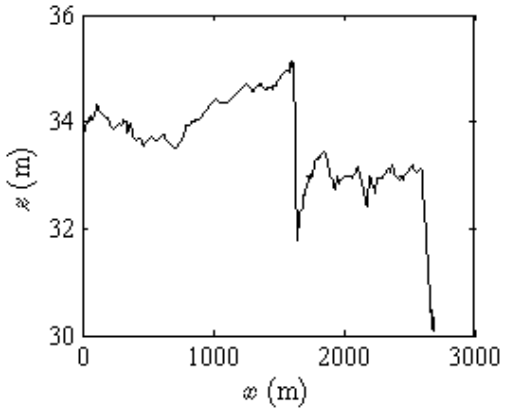

Figure C.6.10. Flix reservoir bathymetry (longitudinal profile)

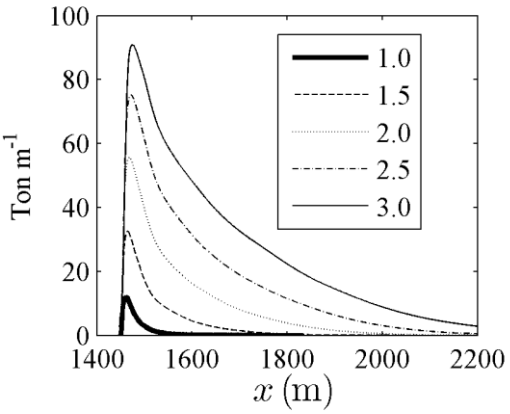

Figure C.6.11. Amount of sediment mobilized for different initial velocities of the density current (m s^{-1})

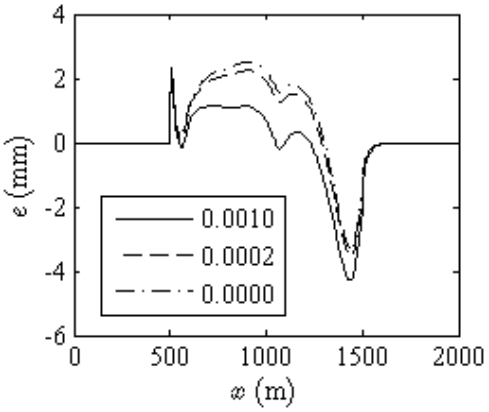

Figure C.6.12. Eroding profiles for a velocity of 1.0 m s^{-1} and different initial concentrations (sed. Volume/water volume)

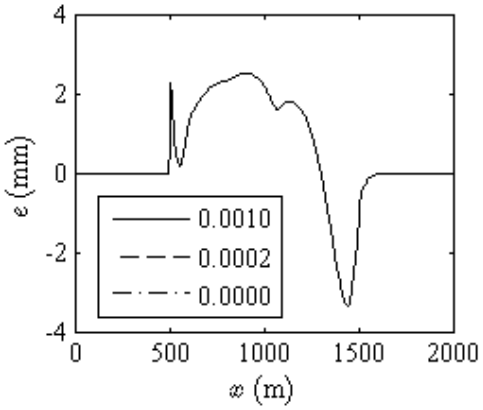

Figure C.6.13. Eroding profiles for a velocity of 3.0 m s^{-1} and different initial concentrations (sed. Volume/water volume)

Another interesting item is the influence of the density current length on the generated eroding profile. In this study, currents of 500, 1000 and 1500 meters were applied (Fig. C.14).

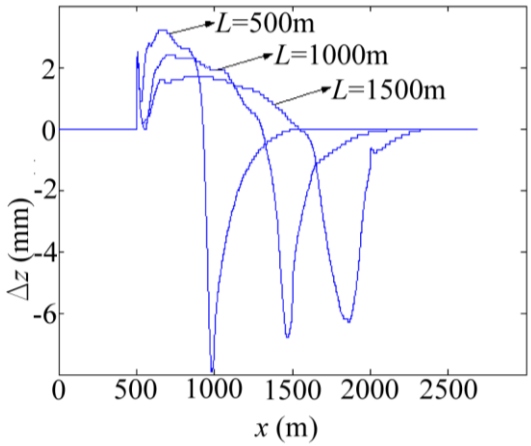

Figure C.6.14. Eroding profiles for different initial lengths

As current length increases, maximum local erosion decreases but total sediment volume mobilized rises.

Once the resuspended amount of sediment has been obtained, the quantity of mercury that is set into motion can be computed, starting from the concentration of this element at the reservoir bed. Its distribution appears in Fig. C.15 (Costa *et al*., 2004):

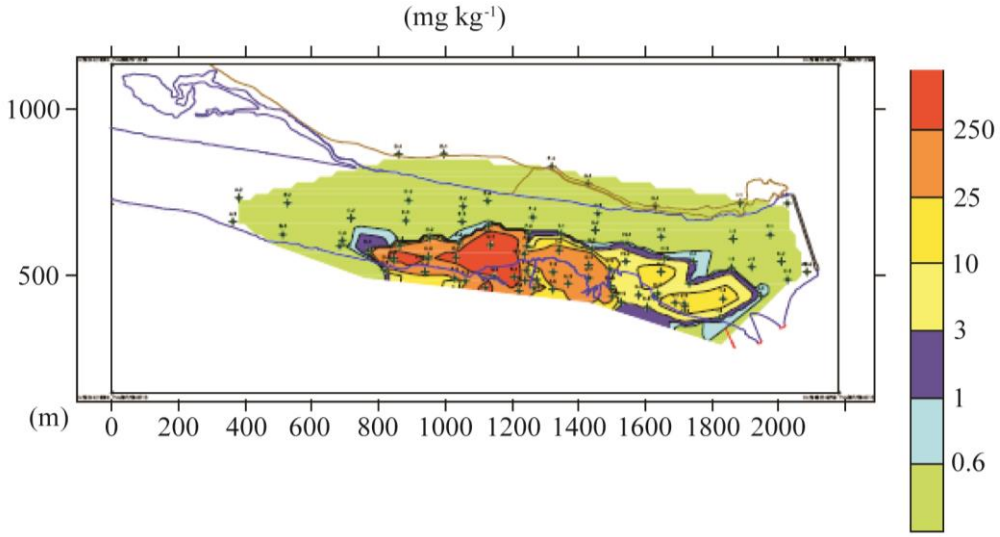

Figure C.6.15. Mercury concentration distribution (mercury mass/sediment mass) in Flix reservoir sediment

According to the eroding profiles obtained for the initial velocities of 1.0 m s^{-1} and 3.0 m s^{-1}, the eroded volume per width unit is shown in Table C.4.

Table C.4. Eroded volume and mercury mobilized for different initial velocities

Initial velocity ($m\ s^{-1}$)	Eroded volume per width unit ($m^3\ m^{-1}$)	Mobilized volume (m^3)	Mobilized mass of mercury (kg)
1.0	1.5	45	23.8
3.0	18	540	286.2

Considering a density current 30 meters wide, these results would imply the mobilized volumes of mercury exposed in Table C.4.

Assuming an average mercury concentration of $2 \cdot 10^{-4} kg\ kg^{-1}$ in sediment affected by the current, and taking $2.65 \cdot 10^{3} kg\ m^{-3}$ as the value for sediment density, the amounts of mobilized mercury shown in Table C.4 are obtained.

It can be observed that for high velocities, or considering the possibility of a wider density current or one which affects a nucleus with a higher contaminant concentration, quantities of mercury mobilized have the same order of magnitude as the ones estimated according to the concentration data measured in water samples, that have been previously commented during the hypothesis discussion (section 2).

Table C.5. Eroded volume and mercury mobilized for different initial concentrations of the density current

Initial concentration ($m^3 sed\ m^{-3} water$)	Eroded volume per width unit ($m^3\ m^{-1}$)	Mobilized volume (m^3)	Mobilized mass of mercury (kg)
0.005	5.1	153.6	61.2
0.01	11.1	332.4	132.9
0.04	43.4	1301.7	520.7

In Table C.5, a similar comparison is shown between density currents with different initial concentrations, showing that a higher amount of sediment implies a greater density difference and, therefore, a density current with more strength to resuspend sediment from the bottom and mobilize mercury.

As already explained, if cold water body is longer, the amount of mercury mobilized would be higher. Unfortunately, the bathymetry of the upstream section of the Ebro River was not available, and longer density currents have not been introduced in the model.

Despite the fact that previous calculations are only an estimation, as the exact conditions in which the fish's death took place are not known, they highlight that in certain circumstances an important sediment resuspension can occur in the Flix reservoir or similar scenarios.

Given the contaminant concentrations of the reservoir bed, these phenomena are an important risk for the organisms that live in that environment and for the activities in the area.

It should also be considered that at the reservoir bed there are important amounts of other kinds of contaminants which are also harmful for animals and plants that live there, in spite of the fact that during this event nobody paid much attention to them. In the following figures, concentration distributions of chrome (Fig. C.16), DDT (Fig. C.17) and PCB (Fig. C.18) are shown (Costa *et al*., 2004).

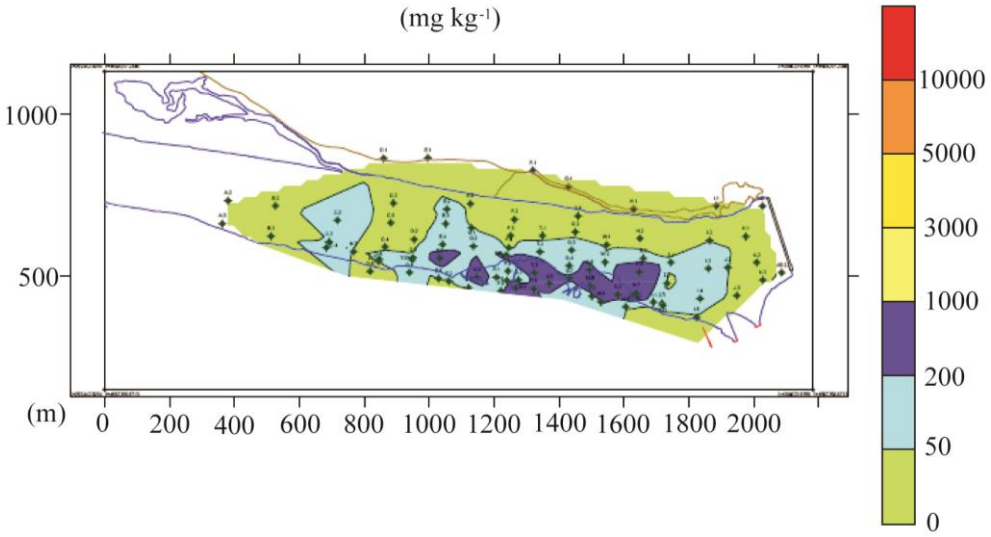

Figure C.6.16. Chrome concentration distribution (mercury mass/sediment mass) in Flix reservoir sediment (Costa et al. 2004)

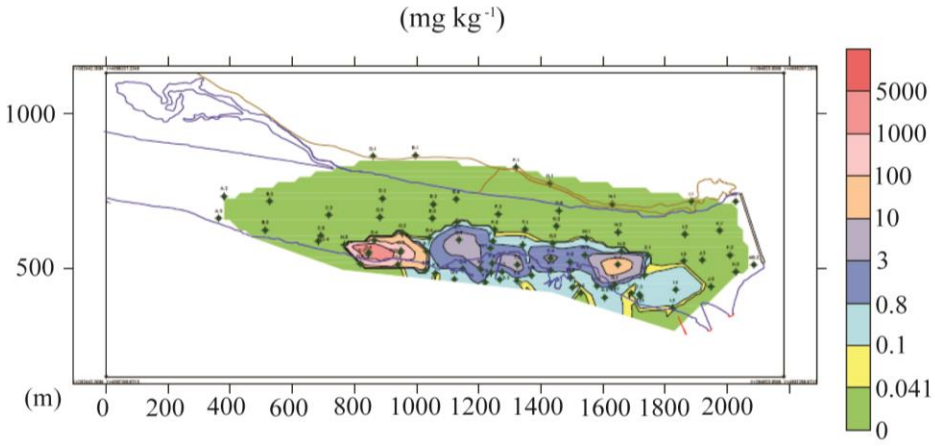

Figure C.6.17. PCB concentration distribution (mercury mass/sediment mass) in Flix reservoir sediment (Costa et al. 2004)

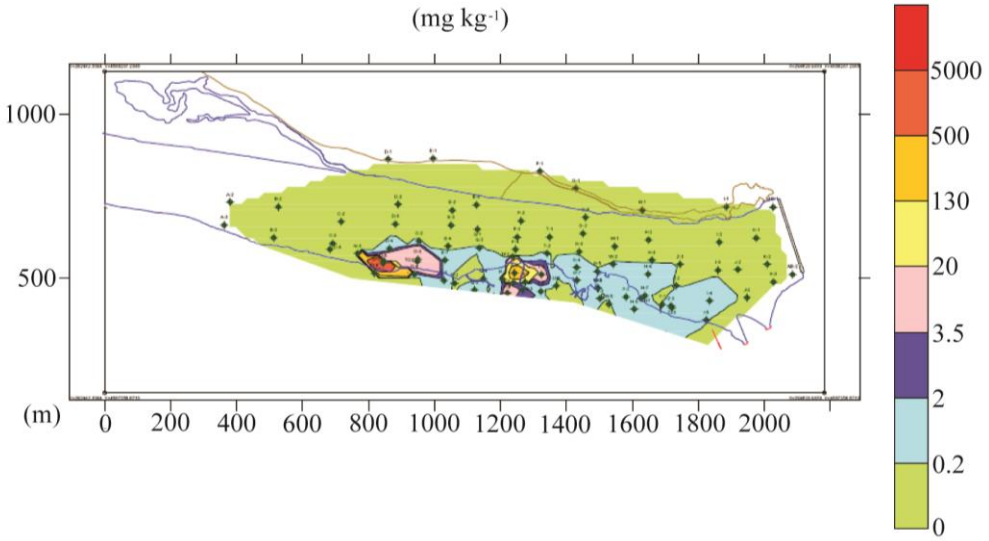

Figure C.6.18. DDT concentration distribution (mercury mass/sediment mass) in Flix reservoir sediment

C.7 Conclusions

In this study, the main possible cause of the fish's deaths in the Flix reservoir in December 2001 has been analyzed.

The large amount of mercury found in the samples, suggests that the pollutant comes from the reservoir bed, instead of from a punctual dumping of Ercros factory. This drop was the first hypothesis to be considered. However, it seems unlikely that anybody threw 400 kilograms of mercury into the water and, even in this case, that the pollutant dispersed all throughout reservoir affecting so many fish species. On the contrary, at the reservoir bed there are $3 \cdot 10^8$kg of

contaminated sediment that could be a more reliable source for the pollutant found in the water and cause of the mentioned consequences.

Following this line of reasoning, we have tried to draw up a hypothesis based on a mechanism which is able to set sediment into motion. In the absence of extraordinary flood events (discharges of those days have ordinary values), density currents have been studied in this article as a possible explanation of the happening.

This phenomenon is generated by the presence of two water bodies with different densities. In this situation the denser water falls to the bed and causes a turbulence that can be able to mobilize the bottom sediment. Density difference between water bodies can be caused by the presence of sediment in suspension or by a temperature difference between both. The extraordinarily low temperatures of the days during which the contamination event took place, motivated the study of the second option. For that purpose, a previous programme BANG 1D (Pratson *et al*. 2001) was modified to create a new version BANG 1DT, in which the new equation proposed in this study to evaluate temperature evolution was introduced. Processes of water and sediment entrainment, diffusion by conduction and turbulent viscosity and the energy dissipation due to viscosity, have been considered.

The results obtained have shown that temperature has little influence on the ability of resuspension of the current, in contrast with other parameters such as initial velocity and sediment concentration, but it can be a crucial factor when it comes to initiating the phenomenon.

After applying Flix reservoir bathymetry, there was an initial section in which erosion was observed and a later one where sediment was deposited. In conditions of high velocities, the amount of sediment mobilized is about 500 m^3, and taking into account the concentrations of mercury measured in the ground, that would imply a mobilization of 300 kg of mercury, in addition to other contaminants present in the ground in significant quantities. Therefore, this hypothesis would justify the large amount of pollutant found in the water and would be a reliable explanation of the fish's death.

In such conditions, it is interesting to think about possible situations that could give rise to density currents. It may occur when draining suddenly from a reservoir upstream, in such a way that water gets cold during its trajectory across the air until falling downstream or during its journey to a lower reservoir. It could also happen that when cleaning the bottom drain of the dam upstream, a certain amount of sediment mixes with the water, triggering a density current.

C.8 Acknowledgements

This work has been developed within the framework of the project "Estudi de la dinàmica dels compostos organoclorats persistents i altres contaminants en els sistemes aquatics continentals". The authors thank GITS research group for its economical and personal help, the Spanish ministry of education for the grant given to the first author for the development of his thesis and the anonymous referees for their constructive criticism, which contributed to the improvement of the manuscript.

C.9 Notation

c: specific heat of the density current (J K^{-1})

$\bar{c}$: depth-averaged concentration of the density current (J K^{-1})

c_0 : specific heat of the external environment water (J K^{-1})

c_s: specific heat of the bed sediment (J K^{-1})

c_w: specific heat of the water inside the density current (J K^{-1})

D_s: mean sediment diameter (m)

E_s: non-dimensional coefficient of erosion

e_w: non-dimensional water entrainment coefficient from the environment water body

g: gravitational acceleration (m s^{-2})

h: depth of the density current (m)

k: water thermal conductivity (W K^{-1} m^{-1})

$\bar{k}$: depth-averaged turbulent kinetic energy of the density current (m^2 s^{-2})

R: non-dimensional submerged specific gravity of the sediment

Re_p: particle Reynolds number

Ri: Richardson number

r_0: non-dimensional coefficient for the bulk concentration at the base of a turbidity current

S: bed slope (radians)

t: time (s)

T: depth-averaged temperature of the density current (K)

T_0: temperature of the external environment water (K)

$\bar{u}$: depth-averaged velocity of the density current (m s^{-1})

u_* : shear velocity at the base of a turbidity current (m s^{-1})

W_s: sediment fall velocity (m s^{-1})

x: distance parallel to the seafloor (m)

ε_0 : vertically averaged viscosity of a turbidity current ($m^2\ s^{-2}$)

ν : kinetic viscosity ($m^2\ s^{-1}$)

ν_T : turbulent viscosity (m^2 s)

ρ : density of the density current (kg m^{-3})

ρ_0 : density of the external environment water (kg m^{-3})

ρ_s : density of the bed sediment (kg m^{-3})

ρ_w : density of the water inside the density current (kg m^{-3})

C.10 References

Altinakar, M. S., Graf, W. H., and Hopfinger, E. J. (1990). Weakly depositing turbidity current on a small slope. *J. Hydraulic Res.* 28(1), 55-80.

Boening, D. (2000). Ecological effects, transport, and fate of mercury: a general. *Chemosphere.* 40(12), 1335-1351.

Bradford, S. & Katopodes, N. (1995). Numerical modeling of turbidity currents. Proc. 4th Int. Conf. on Estuarine and Coastal Modeling, 404–415.

Bradford, S., Katopodes, N. (1999). Hydrodynamics of turbid underflows. i: Formulation and numerical analysis. *J. Hydraulic Eng.* 125(10), 1006–1015.

Bradford, S., Katopodes, N., Parker, G. (1997), Characteristic analysis of turbid underflows. *J. Hydraulic Eng.* 123(5), 420–431.

Cathum, S., Velicogna, D., Obenauf, A., Dumouchel, A., Punt, M., Brown, C., Ridal, J. (2005). Detoxification of mercury in the environment. *Analytical and bioanalytical chemistry.* 381(8), 1491–1498.

Choi, S.-U., García, M.H. (1995). Modeling of one-dimensional turbidity currents with a dissipative-Galerkin finite element method. *J. Hydraulic Res.* 33(5), 623-648.

Costa, J., Villarrubia, M. & Bateman, A. (2004). Contribución y evaluación del "Estudi de la dinàmica dels compostos organoclorats persistents i altres contaminants en els sistemes aquàtics continentals". Noviembre 2003. Propuesta de actuaciones en el Embalse de Flix.

Fer, I. (2001). Dynamics of winter cooling in Lake Geneva. *Thèse EPFL*, nº 2398, Lausanne, Switzerland..

Fer, I., Lemmin, U., Thorpe, S.A. (2002). Winter cascading of cold water in Lake Geneva. *J. Geophys. Res.* 107, 3060, 16pp., 2002.

Fofonoff, N., Millard, R. (1983). Algorithms for computation of fundamental properties of seawater. Endorsed by Unesco/SCOR/ICES/lAPSO Joint Panel on Oceanographic Tables and Standards and SCOR Working Group 51.

García, M. H., Parker, G. (1991). Entrainment of bed sediment into suspension. *J. Hydraulic Eng.* 117(4), 414-435.

García, M. H. (1993). Hydraulic jumps in sediment-driven bottom currents. *J. Hydraulic Eng.*, ASCE, 119(10), 1094-1117.

García, M. (1994), Depositional turbidity currents laden with poorly sorted sediment. *J. Hydraulic Eng.* 120(11), 1240–1263.

García, M. H. (2008). *Sedimentation Engineering*. # ASCE.

Huang, X., Garcia, M. (1998). A herschel–bulkley model for mud flow down a slope. *J. Fluid Mech.* 374(1), 305–333.

Hungr, O. (1995). A model for the runout analysis of rapid flow slides, debris flows and avalanches. *Canadian Geotechnical Journal.* 32(4), 610–623.

Imran, J., Parker, G., Locat, J., Lee, H. (2001). 1D numerical model of muddy subaqueous and subaerial debris flows. *J. Hydraulic Eng.* 127(11), 959–968.

Jameson, A., Schmidt, W., Turkel, E. (1981). Numerical solutions of the Euler equations by finite volume methods using Runge-Kutta time-stepping schemes. *AIAA paper* 81, 1259.

La Rocca, M., Bateman, A. (2010), Experimental and theoretical modeling of 3D gravity currents, Numerical Simulations. Examples and Applications in Computational Fluid Dynamics. *Intech*, 281-310.

Lemmin, U., Jiang, R., Thorpe, S.A. (1998). Finescale dynamics of stratified waters near a sloping boundary of a lake. *Physical processes in lakes and oceans*, Ed. J. Imberger. Amer. Geophys. Un., Washington, DC, Coastal and Estuarine Studies, 54, 461-474.

Newell, L. (1903). *Descriptive chemistry*. DC Heath & co.

Parker, G., Fukushima, Y., Pantin, H. (1986). Self-accelerating turbidity currents. *J. Fluid Mech.* 171, 145–181.

Pratson, L., Imran, J., Hutton, E., Parker, G., Syvitski, J. (2001). Bang1D: a one-dimensional, lagrangian model of subaqueous turbid surges. *Computers & geosciences* 27(6), 701–716.

Ravisangar, V., Dennett, K., Sturm, T., Amirtharajah, A. (2001). Effect of sediment pH on resuspension of kaolinite sediments. *J. Envir. Eng.* 127, 531-538.

Ravisangar, V., Sturm, T., Amirtharajah, A. (2005). Influence of sediment structure on erosional strength and density of kaolinite sediment beds. *J. Hydraulic Eng.* 131, 356-365.

Reddi, L., Bonala, M. (1997). Critical shear stress and its relationship with cohesion for sand-kaolinite mixtures. *Canadian geotechnical journal*, 34(1), 26–33.

Savage, S. B., Hutter, K. (1991). The dynamics of avalanches of granular materials from initiation to run-out. *Acta. Mech.* 86(1), 201–223.

Turner, J. S., (1979). *Buoyancy effects in fluids*. # Cambridge University Press, Cambridge.

Wan, C., Fell, R. (2004). Investigation of rate of erosion of soils in embankment dams. *Journal of geotechnical and geoenvironmental engineering* 130, 373-380.

Wright, S., Parker, G. (2004a). Density stratification effects in sand bed rivers. *J. Hydraulic Eng.* 130(8), 783-795.

Wright, S. and Parker, G. (2004b). Flow resistance and suspended load in sand-bed rivers: simplified stratification model. *J. Hydraulic Eng.* 130(8), 796-805.